

AFRL-PR-WP-TR-2000-2120

**FUEL DEGRADATION AND ALLIED
STUDIES
DELIVERY ORDER 5**

**ANDRE BOEHMAN, SEMIH ESER,
PAT HATCHER, BRUCE MILLER,
HAROLD SCHOBERT, AND CHUNSHAN SONG**

**ENERGY INSTITUTE AND DEPARTMENT OF MECHANICAL AND
NUCLEAR ENGINEERING
THE PENNSYLVANIA STATE UNIVERSITY
UNIVERSITY PARK, PA 16802-2320**



JULY 2000

FINAL REPORT FOR PERIOD OF 01 JUNE 1998 – 31 JULY 2000

Approved for public release; distribution unlimited

**PROPULSION DIRECTORATE
AIR FORCE RESEARCH LABORATORY
AIR FORCE MATERIEL COMMAND
WRIGHT-PATTERSON AIR FORCE BASE, OH 45433-7251**

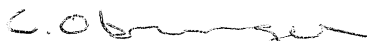
REPORT DOCUMENTATION PAGE			Form Approved OMB No. 0704-0188	
Public reporting burden for this collection of information is estimated to average 1 hour per response, including the time for reviewing instructions, searching existing data sources, gathering and maintaining the data needed, and completing and reviewing this collection of information. Send comments regarding this burden estimate or any other aspect of this collection of information, including suggestions for reducing this burden to Department of Defense, Washington Headquarters Services, Directorate for Information Operations and Reports (0704-0188), 1215 Jefferson Davis Highway, Suite 1204, Arlington, VA 22202-4302. Respondents should be aware that notwithstanding any other provision of law, no person shall be subject to any penalty for failing to comply with a collection of information if it does not display a currently valid OMB control number. PLEASE DO NOT RETURN YOUR FORM TO THE ABOVE ADDRESS.				
1. REPORT DATE (DD-MM-YYYY) 01-07-2000		2. REPORT TYPE Final		3. DATES COVERED (FROM - TO) 01-06-1998 to 31-07-2000
4. TITLE AND SUBTITLE Fuel Degradation and Allied Studies Delivery Order 5 Unclassified			5a. CONTRACT NUMBER F33615-98-D-2802	
			5b. GRANT NUMBER	
			5c. PROGRAM ELEMENT NUMBER	
6. AUTHOR(S) Boehman, Andre ; Eser, Semih ; Hatcher, Pat ; Miller, Bruce ; Schobert, Harold ;			5d. PROJECT NUMBER	
			5e. TASK NUMBER	
			5f. WORK UNIT NUMBER	
7. PERFORMING ORGANIZATION NAME AND ADDRESS Energy Institute and Department of Mechanical and Nuclear Engineering The Pennsylvania State University University Park, PA16802-2320			8. PERFORMING ORGANIZATION REPORT NUMBER	
9. SPONSORING/MONITORING AGENCY NAME AND ADDRESS Propulsion Directorate Air Force Research Laboratory Air Force Materiel Command Wright-Patterson AFB, OH45433-7251			10. SPONSOR/MONITOR'S ACRONYM(S)	
			11. SPONSOR/MONITOR'S REPORT NUMBER(S)	
12. DISTRIBUTION/AVAILABILITY STATEMENT APUBLIC RELEASE				
13. SUPPLEMENTARY NOTES				
14. ABSTRACT Experimental and theoretical efforts were undertaken to further the understanding of the thermal degradation of coal-derived and petroleum-derived jet fuels. Thermal degradation includes both thermal-oxidative and pyrolytic degradation and deposition.				
15. SUBJECT TERMS Fuel; Coal Derived Fuel; Thermal Stability; High Temperature Fuels; Pyrolysis; Thermal Oxidation				
16. SECURITY CLASSIFICATION OF:		17. LIMITATION OF ABSTRACT	18. NUMBER OF PAGES	19. NAME OF RESPONSIBLE PERSON
		Same as Report (SAR)	102	Fenster, Lynn lfenster@dtic.mil
a. REPORT Unclassified	b. ABSTRACT Unclassified	c. THIS PAGE Unclassified		19b. TELEPHONE NUMBER International Area Code Area Code Telephone Number 703767-9007 DSN 427-9007
				Standard Form 298 (Rev. 8-98) Prescribed by ANSI Std Z39.18

NOTICE

USING GOVERNMENT DRAWINGS, SPECIFICATIONS, OR OTHER DATA INCLUDED IN THIS DOCUMENT FOR ANY PURPOSE OTHER THAN GOVERNMENT PROCUREMENT DOES NOT IN ANY WAY OBLIGATE THE US GOVERNMENT. THE FACT THAT THE GOVERNMENT FORMULATED OR SUPPLIED THE DRAWINGS, SPECIFICATIONS, OR OTHER DATA DOES NOT LICENSE THE HOLDER OR ANY OTHER PERSON OR CORPORATION; OR CONVEY ANY RIGHTS OR PERMISSION TO MANUFACTURE, USE, OR SELL ANY PATENTED INVENTION THAT MAY RELATE TO THEM.

THIS REPORT IS RELEASABLE TO THE NATIONAL TECHNICAL INFORMATION SERVICE (NTIS). AT NTIS, IT WILL BE AVAILABLE TO THE GENERAL PUBLIC, INCLUDING FOREIGN NATIONS.

THIS TECHNICAL REPORT HAS BEEN REVIEWED AND IS APPROVED FOR PUBLICATION



CYNTHIA OBRINGER
Fuels Branch
Turbine Engine Division
Propulsion Directorate



WILLIAM E. HARRISON III
Chief, Fuels Branch
Turbine Engine Division
Propulsion Directorate



JOHN T. DATKO, JR.
Acting Chief of Technology
Turbine Engine Division
Propulsion Directorate

Do not return copies of this report unless contractual obligations or notice on a specific document requires its return.

REPORT DOCUMENTATION PAGE			Form Approved OMB No. 0704-0188	
Public reporting burden for this collection of information is estimated to average 1 hour per response, including the time for reviewing instructions, searching existing data sources, gathering and maintaining the data needed, and completing and reviewing the collection of information. Send comments regarding this burden estimate or any other aspect of this collection of information, including suggestions for reducing this burden, to Washington Headquarters Services, Directorate for Information Operations and Reports, 1215 Jefferson Davis Highway, Suite 1204, Arlington, VA 22202-4302, and to the Office of Management and Budget, Paperwork Reduction Project (0704-0188), Washington, DC 20503.				
1. AGENCY USE ONLY (Leave blank)		2. REPORT DATE July 2000		3. REPORT TYPE AND DATES COVERED FINAL, 06/01/1998 – 07/31/2000
4. TITLE AND SUBTITLE Fuel Degradation and Allied Studies Delivery Order 5			5. FUNDING NUMBERS C F33615-98-D-2802 PE 62203F PR 3048 TA 05 WU EX	
6. AUTHOR(S) Andre Boehman, Semih Eser, Pat Hatcher, Bruce Miller, Harold Schobert, Chunshan Song				
7. PERFORMING ORGANIZATION NAME(S) AND ADDRESS(ES) Energy Institute and Department of Mechanical and Nuclear Engineering The Pennsylvania State University University Park, PA 16802-2320			8. PERFORMING ORGANIZATION REPORT NUMBER D.O. 0005	
9. SPONSORING/MONITORING AGENCY NAME(S) AND ADDRESS(ES) Propulsion Directorate Air Force Research Laboratory Air Force Materiel Command Wright-Patterson AFB, OH 45433-7251 POC: Cindy Obringer, AFRL/PRTG, 937-255-6390			10. SPONSORING/MONITORING AGENCY REPORT NUMBER AFRL-PR-WP-TR-2000-2120	
11. SUPPLEMENTARY NOTES				
12a. DISTRIBUTION AVAILABILITY STATEMENT Approved for Public Release; Distribution Unlimited			12b. DISTRIBUTION CODE	
13. ABSTRACT (Maximum 200 words) Experimental and theoretical efforts were undertaken to further the understanding of the thermal degradation of coal-derived and petroleum-derived jet fuels. Thermal degradation includes both thermal-oxidative and pyrolytic degradation and deposition.				
14. SUBJECT TERMS Fuel, Coal Derived Fuel, Thermal Stability, High Temperature Fuels, Pyrolysis, Thermal Oxidation			15. NUMBER OF PAGES 104	
			16. PRICE CODE	
17. SECURITY CLASSIFICATION OF REPORT UNCLASSIFIED	18. SECURITY CLASSIFICATION OF THIS PAGE UNCLASSIFIED	19. SECURITY CLASSIFICATION OF ABSTRACT UNCLASSIFIED	20. LIMITATION OF ABSTRACT SAR	

THIS PAGE INTENTIONALLY LEFT BLANK

Table of Contents

	Page
List of Figures	v
List of Tables.....	ix
 SECTION	
1.0 MINIMIZE THERMAL DEGRADATION OF FUELS	1
1.1 Construction of a Flow Reactor	1
1.2 Thermal-Stability Testing of Coal- and Petroleum-Derived Fuels.....	1
 2.0 THERMAL OXIDATIVE MODELING	 3
 3.0. JP-8+225 DEVELOPMENT	 5
 4.0 FUEL STABILIZERS: FLOW-REACTOR STUDIES OF PETROLEUM-DERIVED JET FUELS	 6
 5.0 FUEL STABILIZERS: NUMERICAL SIMULATION OF JET-FUEL DEGRADATION IN FLOW REACTORS	 7
 6.0 FUEL STABILIZERS: MANUSCRIPT SUBMITTED TO <i>ENERGY & FUELS</i> — “NUMERICAL SIMULATION OF JET-FUEL DEGRADATION IN FLOW REACTORS” ...	 11
6.1 Abstract	11
6.2 Introduction	11
6.3 Numerical	13
6.4 Experimental.....	17
6.5 Results and Discussion.....	18
6.6 Conclusions	28
 7.0 DEGRADATION OF INDIVIDUAL COMPONENTS IN FUEL	 30
7.1 Introduction	30
7.2 Experimental Section	31
7.3 Results and Discussion.....	39
7.4 Conclusions	50
 8.0 CLARIFICATION OF KEY INTERACTIONS AMONG FUEL COMPONENTS UNDER PYROLYTIC AND OXIDATIVE CONDITIONS.....	 52
8.1 Suppression of Pyrolytic Degradation of n-Alkanes in Jet Fuels by Hydrogen Donors....	52
8.2 Synergistic Effects of Hybrid Hydrogen Donors toward Stabilization of Paraffinic Jet Fuels in the Pyrolytic Regime	55
8.3 Thermal Stability of Coal-Derived Jet Fuels in the Autoxidative and Pyrolytic Regimes	59
 9.0 DECOMPOSITION AND SOLID DEPOSITION FOR COAL-BASED FUELS: FUEL COMPOSITION/PHASE AND SURFACE EFFECTS	 69
9.1 Introduction	69
9.2 Experimental.....	69

9.3 Results and Discussion	69
9.4 Conclusions	82
10.0 REFERENCES	83
List of Symbols, Abbreviations, and Acronyms	89

List of Figures

	Page
1. Schematic Drawing of the Flow Reactor	2
2. Comparison of Preheater-Tube Deposits.	4
3. Comparison of Heater-Tube Deposits.....	4
4 .Measured and Predicted Fuel-Temperature Profiles.	5
5. Carbon Deposition and Wetted-Wall Temperature as a Function of Axial Distance for Three Fuels.....	8
6. Heat of Combustion of Unstressed and Stressed Fuels.....	8
7. Experimental and Calculated Bulk-Temperature Profiles.	10
8. Experimental and Calculated Unreacted Fuel-Fraction Profiles.	10
9. Coordinate System for the Flow-Reactor Model.....	14
10. Temperature Profiles for Dodecane Stressing.....	20
11. Unreacted Fuel Fraction Profiles for Dodecane Stressing.	20
12. Arrhenius Plots of $\ln(k)$ vs. T^{-1} for Pure Dodecane and the Dodecane Mixtures Containing 10-mol percent BzOH and THQ.....	22
13. Experimental and Calculated Bulk Temperature Profiles.....	26
14. Experimental and Calculated Unreacted Fuel-Fraction Profiles.	27
15. Temperature Profiles Predicted by Nonpyrolysis and Pyrolysis Model for NORPAR-13 Stressing.....	28
16. Variation of Local Nusselt Number Along the Flow Reactor for Dodecane Stressing.	29
17. Schmatic Presentation of the Procedure Used for the Synthesis of the Labeled Compound 1- ^{13}C -Hexylbenzene.	32
18. Schematic Presentation of the Stainless-Steel Autoclave Reactor for Jet-Fuel Stressing.	36
19. Schematic of the Flowing Reactor.....	38

	Page
20. First-Order Plots of the Thermal Degradation of Neat Unlabeled Hexylbenzene Quantified by GC-FID and GC-SIM-MS, Compared with the GC-FID Data Obtained by McKinney [51].....	41
21. Gas Chromatograms of ^{13}C -Hexylbenzene Mixed with JP-8 (a) and Pyrolyzed in a Static Reactor at 400 °C for 1 (b); 2 (c); 4 (d); and 6 Hours (e).	43
22. First-Order Plots for the Thermal Degradation of Neat Hexylbenzene and When Mixed in JP-8, Quantified by GC-SIM-MS.	45
23. First-Order Plots for the Thermal Degradation of Hexylbenzene Mixed in JP-8, Compared with the Same Fuel in the Static Reactor as Quantified by GC-SIM-MS.....	46
24. Comparison of Remaining TD Content Divided by its Initial Concentration for Different Mixtures with THNol, Stressed at 425, 450, and 475 °C for 30 Minutes.....	53
25. Comparison of the Ratio of the Remaining TD Content to its Initial Concentration for TD Alone and with 0.5-Mole Percent THNol Added, Stressed at 425, 450, and 475 °C for 30 Minutes	54
26. Comparison of Remaining TD Content Divided by its Initial Concentration for Different Mixtures with THQ, Stressed at 425, 450, and 475 °C for 30 Minutes.....	54
27. Changes in the Enhancement of the TD_t/TD_0 ratio with 0.5-Mole Percent THQ Added, Stressed at 425, 450, and 475 °C for 30 Minutes (TD_t/TD_0 for TD only is baseline)	55
28. Ratio of the 1-Alkene Peak Area to that of the Corresponding Alkane for TD Alone and with 0.5-Mole percent THN and 0.5-Mole percent BA Addition Stressed at 475 °C for 30 Minutes.	56
29. Simplified Role of the Hydrogen Donors, BA, THN, and THNol in the Thermal Stabilization of TD in the Pyrolytic Regime.	57
30. Comparison of the Ratio of TD Remaining to the Initial Amount for TD Mixed with 1- mole percent of the Single Hydrogen Donors BA, THN, and THNol, Individually, and with Hybrids at 450 °C.....	58
31. Comparison of the Ratio of TD Remaining to the Initial Amount for TD Mixed with 1 Mole percent of the Single Hydrogen Donors BA, THN, and THNol, Individually, and with Hybrids at 475 °C.....	58

	Page
32. Comparison of Liquid Remaining for Tetradecane, Decahydronaphthalene, and the Coal-Derived Jet Fuel JP-8C Stressed Under the Influence of Air in the Temperature Range 250 to 500 °C.	61
33. Comparison of Solid Deposition for Tetradecane, Decahydronaphthalene, and the Coal-Derived Jet Fuel JP-8C Atrressed Under the Influence of Air in the Temperature Range 250 to 500 °C.	61
34. General Composition of the Coal-Derived Jet-Fuel JP-8C.	62
35. Variation in the Remaining Concentration of Tetradecane (TD) and Decahydronaphthalene (DHN) with Temperature.	62
36. GC/MS Traces of the Reaction Products from Stressing Tetradecane in Air Up to 250, 350, 450, and 500 °C (listed from bottom to top and not to scale).	64
37. GC/MS Traces of the Reaction Products from Stressing Decahydronaphthalene in Air at 250, 350, 450, and 500 °C (listed from bottom to top and not to scale).	66
38. Major Oxygenated Compounds from Decahydronaphthalene Stressed Under Air and Heated to 250 °C.	67
39. GC/MS Traces of the Coal-Derived Jet Fuel JP-8C Stressed Under Air at 250 °C (bottom) and 500 °C (top).	68
40. TPO Profiles of Carbon Deposits from Thermal Stressing of Dodecane, Toluene, and Methylcyclohexane at 500 °C and 500 psig for 5 h with a 1 mL/min Flow Rate.	71
41. SEM Micrographs of Carbon Deposits from Dodecane (a), Toluene (b), and Methylcyclohexane (c) at 500 °C and 500 psig for 5 h with a 1 cc/min Flow Rate.	72
42. TPO Profiles of Carbon Deposits from Stressing Toluene, Dodecane, and Methylcyclohexane on Inconel 600 in a Glass-Lined Flow Reactor at 600 °C.	73
43. SEM Micrographs of Deposits from Dodecane (a), Toluene (b), and Methylcyclohexane (c) Decomposition at 600 °C and 500 psig for 5 h with a 1 cc/min Flow Rate.	74
44. TPO Profiles of Carbon Deposits and SEM Micrographs of Carbon Deposits Formed from Dodecane and Methylcyclohexane.	76
45. TPO Profiles of Deposits from Thermal Stressing of a Ternary Mixture of Dodecane, Toluene, and Methylcyclohexane for Different Pressures at 500 °C.	78
46. SEM Images of Deposits from Thermal Stressing of an n-Dodecane, Toluene, and Methylcyclohexane Mixture at Various Pressures.	79

	Page
47. Carbon Burn-Off Profiles Showing the Effect of 100-ppm Thiophene Addition to Dodecane and Methylcyclohexane.	81
48. SEM Micrograph of a Carbon Deposit on Inconel 600 (100-ppm Thiophene).	82

List of Tables

	Page
1. Brief Descriptions of Fuels Studied.....	6
2. Kinetic Parameters for Model Jet Fuels and Additives.....	16
3. Values of Experimental Parameters.....	19
4. Predicted Outlet Bulk Temperatures and Unreacted Fuel Fraction.....	21
5. Calculated Outlet Bulk Temperatures and Unreacted Fuel Fraction.....	23
6. Mean Residence Time for Dodecane Stressing at Different Flow Rates.....	24
7. Comparison of Experimental and Calculated Outlet Bulk Temperatures.....	24
8. Comparison of Experimental and Calculated Outlet Unreacted Fuel Fraction.....	25
9. Conversion percentage of Neat Unlabeled Hexylbenzene Pyrolyzed in a Tubing Bomb at 400 °C at Each Time Interval.....	40
10. Percentage of Conversion of ¹³ C-Labeled Hexylbenzene Spiked into JP-8 and Pyrolyzed in a Tubing Bomb at 400 °C at Each Time Interval	42
11. Percent Change of Abundance Relative to Initial Concentration of Peaks 1 to 20 (Figure 7.4a) during 6-Hour Pyrolysis.	44
12. Percentage of Conversion of ¹³ C-Labeled Hexylbenzene Spiked into JP-8 and Pyrolyzed in a Flowing Reactor at 400 °C at Each Time Interval, as Defined by the Flow Rate of the Pump and the Reactor Length	46
13. Mass Balance of the ¹³ C from the Thermal Degradation (flow reactor, 4 hours) of ¹³ C-Hexylbenzene Spiked in JP-8 and Showing the Redistribution of the Label into Other Compounds	49
14. Relative Abundance of the ¹³ C-Enriched Compounds Characterized by GC-SIM-MS	49
15. percentage of Conversion of ¹³ C-Labeled Hexylbenzene Spiked into JP-8 and Pyrolyzed in a Flow Reactor at 400 °C at Each Time Interval, as Defined by the Flow Rate of the Pump and the Reactor Length.....	50
16. Carbon Deposits from Stressing Dodecane, Toluene, and Methylcyclohexane on an Inconel 600 Alloy.....	70

17. The Amount of Deposit Formed from Toluene, Dodecane, and Methylcyclohexane at 600 °C and 500 psig with 1 cc/min Flow Rate for 5 h.	71
18. Carbon Deposits from Dodacane+Methylcyclohexane and Dodecane+Toluene Mixtures on Inconel 600.....	75
19. The Amount of Carbon Deposit Obtained from Thermal Stressing n-Dodecane, Methylcyclohexane, and Toluene at 500 °C.....	77
20. The Amount of Deposit Formed from Dodecane and Methylcyclohexane on Inconel 600 with and without Added Thiophene at 500 °C, 500 psig, with 1-cc/min Flow Rate for 5 h.....	80

1.0 MINIMIZE THERMAL DEGRADATION OF FUELS

1.1 Construction of a Flow Reactor

In order to study further the thermal stability of petroleum-derived jet fuels, a second flow reactor was constructed at Penn State. The following is a brief description of the flow reactor construction and operation.

Figure 1 shows the overall layout of the flow reactor system. Fuel is held in a 20-liter stainless-steel reservoir tank. A nitrogen purge is passed through this tank in order to remove oxygen from the fuel and also reduce autoxidative reactions. A Waters 515 high-pressure liquid-chromatography pump draws fuel from the reservoir tank and pumps it throughout the system. A 0.5-micron sintered filter removes any insoluble particles from the flow. The fluid then passes through a TVS 12/60/900 Carbolite furnace to raise the temperature of the fuel. The heated region of the furnace is 0.89 meter (35 inches) in length. Thirteen K-type thermocouples, spaced 2.5 inches apart, monitor the wetted-wall temperature of the stainless-steel flow tube inside the furnace.

The fluid then passes through a counterflow heat exchanger where it cools to room temperature. A Polyscience model 6506 Recirculator circulates the heat-exchanger coolant, which consists of a 50/50 mixture of ethylene glycol and water. The reaction products are then separated into liquid and gaseous fractions and collected for sampling.

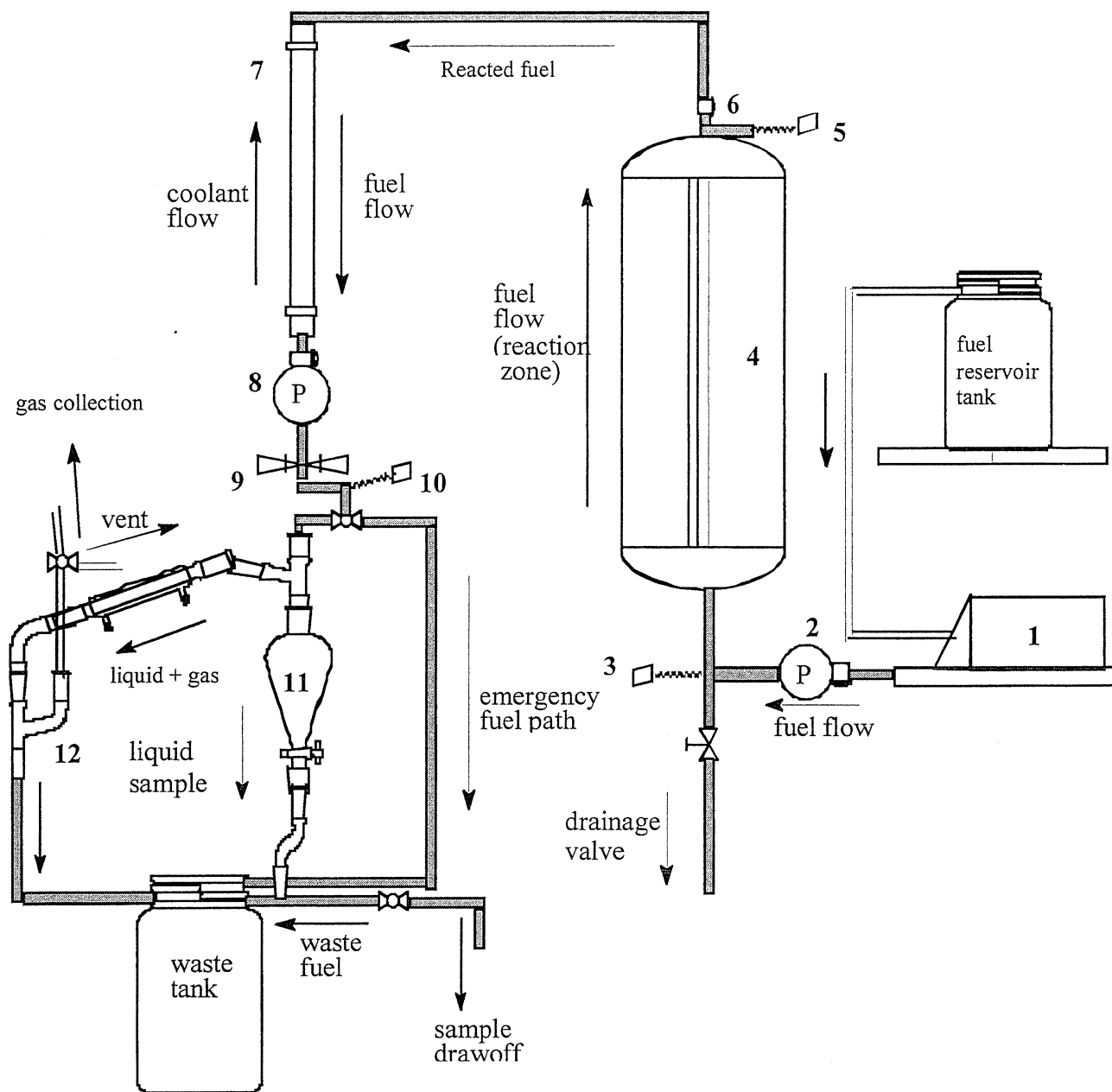
The system pressure is controlled by a Nupro metering valve and is monitored both by an electronic transducer and simple analog dial gauges. This pressure-transducer signal is then used in the Visual Basic data acquisition and control program and compared with a user-defined set point. The program then adjusts the position of the Nupro metering valve accordingly via a stepping motor.

The following are typical flow-reactor test conditions. The sample temperature is 700 °C and the pressure is 700 psig. The typical test duration is 7 hours with a fuel flow rate of 10 mL/min. The fuel in the reservoir tank is sparged with ultra high purity nitrogen for 2 hours.

1.2 Thermal-Stability Testing of Coal- and Petroleum-Derived Fuels

Work under this task was performed by the University of Dayton Research Institute under SUBCONTRACT NO. USAF-TPSU-UDRI-2802-1494. The objective of this task was to utilize the Extended-Duration Thermal-Stability Tests (EDTST) to evaluate coal- and petroleum-derived fuels.

We performed a test with Jet Propellant Thermally Stable fuel under the same conditions used previously (Report 4) for evaluating JP-8+100 fuel. The temperatures were 360 °F (bulk) and 600 °F (wetted wall). The purpose of this test was to evaluate the thermal stability of JPTS at elevated temperatures. The carbon deposits in the heater and preheater tubes that resulted from this test are shown in Figures 2 and 3, respectively. The previous results with JP-8+100 fuel are



Legend:

- | | |
|------------------------------|--------------------------------------|
| 1. HPLC pump | 7. Heat exchanger |
| 2. Pressure gauge and filter | 8. Pressure gauge and filter |
| 3. Inlet thermocouple | 9. Backpressure valve |
| 4. Furnace | 10. Post heat exchanger thermocouple |
| 5. Outlet thermocouple | 11. Separatory funnel |
| 6. Filter | 12. Gas collection system |

Figure 1. Schematic Drawing of the Flow Reactor

shown for comparison purposes. The heater deposits for JPTS fuel are considerably lower than for the JP-8+100 fuel at the tube location (section 15) where the maximum wetted-wall temperature was experienced. However, JPTS had significant deposits downstream from the maximum wetted-wall temperature location. This is an indication that the thermal-stability additive for JPTS was virtually depleted or the oxygen was completely consumed at the end of the heater tube where the peak deposit was experienced. The preheater deposits with JPTS were higher than deposits with the JP-8 +100 fuel.

2.0 THERMAL OXIDATIVE MODELING

The objective of this task was to model the chemical reactions that occur upon fuel heating. To this extent, we continued the development of a new one-dimensional model for the simulation of thermal oxidative and deposition processes in flowing systems. Accurate predictions of the fuel temperature are important, as the fuel temperature has a large role in the chemical kinetics of fuel degradation. As further confirmation of the model's accuracy, simulations of the fuel temperature profile along the tube were performed, and the results were compared with both experimental measurement and predictions from a two-dimensional axisymmetric finite-difference solution of the governing equations (see Figure 4). For flow rates less than 50 mL/min, the main flow is anticipated to be laminar because the Reynolds numbers for these conditions are well below 3000. Interestingly, the two-dimensional, turbulent-flow predictions follow the measurements better than the two-dimensional laminar calculations for flow rates where laminar behavior might otherwise be expected.

Katta and Roquemore [1] proposed that buoyancy induced vortices that are superimposed on the main flow significantly enhance the heat transfer. In the present work, the heat-transfer coefficients used for flow rates below 50 mL/min come from the mixed natural- and forced-convection heat-transfer correlation of Oliver [2]. Figure 4 shows that the present model, which incorporates buoyancy effects by means of the mixed-convection heat-transfer coefficient, supports the hypothesis for the formation of streamwise vortices [1]. Figure 4 also shows that for flow rates greater than 50 mL/min, the measured temperatures approach those obtained from the two-dimensional laminar calculations. The heat-transfer correlation used for flow rates between 80 and 100 mL/min in the present analysis is for laminar conditions without buoyancy effects ($Re < 3000$ [3]). Thus, the present analysis together with the axisymmetric laminar solution support the suggestion [1] that the flow relaminarizes as the flow rate is increased beyond 80 mL/min. For flow rates between 100 mL/min and 175 mL/min ($Re \sim 3200$ and $Re \sim 3900$), the main flow changes from laminar to turbulent flow ($Re > 3000$). Thus, another heat-transfer correlation (Gnielinski [4]; $3000 < Re < 5 \times 10^6$) was chosen to represent turbulent (and mixed turbulent-laminar) conditions. The complex fluid dynamics and heat transfer that occur within the tube between 50 and 80 mL/min is not well represented by the correlations selected here. Moreover, this complex three-dimensional behavior was not captured by the more complicated two-dimensional simulations. However, from a practical point of view, greater accuracy in this flow range is unwarranted because flow rates in aircraft are generally large (> 120 mL/min).

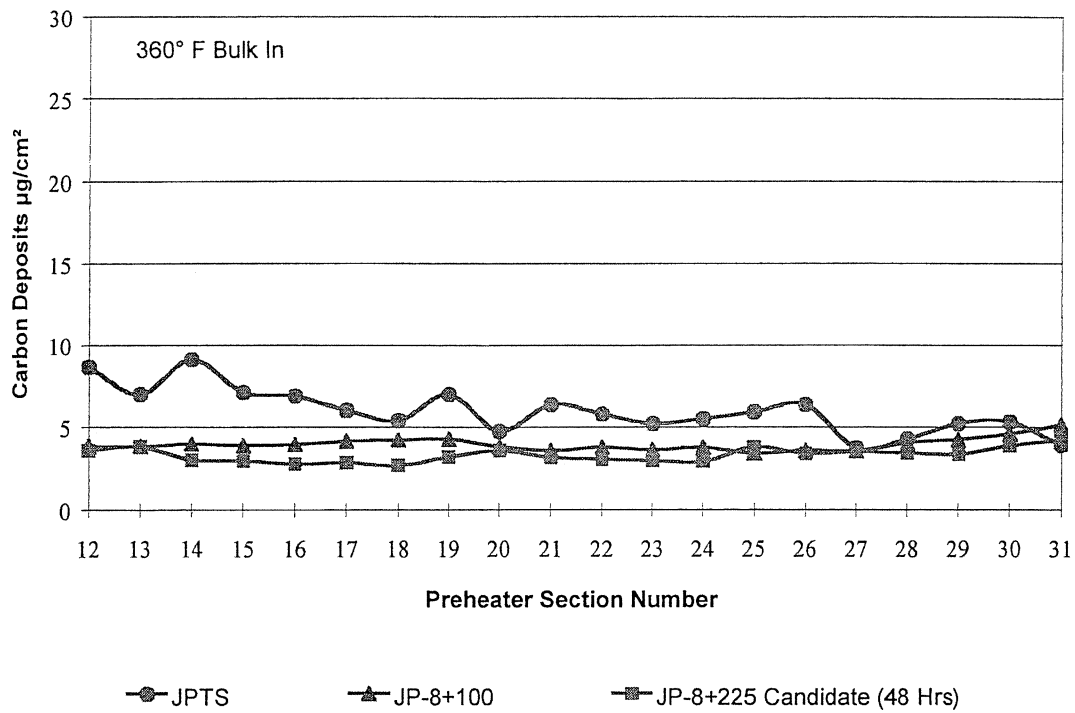


Figure 2. Comparison of Preheater-Tube Deposits

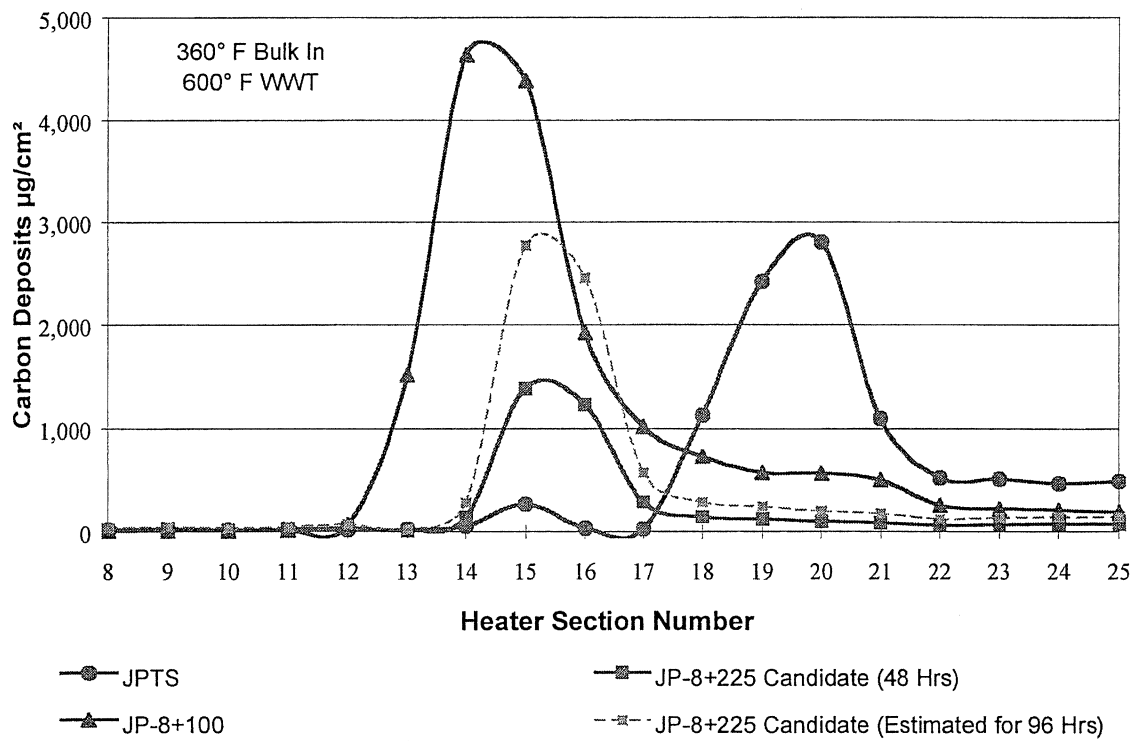


Figure 3. Comparison of Heater-Tube Deposits.

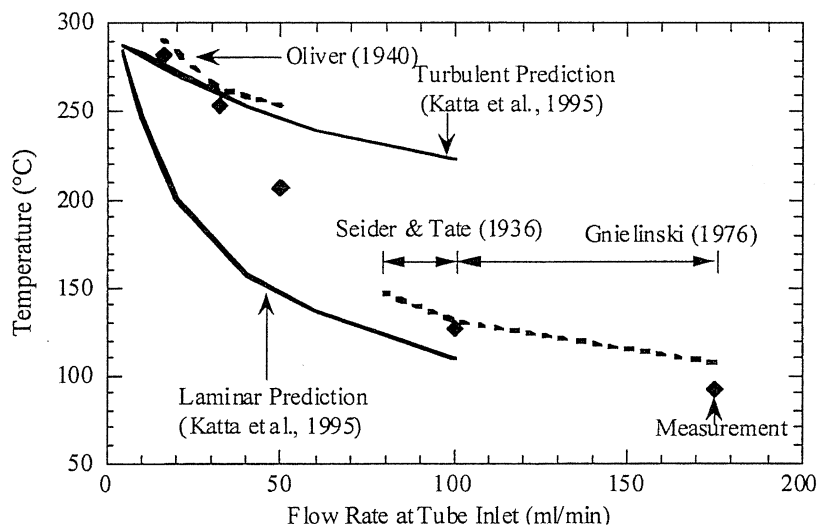


Figure 4. Measured and Predicted Fuel-Temperature Profiles

3.0 JP-8+225 DEVELOPMENT

We began evaluation of new test conditions for the formulation of additives and additive packages for JP-8+225 in the quartz crystal microbalance/Parr bomb system. A test temperature of 180 °C was selected. It was thought that this temperature would be high enough to provide a reasonably realistic screening of potential additives, while being low enough to observe oxidation and deposition over the time period of minutes to hours. Higher temperatures would result in oxidation and deposition occurring too rapidly for *in situ* measurement in the QCM apparatus. Initially, we tried some runs where the fuel and reactor were sparged with nitrogen prior to heat-up, with subsequent addition of air after temperature equilibration at 180 °C. We found that this labor-intensive process was unnecessary for most jet fuels, as no significant deposition occurred during the heat-up period in the presence of air. A series of runs was performed for various Jet A, JP-8, and JP-7 fuels to determine typical oxidation times and deposition quantities under these test conditions. The JP-7 fuels produce deposits of approximately 0.5 $\mu\text{g}/\text{cm}^2$, whereas less-refined fuels yield deposits from 1 to 4 $\mu\text{g}/\text{cm}^2$. Our original JP-8+100 baseline fuel, POSF-2827, exhibits one of the higher-deposit quantities at these high temperatures, so it was selected as the preliminary JP-8+225 baseline fuel for this test.

Analysis of oxygen consumption in fuel systems under various realistic temperature/time conditions shows that oxygen consumption will be much higher under JP-8+225 conditions than JP-8+100 conditions. In fact, most reasonable residence times will result in complete oxygen consumption at 288 °C (550 °F) fuel temperatures. Thus, production of polar species and particles, which result in deposition, will likely be about one order of magnitude higher at JP-8+225 temperatures. These observations lead us to the conclusion that antioxidants such as hindered phenols and metal deactivators will have little effect at these temperatures. Detergents and dispersants appear to be more promising in providing the needed reductions in deposition. The order of magnitude greater production of polar species and particles, however, means that significantly greater levels of dispersants and/or detergents will be required. We have tested this hypothesis in POSF-2827 at 180 °C with two dispersant additives: Ethyl POSF-3557 and

BetzDearborn 8Q405. It was found that a significant reduction in deposition was observed as the additives were increased from the JP-8+100 levels (100-200 mg/L) to 1000 mg/L. These high-dispersant concentrations look very promising for providing the deposition reduction required for the development of JP-8+225.

4.0 FUEL STABILIZERS: FLOW-REACTOR STUDIES OF PETROLEUM-DERIVED JET FUELS

In this work we seek to assess the stability of various fuel basestocks in a flowing system to determine their suitability for blending in a highly thermally stable jet fuel. This in turn will assist in determining what fuel processing routes yield basestocks with higher inherent stability.

Six fuels are being tested in a flow reactor for thermal stability. A flow reactor provides a somewhat more realistic environment than the batch reactors that are predominately used. The six fuels tested are shown in Table 1 with brief descriptions. All fuels except for the Norpar-13 were manufactured by BP. Norpar-13 is a solvent manufactured by Exxon Chemical Co. The fuels are sparged with UHP nitrogen in order to remove any dissolved oxygen that may be present. All six fuels were tested at a furnace temperature of 700 °C and a reactor pressure of 700 psig. A flow rate of 10 mL/min was used. Most of the fuels were tested for 7 hours to ensure measurable deposition formation. However, the hydrotreated light cycle oil and the light cycle oil were tested for only 3 hours, in order to avoid blocking the tube.

Table 1. Brief Descriptions of Fuels Studied

Fuel	Description
Kerosene	Straight-run kerosene often serves as a base for jet fuels. The kerosene used in this study is largely made up of alkanes and cyclic alkanes.
JP-8	JP-8 is the current military combat fuel, and is used for air- and ground-based vehicles. It consists mainly of alkanes. It also contains an additive package.
De-aromatized hydrotreated light cycle oil	De-aromatized hydrotreated light cycle oil is an attempt to increase the usefulness and value of heavier stocks as well as to mimic a coal-derived jet fuel. The fuel is mostly made up of cyclic alkanes.
Hydrotreated light cycle oil	Hydrotreated light cycle is aromatic in nature, but has been treated to a lower sulfur content than its parent feedstock.
Light cycle oil	Light cycle oil is a product of catalytic cracking. It is very aromatic in nature.
Norpar-13	Norpar-13 is a solvent produced by Exxon Chemical Co. It consists mostly of normal alkanes, and is often used as a model fuel in jet-fuel degradation studies.

The fuels are analyzed for solid formation, liquid composition, post-stressing fuel properties, and gas composition. At this point, the only results available are the carbon profiles from some of the fuels (Figure 5). The carbon profiles are obtained by analyzing sections of the reactor tube with an LECO R412 Multiphase Carbon Analyzer. The wetted-wall temperatures are measured by spot-welding thermocouples to the outside of the reactor tube.

As Figure 5 shows, both kerosene and dearomatized hydrotreated light cycle oil demonstrate a marked decrease in carbon deposition from JP-8. The JP-8 also lost more liquid mass to solid and gas production than did the other two fuels. Preliminary results indicate that the straight-run kerosene contains a higher percentage of hydroaromatics, which have been shown to be effective additives in decreasing pyrolytic deposition in an anaerobic environment, than does the JP-8. The dearomatized hydrotreated light cycle oil lacks the hydroaromatics but consists largely of cyclic alkanes, which appear to be more stable than the long-chain alkanes which are the main constituents of JP-8.

Studies have also been performed on the calorific value of the stressed jet fuel (Figure 6). The calorific value of the stressed fuel decreases for all fuels tested. In addition, liquid fuel is lost to solid and gas formation, decreasing further the fuel that can be delivered to the combustor, and hence the energy that can be used to propel the aircraft.

The JP-8 shows a slightly larger decrease in calorific value than do kerosene and dearomatized light cycle oil, and the light cycle oil shows the greatest loss in calorific value. The magnitude of the losses may be accounted for by the loss of some of the liquid fuel to gas and solid formation.

From a preliminary examination of the results, it appears that kerosene and dearomatized hydrotreated light cycle oil are the most thermally stable of the six fuels studied, and could provide an acceptable base for a prototype JP-900.

5.0 FUEL STABILIZERS: NUMERICAL SIMULATION OF JET-FUEL DEGRADATION IN FLOW REACTORS

We are developing a mathematical model for estimating the degradation of jet fuels in a simulated heated-flow environment. Since many of the physical and chemical processes involved in the decomposition of real jet fuel in an aircraft are not well understood at this point, this model is formulated by incorporating an accurate description of the transport phenomena, but with a simplified global chemistry model. This model is also capable of utilizing the existing kinetic data from batch reactors and predicting the jet-fuel degradation in heated-flow reactor systems. In order to develop and validate this mathematical model, however, it is necessary to have data from carefully instrumented experiments. The proposed model is validated using experimental data obtained at different flow rates after stressing the model jet fuel, dodecane. For the conditions examined, the model predictions agree well with the experimentally measured results. The numerical model also serves as a comprehensive simulation tool to examine the effects of various physical and experimental parameters on jet-fuel degradation and to evaluate additive effectiveness in flow reactors.

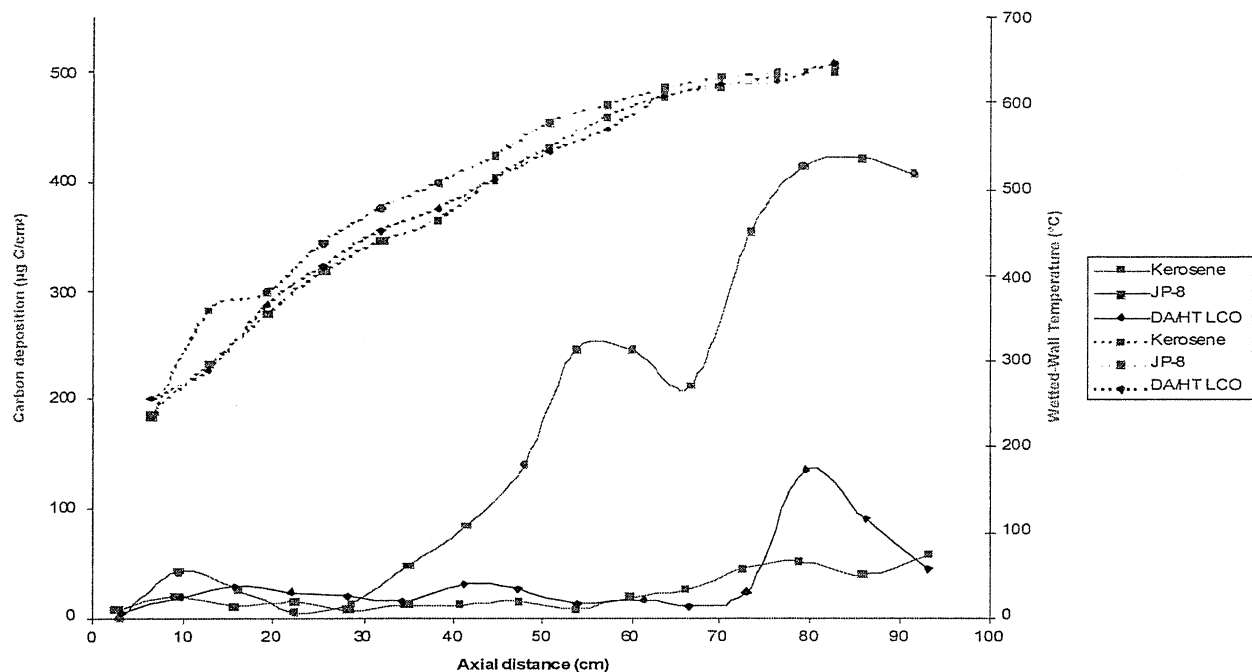


Figure 5. Carbon Deposition and Wetted-Wall Temperature as a Function of Axial Distance for Three Fuels
(Furnace temperature = 700 °C, pressure = 700 psig, duration of run = 7 hours, heated zone = 90 cm)

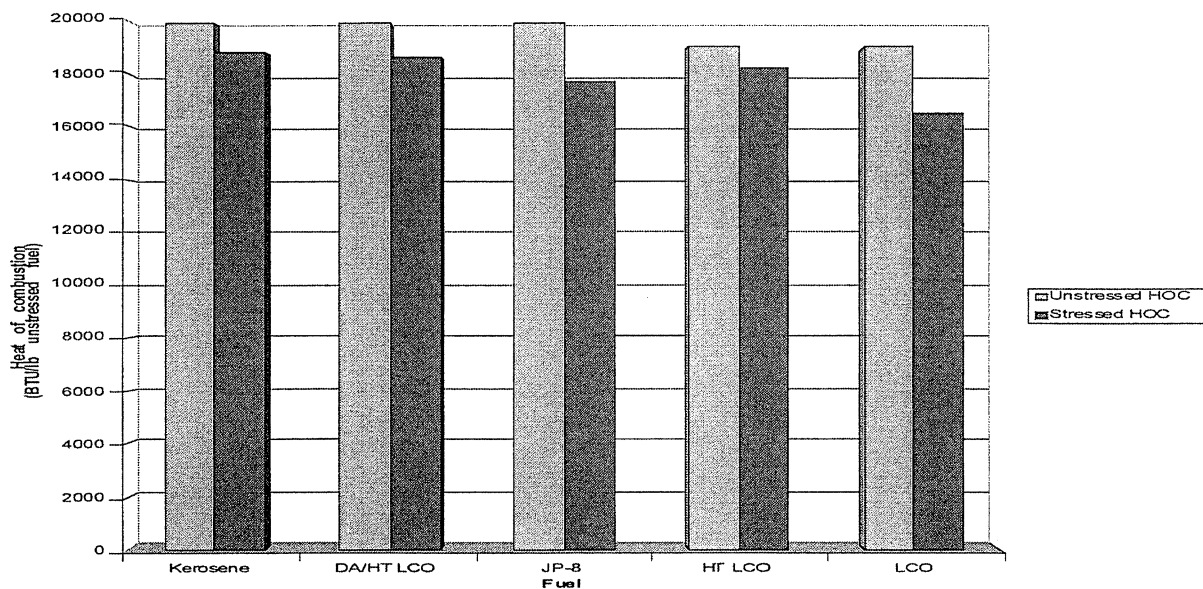


Figure 6. Heat of Combustion of Unstressed and Stressed Fuels

Figure 7 shows the outlet bulk temperatures measured experimentally after stressing dodecane at five different flow rates through the flow reactor. The experimentally measured outlet temperatures are accurate to within ~ 2 °C. It also shows the calculated bulk temperatures from the simulation runs at two different sets of densities. The calculated bulk temperature values show a deviation in the range of 2-20 percent from the experimentally measured values, when the dodecane density was estimated at the experimentally measured outlet bulk temperatures. However, the calculated bulk temperatures show a deviation only in the range of 3-7 percent, when the dodecane density was estimated at 500 °C. This shows that the calculated values are in reasonable agreement with the experimentally measured values, but show variation with changing density. The simulation results calculated with the dodecane density estimated at 500 °C are closer to the experimentally measured outlet bulk temperatures. This shows that the simulation results are sensitive to the density parameter. Figure 7 also shows that the calculated outlet bulk temperature increases with the decreasing value of density and vice versa. For example, at a fuel flow rate of 20 mL/min, the calculated outlet bulk temperature was found to be 397 °C when the density was estimated at 500 °C, but was found to be 343 °C when the density was estimated at the experimentally measured outlet temperature of 430 °C.

Figure 8 shows the plots of experimentally measured outlet unreacted-fuel fractions and the calculated numerical results for two different sets of densities at varying flow rates. The experimentally measured unreacted dodecane was estimated by averaging the results from three samples of the unreacted dodecane at each flow rate to reduce experimental error. However, the calculated results for the unreacted dodecane fraction may be accurate only up to ~ 10 percent because of extreme sensitivity to the kinetic parameters of dodecane degradation. The calculated results for two different sets of densities show a deviation in the range of 1-18 percent from the experimentally measured values. However, the variation in the calculated unreacted fuel-fraction shows very little variation with changing density compared with that observed for the outlet bulk temperatures. It appears that the density parameter has a much greater impact on the temperature profiles compared with the unreacted fuel-fraction profiles.

Both the experimental and numerical results also show that as the fuel flow rate increases, the outlet bulk temperature decreases, while the unreacted fuel-fraction increases. These trends can be justified on the basis of residence time of the fuel in the flow reactor and the temperature experienced by the fuel during that period. At a lower flow rate, the fuel spends more time in the flow reactor, hence absorbing more heat and in the process suffering more degradation.

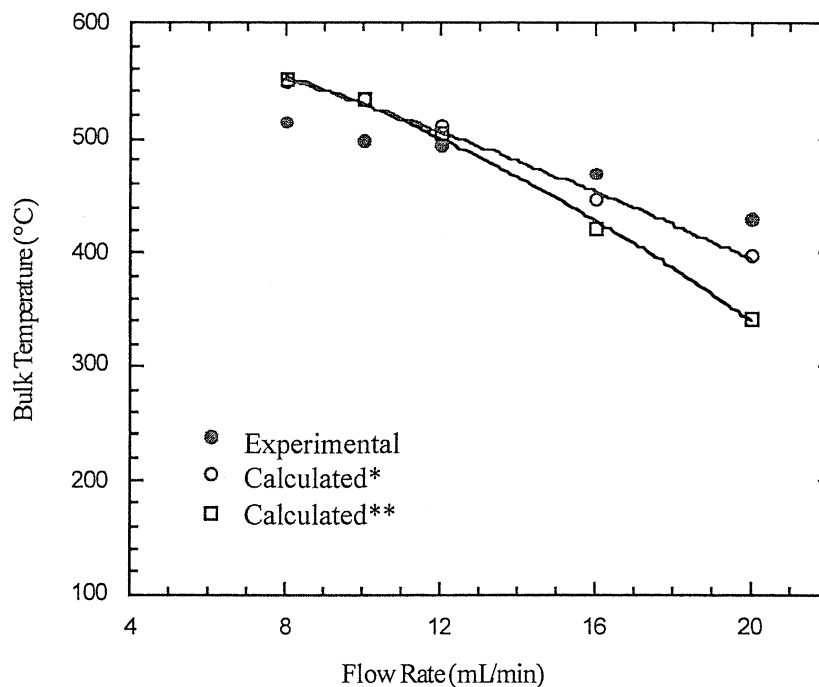


Figure 7. Experimental and Calculated Bulk-Temperature Profiles

* Simulation results for density of dodecane estimated at experimentally measured outlet bulk temperatures

** Simulation results for density of dodecane estimated at experimentally measured outlet bulk temperatures at a temperature of 500 °C

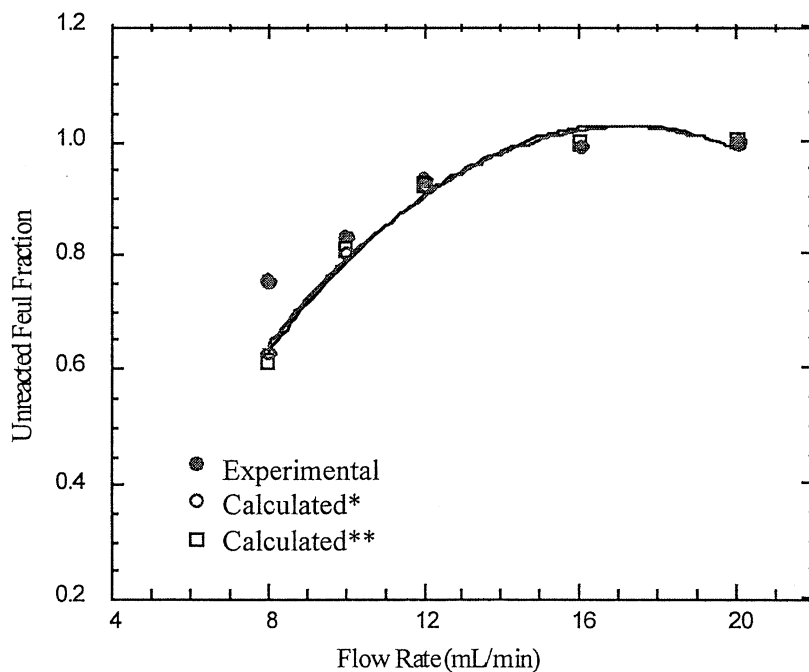


Figure 8. Experimental and Calculated Unreacted Fuel-Fraction Profiles.

* Simulation results for density of dodecane estimated at experimentally measured outlet bulk temperatures

** Simulation results for density of dodecane estimated at experimentally measured outlet bulk temperatures at a temperature of 500 °C

6.0 FUEL STABILIZERS: MANUSCRIPT SUBMITTED TO *ENERGY AND FUELS* — “NUMERICAL SIMULATION OF JET-FUEL DEGRADATION IN FLOW REACTORS”

6.1 Abstract

In modern high-speed military aircraft, the jet fuel has a secondary function, acting as primary coolant to absorb the heat generated at high flight speeds and by on-board equipment. The present study deals with the development of a mathematical model for estimating the degradation of jet fuels in a simulated heated-flow environment. Since many of the physical and chemical processes involved in the decomposition of real jet fuel in an aircraft are not well understood at this point, this model is formulated by including an accurate description of the transport phenomena, but with a simplified global chemistry model. This model is also capable of utilizing the existing kinetic data from batch reactors and predicting the jet-fuel degradation in heated-flow reactor systems. In order to develop and validate this mathematical model, however, it is necessary to have data from carefully instrumented experiments. The proposed model is validated using experimental data obtained at different flow rates after stressing the model jet fuel, dodecane. For the conditions examined, the model's predictions agree well with the experimentally measured results. The numerical model also serves as a comprehensive simulation tool to examine the effects of various physical and experimental parameters on jet fuel degradation and to evaluate additive effectiveness in flow reactors.

6.2 Introduction

With the advancement of aeropropulsion technologies into the twenty-first century, increasingly severe demands are being placed on the structural and thermal capabilities of the engine, fuel economy, and pollutant-emissions control [5]. At supersonic and hypersonic flight speeds, the temperature of the ram air taken on board the vehicle is too high to cool the engine. Use of mechanical cooling units on board is undesirable because they increase both the weight and complexity of the aircraft [6]. These conditions make it necessary to seek an alternative strategy utilizing the jet fuel as the primary coolant. To provide this necessary cooling, the fuel must be resistant to degradation under both autoxidative and pyrolytic conditions. These advanced "high heat-sink" fuels will require development of new fuel additives that can suppress autoxidation and pyrolysis at temperatures as high as 450 °C [7]. Simulating the behavior of these fuels with additives at supercritical or cracking temperatures requires development of new test modules. These test modules can be used to determine fuel reaction chemistry, kinetics, heat transfer, as well as chemical and physical properties at supercritical conditions.

Advanced computational fluid-dynamic models coupled with fuel-degradation chemistry and advanced high-temperature fuel-system-component simulators are required to determine the impact of fuel degradation in advanced high-speed aircraft and engine fuel systems. A realistic numerical model can help to identify the major factors governing the complex processes occurring during fuel degradation and predict the flow-system behavior under different operating conditions. It is very difficult to build a comprehensive model of real jet-fuel decomposition in an aircraft because many of the physical and chemical processes involved are not well

understood at this point [8]. Two general approaches followed to tackle these kinds of problems are:

1. Develop a model with an accurate description of transport phenomena, but with a simplified global chemistry model.
2. Develop a model with a detailed chemical-kinetics simulation, but neglecting effects from flow conditions.

Some work has already been done using the second approach to predict the thermal stability of hydrocarbons using the Structure-Property Relationship (SPR) method [8]. Here a more practical approach to study the degradation of jet fuel in a heated-flow environment will be proposed and tested using a detailed treatment of transport phenomena, but with a global chemical kinetic model. This mathematical model will be used for predicting bulk-fuel temperatures and fuel degradation in a simulated heated-flow environment for specific boundary conditions and parameters. The simulated heated-flow environment under consideration is a flow reactor in which the temperature of the fluid varies, not only in the axial direction, but also radially in the reactor tubing. Therefore, it is possible for the jet fuel to experience higher wall temperatures (e.g., 600 °C) with the bulk of the fuel remaining at a significantly lower temperature (e.g., 460 °C). Understanding these issues could be critical to the use of these jet fuels at much higher temperatures than has been typical in the past.

Because the development of this model will also require kinetic data for the reactions occurring in the flow reactor, use is made of existing kinetic data from batch reactors [9,10]. This numerical model coupled with the reaction kinetics of model jet-fuel compounds would be able to predict the fraction of fuel that is likely to decompose in the flow reactor system, i.e., bulk-fuel decomposition, provided that the batch kinetic data are applicable to conditions in the flowing system. The model would thus serve as a comprehensive simulation tool that can utilize kinetic data from batch reactor studies to predict the outcome in flow reactor systems. In order to develop and validate this mathematical model, however, it is necessary to have data from carefully instrumented experiments that have isolated the different mechanisms in the overall process. These models will be formulated from experimental data and will be simplified to make the numerical solution of the coupled equations practical. The numerical model will thus help in interpreting the observations in the flow-reactor experiments to determine the thermal stability of the fuel.

In the literature, there are at least two different approaches that are used to measure high-temperature thermal stability of aviation fuels or model jet-fuel compounds [11]. The first approach characterizes thermal stability in terms of the amount of the original fuel remaining after stressing the fuel in batch reactors [12,13]. The second approach is based on determining the amount of carbonaceous solid deposit formation after stressing the fuel at high temperatures [14,15].

The main focus in jet-fuel modeling has traditionally been in the area of thermal-oxidative deposition with maximum fuel temperatures of about 350 °F [16-19]. The deposits formed in such a temperature range are mainly autoxidative. Therefore, the deposition mechanisms

developed in earlier studies cannot be used to simulate jet-fuel decomposition under pyrolytic conditions. A few studies were conducted on the modeling of pyrolytic deposition from hydrocarbon fuels [20-22]. However, the models developed by these workers are for use in the petroleum industry and are applicable for low-pressure and high-temperature conditions. A typical fuel system in a military or jet aircraft is operated at high pressures (between 3.4 and 6.9 MPa) and relatively low temperatures ($< 600\text{ }^{\circ}\text{C}$) [23]. Using these models without any modification to predict the pyrolytic deposition of aviation fuels may not be suitable [24].

The thermal decomposition of aviation fuel is a complex process involving a wide variety of physical and chemical phenomena. Thermal decomposition and deposition can be divided into four areas: fuel chemistry, transport processes, surface adhesion, and deposit-removal mechanism [25]. The fundamental process responsible for the thermal degradation of the fuel is the convective heat transfer from the wall to the fluid. The increase in fuel temperature in layers adjacent to the wall results in a series of chemical reactions eventually producing insoluble species, which deposit onto the solid surfaces. Thus, determination of the near-wall temperature distribution and fuel flow rates are essential for predicting the rate of fuel decomposition. A rough estimate of cracking in tube tests could be obtained by dividing the tube into sections and estimating the cracking in each section using the average fuel temperature in that section.

One key piece of data that is not easily available is the bulk-fuel temperature profile through the heated section, since usually only the fuel-outlet bulk temperature is obtained [26]. A knowledge of bulk-fuel temperature is important because in addition to the wall-temperature profile, the deposition process is also influenced by reactions occurring in the bulk of the fuel. Another piece of information, which can indicate the thermal stability of aviation fuels, is the amount of unreacted fuel left after stressing at high temperatures in the flow reactor. To determine the amount of unreacted fuel numerically, it is necessary to know the temperature experienced by the fuel in the flow reactor. Experiments can easily provide a measure of the fuel inlet and outlet temperatures and the wall temperatures, but the actual temperatures experienced by the fuel will be different from the wall temperatures because of radial temperature gradients and flow conditions existing in the flow reactor. This study develops a comprehensive simulation tool to predict the temperature profile in the fuel and the fraction of unreacted fuel when the flow reactor is subjected to varying wall temperatures and compares the results obtained from the numerical model with the experimental results obtained from stressing dodecane.

6.3 Numerical

The computational model for the flow reactor reduces to a forced-convection heat-transfer problem with laminar flow inside a circular tube with varying wall temperature. The flow reactor is assumed to be axisymmetric. The flow is assumed to be hydrodynamically fully developed at the inlet of the flow reactor, but since the wall temperature varies along the length of the reactor, the thermal flow field does not reach the fully developed state. For laminar flow, the velocity profile is parabolic, with the fluid in the center of the tube spending the shortest amount of time in the reactor [27-29]. This parabolic velocity profile in a pipe of outer radius r_w is given by:

$$u = u_{\max} \left[1 - \left(\frac{r}{r_w} \right)^2 \right] \quad (1)$$

where, u_{\max} is the centerline velocity through the flow reactor. Thus, at a given location along the length of the tube, the velocity is a function of radius. This parabolic velocity profile results in a flow field inside the reactor in which both radial and axial gradients of temperature and concentration need to be considered.

The design of tubular flow reactors has generally been based upon a one-dimensional model. Some plug-flow one-dimensional models assume that concentration and temperature gradients occur only in the axial direction, and that the transport mechanism operating in this direction is the overall flow itself, considered to be of the plug-flow type [30]. In the present study, however, radial temperature gradients are inevitable, and the velocity profile is parabolic. Hence, the use of a one-dimensional plug-flow model here will lead to average values for the temperatures and conversions and will provide no information concerning excessive temperatures along the axis, which may be markedly different from the bulk temperatures. Therefore, the equations needed to model this flow reactor will be taken as the two-dimensional energy- and mass-balance equations. The applicable two-dimensional governing equations for such axisymmetric flow conditions in a tubular flow reactor are well established [31-34] and are described as follows. The coordinate system for this flow reactor is shown in Figure 9.

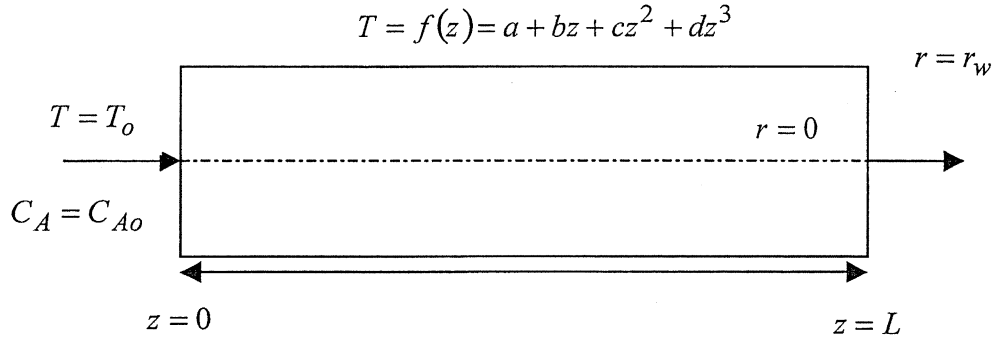


Figure 9. Coordinate System for the Flow-Reactor Model

The energy-balance equation with the initial and boundary conditions written in an axisymmetric z - r coordinate system is:

$$\rho C_p u_{\max} \left[1 - \left(\frac{r}{r_w} \right)^2 \right] \frac{\partial T}{\partial z} = K \left(\frac{\partial^2 T}{\partial r^2} + \frac{1}{r} \frac{\partial T}{\partial r} \right) + \Delta H(-r_a) \quad (2)$$

$$T(r, z=0) = T_0 \quad (3)$$

$$\frac{fT}{fr}(r=0, z) = 0 \quad (4)$$

$$T(r=r_w, z) = f(z) = a + bz + cz^2 + dz^3 \quad (5)$$

Equation (3) shows that the entering fuel temperature is constant and uniform at the inlet of the flow reactor. The first boundary condition, equation (4), is the result of the axisymmetric

flow conditions existing in the flow reactor. The second boundary condition, equation (5), is based on the measured experimental wall temperatures. In the mathematical model, the experimentally measured wall temperatures along the length of the reactor are fit with a third-order polynomial to determine the values of constants a , b , c , and d .

The mass-balance equation with the specified initial and boundary conditions in z - r cylindrical coordinates is:

$$u_{\max} \left[1 - \left(\frac{r}{r_w} \right)^2 \right] \frac{\partial C_A}{\partial z} = D \left(\frac{\partial^2 C_A}{\partial r^2} + \frac{1}{r} \frac{\partial C_A}{\partial r} \right) + (-r_a) \quad (6)$$

$$C_A(r, z = 0) = C_{A0} \quad (7)$$

$$\frac{fC_A}{fr}(r = 0, z) = 0 \quad (8)$$

$$\frac{fC_A}{fr}(r = r_w, z) = 0 \quad (9)$$

Equation (7) shows that the concentration of the fuel at the flow-reactor inlet is constant and uniform. Again, the axisymmetric conditions at the center of the flow reactor lead to the first boundary condition given by equation (8).

The rate of reaction, r_a , in the governing equations is the rate of decomposition of the fuel and is given by first-order kinetics [9].

$$r_a = kC_A \quad (10)$$

The rate constant in the above rate expression has a temperature dependence expressed in the Arrhenius form:

$$k = A_o \exp\left(\frac{-E_a}{RT}\right) \quad (11)$$

The Arrhenius parameters, E_a and A_o , for the rate constant in equation (11) are determined from the batch-reactor experiments for the fuels used [9,10]. The value for the heat of reaction over the observed temperature range was assumed constant and taken from Edwards *et al.* [35]. The value for the diffusion constant in equation (6) was also assumed to be constant and was calculated at the mean wall temperature from Krazinski *et al.* [36].

To obtain the above forms of the governing equations, the following additional assumptions were made:

1. The flow is independent of time, i.e., a steady-state solution is obtained.
2. The physical properties such as density, specific heat, thermal conductivity, and viscosity of the fuel are constant and are evaluated using the National Institute of Standards and Technology database 4 SUPERTRAPP.
3. The fuel flow is in the laminar regime with a Reynolds number less than about 2100.
4. There is no slip at the wall.
5. The flow is fully developed at the entrance of the reactor, and the velocity profile is parabolic.
6. The fluid is not well mixed in the radial direction, so radial heat conduction is considered.

7. The axial dispersion of mass and energy is negligible as compared with the axial-convection terms.
8. The inlet fuel temperature and concentration are uniform (do not vary in radial direction).
9. The tube material has a high thermal conductivity, so the temperature gradient across the tube wall is negligible.
10. The rate constant is a function of temperature given by the Arrhenius equation but is independent of the pressure variations.
11. The pre-exponential factor A_o and activation energy E_a are assumed to be constant over a temperature range of 20 to 600 °C.

The kinetic parameters used in the numerical model have been taken from batch-reactor studies for the model jet-fuel compounds and additives. The fuels chosen were dodecane ($C_{12}H_{26}$), tetradecane ($C_{14}H_{30}$), NORPAR-13, dodecane with 10 mol percent of tetrahydroquinoline (THQ), dodecane with 10 mol percent of benzyl alcohol (BzOH), and tetradecane with 10 mol percent of tetralin. NORPAR-13 is made up of 0.2 wt percent undecane, 14.4 percent dodecane, 52.9 percent tridecane, 32.0 percent tetradecane, and 0.5 percent pentadecane. Table 2 lists the kinetic parameters for some of these fuels taken from the available literature on degradation of these fuels in batch reactors.

Table 2. Kinetic Parameters for Model Jet Fuels and Additives

Fuel	E_a (J/mol)	A_o (sec ⁻¹)
Dodecane	242.4×10^3	5.40×10^{13}
Tetradecane	282.6×10^3	1.20×10^{17}
NORPAR-13	263.3×10^3	4.45×10^{15}
Dodecane/10-mol percent THQ	296.8×10^3	9.20×10^{16}
Dodecane /10-mol percent BzOH	280.1×10^3	2.40×10^{16}
Tetradecane/10-mol percent Tetralin	314.3×10^3	6.90×10^{18}

The kinetic parameters for dodecane, dodecane/THQ, and dodecane/BzOH were taken from Yoon *et al.*, [9] for tetradecane from Song *et al.*, [10] for NORPAR-13 from Yu *et al.*, [37] and for tetradecane/tetralin from experimental data. Since these constants were determined by fitting the rate constants as a function of temperature up to a temperature of 460 °C, the constants will be valid only up to 460 °C. In the absence of additional experimental data for higher temperatures, the constants E_a and A_o will be used for temperatures up to 600 °C. In other words, the kinetic data for these fuels will be extrapolated to the temperatures occurring in the flow reactors.

The two governing equations of energy- and mass-balance are both nonlinear, parabolic, partial differential equations. These equations are coupled by the presence of the reaction rate, r_a , which results in an inherently stiff system. The solution of this system of equations requires a simultaneous solution with the specified boundary conditions. The method used to solve this system of equations is the method of lines [38,39]. The method of lines (MOL) is an approach to the numerical solution of partial differential equations (PDEs). The partial derivatives with respect to one of the variables, r (radial coordinate), are discretized to result in an approximate system of ordinary differential equations (ODEs) in the other variable, z (axial coordinate). Such

a semi-discretization is often an intermediate step in the derivation of a fully discrete scheme, but in the MOL approach, the resulting set of coupled ODEs is integrated directly with a standard ODE integrator code. The ODE integrator used here is a commercially available code ODE15s, which is part of the Matlab programming package. It is a multistep solver and works very well for stiff problems [40].

The solutions of these equations give the values of the temperature and unreacted-fuel fraction at all mesh points inside the reactor. Once the temperature and unreacted-fuel fraction are known inside the reactor, the bulk values are calculated as a function of axial distance in the reactor using the mass-average temperature and mass-average concentration given by equations (12) and (13), respectively. The bulk temperature, T_b , is the mean temperature of the fluid at a given cross section of the tube. It is the temperature one would measure if the tube were chopped off at z and if the fluid issuing forth were collected in a container for a short period of time and thoroughly mixed without allowing it to exchange energy with the surroundings [28,41].

$$T_b(z) = \frac{\int_0^{2\pi} \int_0^R u_z(r) T(r, z) r dr d\theta}{\int_0^{2\pi} \int_0^R u_z(r) r dr d\theta} \quad (12)$$

$$C_A(z) = \frac{\int_0^{2\pi} \int_0^R u_z(r) C_A(r, z) r dr d\theta}{\int_0^{2\pi} \int_0^R u_z(r) r dr d\theta} \quad (13)$$

Equations (12) and (13) were solved numerically to calculate the bulk values of temperature and unreacted-fuel fraction using Simpson's one-third rule of integration. The discretization scheme used here in the radial direction is a finite-difference scheme with central differencing for both first- and second-order partial derivatives with respect to r (radial coordinate) in both the equations. Before discretizing, the two equations were converted into nondimensional forms to give better numerical accuracy. The simulations presented were obtained using 301 radial points from the centerline. This number was chosen by doing a grid-refinement study on the simulation results.

6.4 Experimental

For verifying the simulation results from the numerical model, experiments were conducted using the model compound, dodecane. The anhydrous dodecane fuel (purity, 99+ percent) used was obtained from Aldrich. The flow-reactor apparatus consists of a fuel tank and a single tube running through an actively heated zone in an electric furnace. The furnace is insulated, and the temperature inside is measured by K-type thermocouples. The fuel is pumped through the system using a high-pressure liquid-chromatography (HPLC) pump and a backpressure valve, which regulates the system pressure.

Outside tube-wall temperatures were measured by thermocouples, which were spot-welded to the outside of the tube at regular spacing for each run. Thermocouples were also inserted at the inlet and outlet of the tube section to measure the initial and final fuel temperatures, respectively, within ± 2 °C. The tube dimensions such as the length of the heated section of the tube and the inner and outer radii of the tube were recorded before the start of each run.

The experimental procedure involved both setting up the flow reactor and stressing the fuel through the flow reactor at five different flow rates 8, 10, 12, 16, and 20 mL/min. The dimensions of the flow-reactor tube including the inner and outer diameter and the length were recorded. Thermocouples were spot-welded to the outer surface of the tube at intervals of 0.0635 m (2.5 inches) along the length. The flow-reactor tube with the thermocouples was then placed inside the furnace. Before starting a run, the fuel tank was completely emptied of the previous fuel, rinsed, and refilled with new fuel. The flow reactor was sparged with N₂ to eliminate dissolved oxygen throughout the experimental matrix. The fuel flow rate was set using the HPLC pump, and the pressure was set to 4.8 MPa (700 psi) using the backpressure valve. Once the reactor had been brought up to the required pressure, the furnace was turned on. The furnace was allowed to reach a stable temperature of 700 °C and was maintained at that temperature for the entire experiment. As the run began, a Visual Basic program monitored and recorded the inlet and outlet fuel temperatures, outside wall temperatures, and the pressure inside the flow reactor.

The outlet bulk-fuel temperatures were recorded for each run for comparison with the results predicted from the numerical model. Three outlet fuel samples were taken for each run by closing the separatory funnel and allowing the liquid sample to build up for a fixed time period. The cracked products from each run were then analyzed using a gas chromatography-mass spectrometry technique to determine the amount of unreacted dodecane. An average value determined from three samples was calculated when reporting the unreacted dodecane for each run to reduce experimental error. The GC-MS instrument used to analyze the collected liquid sample was a Shimadzu GC-MS-QP5000 equipped with a compact, high-performance quadrupole mass spectrometer.

6.5 Results and Discussion

The numerical simulations were carried out for six different fuels to compare the outlet bulk-fuel temperatures and unreacted fuel fractions after stressing each fuel mixture in the flow reactor at a flow rate of 2 by 10⁻⁷ m³/sec (12mL/min). The fuels chosen for the simulation runs were dodecane, tetradecane, NORPAR-13, dodecane/10-mol percent BzOH, dodecane/10-mol percent tetrahydroquinoline, and tetradecane/10-mol percent tetralin. This set of fuels and fuel/additive mixtures was chosen because these systems have well established kinetics and are ideal model compounds representing jet fuels.

The physical properties of these fuel and fuel/additive mixtures were calculated at a mean wall temperature of 425 °C using the NIST database SUPERTRAP IV. The experimental parameters for each of these simulations, such as tube dimensions, flow rates, pressure, and wall temperatures, were chosen to be consistent with the flow reactor used by Atria *et al.* [42,43]. Table 3 lists the experimental parameters used for the numerical simulation of the selected fuels.

Table 3. Values of Experimental Parameters

Parameter Name	Parameter Value
Tube ID (m)	0.0047
Tube OD (m)	0.0064
Tube Length (m)	1.2
Pressure (MPa)	4.8 (700 psi)
Fuel Flow Rate (m ³ /sec)	2×10^{-7} (12 mL/min)
Inlet Fuel Temperature (°C)	20
Maximum Wall Temperature (°C)	600

The total reactor length was 1.2 m, but only 91.5 cm of the tube was in the actively heated zone. Simulation runs were carried out for these fuels using the experimental parameters and the batch-reactor kinetic data. Since the temperatures in the flow reactor reached 600 °C, the batch-reactor kinetic data were extrapolated to calculate the rate constants at temperatures above 460 °C. Each simulation run for a fuel provided two distinct results, temperature profiles and unreacted fuel-fraction profiles. The results from the numerical simulations for dodecane are shown in Figures 10 and 11.

Figure 10 shows the temperature profiles along the length of the flow reactor. The bulk mean temperature, the centerline temperature, and the experimentally obtained wall-temperature profiles are plotted on the same scale along the length of the reactor. The wall temperature decreases after 1 m because the reactor tube is no longer in the actively heated zone. All three temperature profiles start at the fuel entrance temperature of 20 °C, but as the fuel progresses along the heated length of the tube, the effect of the heat is felt most strongly at the wall and least at the center line. The most important piece of information obtained from this figure, however, is the bulk-temperature profile for the fuel. Since the wall temperature varies along the length of the flow reactor, the flow cannot become fully developed thermally. The mean bulk-temperature profile, therefore, is neither equal to the wall-temperature profile nor parallel to the wall-temperature profile as would occur with a constant wall temperature or a constant heat-flux boundary condition at the wall, respectively. Also, the fact that the temperature profiles are not the same at the center of the tube and at the wall shows that the model can account for radial temperature gradients. The inclusion of radial temperature differences makes the predicted bulk temperature more accurate compared with that predicted by a one-dimensional, plug-flow model.

Figure 11 shows the fuel fraction left unreacted along the length of the flow reactor. The reacted-fuel fraction inside the reactor is actually a complex mixture of species formed by the degradation of the original fuel and may vary from point to point inside the flow reactor. The three unreacted fuel-fraction profiles shown are again the bulk, wall, and centerline fractions. These results are obtained by considering the effect of changing temperature on the kinetics of the fuel decomposition and hence present a more detailed analysis for the unreacted fuel fraction compared with an earlier study done with a less rigorous analysis of kinetics [44]. The three concentration profiles show that the fuel remains unreacted in the upstream region for approximately half the reactor length (0.6 meter), although slight differences exist for each distinct fuel and fuel/additive mixture. This effect is observed because, in the upstream region of the flow reactor, the fuel temperatures are too low to cause any degradation of the fuel. In the

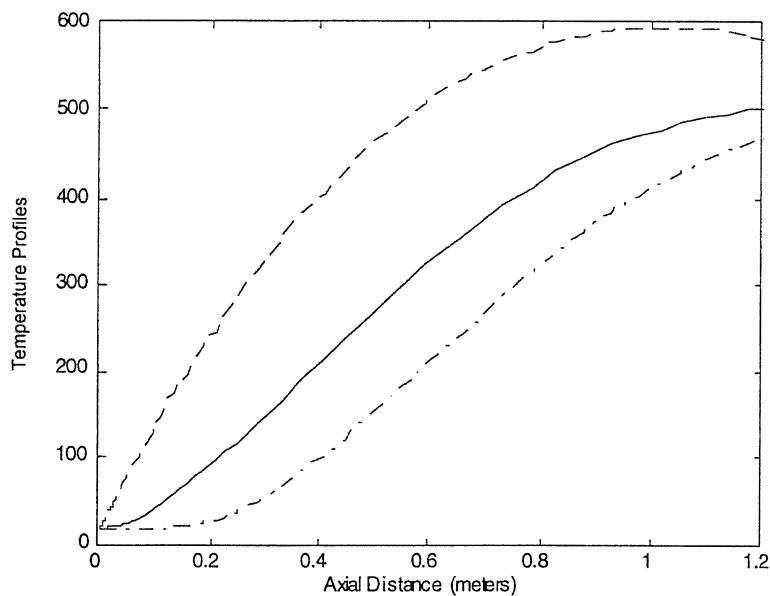


Figure 10. Temperature Profiles for Dodecane Stressing
(---wall temperature, -.-.-.- centerline temperature, — bulk temperature)

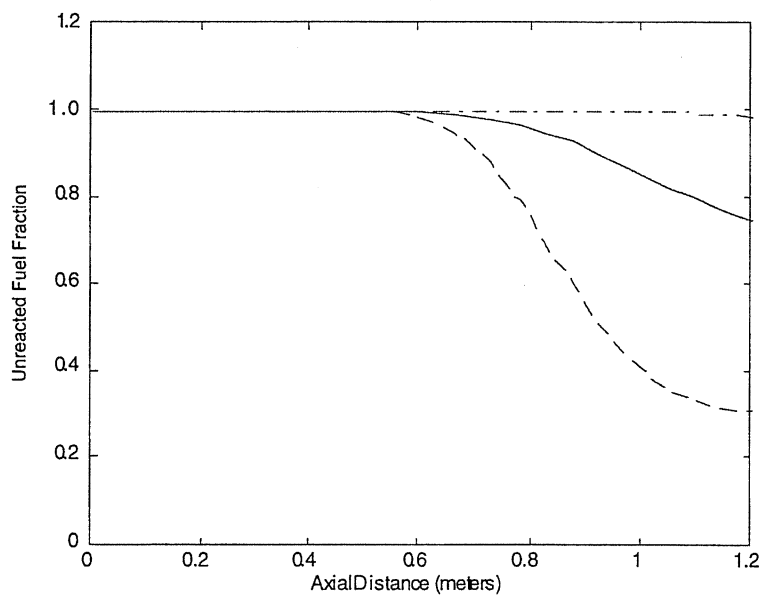


Figure 11. Unreacted Fuel Fraction Profiles for Dodecane Stressing
(-----wall fuel fraction, -.-.-.- centerline fuel fraction, — bulk fuel fraction)

downstream region (from an axial distance of 0.6 meter to the reactor outlet), however, the fuel starts degrading. This can be attributed to the fact that the fuel temperatures in the downstream region start rising (as shown in the temperature profiles), causing the pyrolytic kinetics to come into play. Also, the maximum fuel degradation occurs at the surface of the reactor because the wall is hotter. The unreacted fuel fraction in Figure 11 varies from 90 percent at the center of the reactor to a mere 30 percent at the reactor wall. Such steep concentration gradients in the radial direction are observed because the flow in the reactor is assumed to be in the laminar regime, and radial diffusion of the species occurs at molecular diffusion rates. The concentration gradients in the radial direction are also influenced by changes in the diffusion coefficient. A lower diffusion coefficient would result in steeper gradients. However, in practice, fluid mixing in the flow reactor may reduce these steep concentration gradients in the radial direction, and the large differences between the unreacted fuel fractions at the wall and at the center of the reactor would be lessened.

The unreacted fuel fraction at the wall shows a flattening trend toward the end of the flow reactor because the temperature decreases in that section of the reactor. The most important profile, however, is the unreacted bulk fuel-fraction profile because it represents the behavior of the bulk of fuel. Additionally, this information can also be used to compare the simulation results with the experimentally obtained unreacted bulk-fuel fraction at the reactor outlet.

The simulations for the other five fuels show similar trends. Table 4 shows the results for the outlet bulk temperature and outlet unreacted fuel fraction predicted from simulation runs for each of the fuels. A comparison between the outlet bulk temperatures and unreacted fuel fractions indicates that the dodecane mixture containing 10 mol percent (THQ) gives the best performance with 78.3 percent of the fuel remaining unreacted when experiencing an outlet bulk temperature of 512 °C. The results also show that the THQ additive in the dodecane/THQ mixture suppresses the degradation of pure dodecane.

Table 4. Predicted Outlet Bulk Temperatures and Unreacted Fuel Fraction

Fuel	Outlet Bulk Temperature (°C)	Unreacted Fuel Fraction
Dodecane	503	0.745
Tetradecane	484	0.610
NORPAR-13	488	0.634
Dodecane/10-mol percent THQ	512	0.783
Dodecane /10-mol percent BzOH	503	0.680
Tetradecane/10-mol percent Tetralin	492	0.646

The results from the numerical simulation also show that the tetradecane mixture containing 10-mol percent tetralin degrades less compared with the pure tetradecane. However, the dodecane mixture containing 10 mol percent BzOH shows more degradation when compared with pure dodecane. This behavior can be attributed to the kinetic parameters used for the dodecane/BzOH mixture. These rate constants were estimated by using the kinetic parameters developed by Yoon *et al.* [9]. An extrapolation of these rate constants to 600 °C is shown in Figure 12. It can be seen that the rate of degradation of the dodecane/BzOH mixture exceeds

that of pure dodecane at an abscissa value of 1.27. The temperature corresponding to this value is 514 °C. This means that if the extrapolation of the kinetic parameters is assumed to be accurate, the dodecane mixture with 10 mol percent BzOH should show a higher degradation than does pure dodecane, which is demonstrated by comparison with the numerical predictions. Similar effects were also observed by Minus *et al.* [45], when BzOH was found to increase the pyrolytic deposition of JP-8. The pyrolytic reactions appeared to start at a much lower temperature than for the baseline fuel indicating that BzOH may act as an initiator of pyrolytic reactions.

However, if the extrapolation of the dodecane/BzOH kinetics is invalid, a different approach to incorporate the kinetics of dodecane can be followed by dividing it into two different kinetic regimes. The first regime using the kinetic parameters from the dodecane/BzOH Arrhenius curve is followed until an abscissa value of 1.27 (514 °C), and the second regime using the kinetic parameters from the dodecane Arrhenius curve is followed after an abscissa value of 1.27. The simulation using the two different kinetic regimes for dodecane degradation in the dodecane/BzOH mixture gives a value of 504 °C for the outlet bulk temperature and a value of 0.737 for the unreacted fuel fraction. This value for the unreacted fuel fraction is higher than the one predicted by the simulation run with a single kinetic regime but is still less than the fraction predicted for neat dodecane.

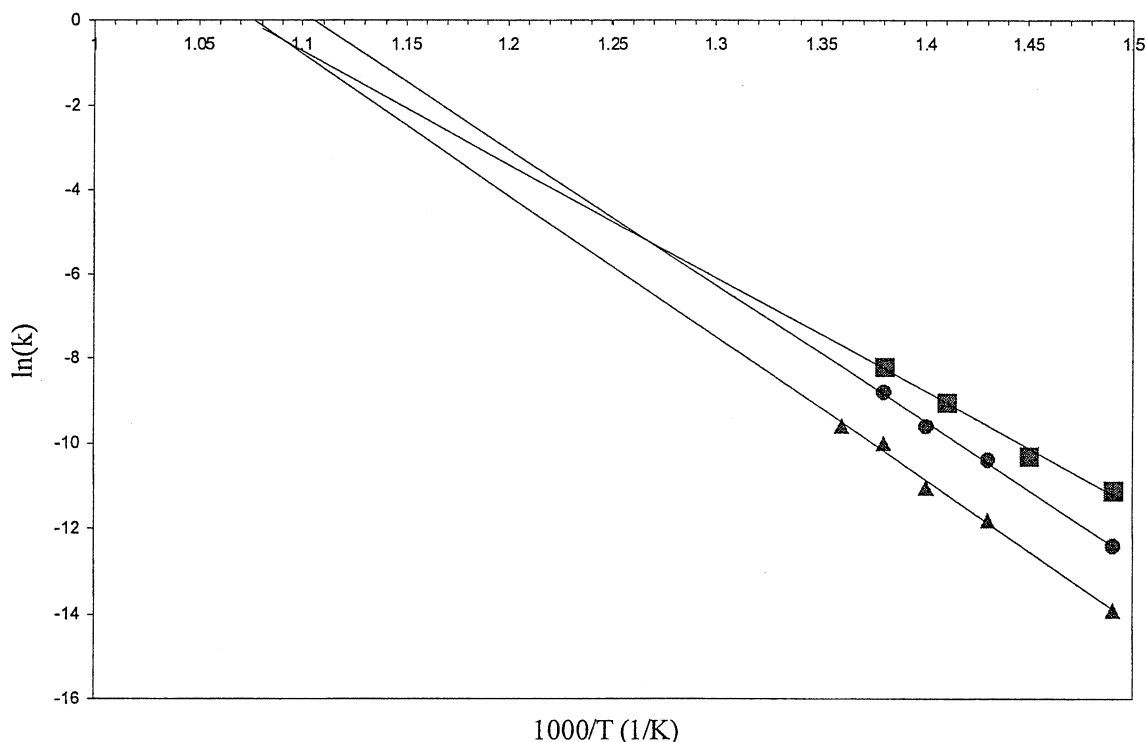


Figure 12. Arrhenius Plots of $\ln(k)$ vs. T^{-1} for Pure Dodecane and the Dodecane Mixtures Containing 10-mol Percent BzOH and THQ
(■ dodecane, ● dodecane/BzOH, ▲ dodecane/THQ)

This analysis shows that the results predicted from the numerical model are highly sensitive to the kinetic parameters. The chemical rate constants from the batch-reactor experiments are semiquantitative formulas extracted from experiments and fundamental calculations. Any uncertainty in the estimation of these kinetic parameters can have a large effect on the numerical predictions for the unreacted fuel fractions.

Also, since the results shown in Table 4 are based upon the extrapolation of the batch-reactor kinetics to a much higher temperature of 600 °C, additional errors in the predictions from the numerical model may occur. To minimize these errors, a similar set of simulations was done for the same fuels in the temperature range over which the kinetic parameters should be valid. The wall temperature profile was chosen to give an outlet bulk temperature of less than 460 °C. Since the fuel experiences a lower bulk temperature in the flow reactor, it shows very little degradation. To observe appreciable degradation differences among various fuels, the flow rate chosen for this set of simulations was reduced to $1.67 \times 10^{-7} \text{ m}^3/\text{sec}$ (10 mL/min), leading to a longer residence time for the fuel in the flow reactor. Table 5 shows the results for the outlet bulk temperature and outlet unreacted fuel fraction predicted from simulation runs for each of the fuels.

Table 5. Calculated Outlet Bulk Temperatures and Unreacted Fuel Fraction

Fuel	Outlet Bulk Temperature(°C)	Unreacted Fuel Fraction
Dodecane	455	0.988
Tetradecane	445	0.966
NORPAR-13	448	0.970
Dodecane/10-mol percent THQ	457	0.996
Dodecane/10-mol percent BzOH	456	0.987
Tetradecane/10-mol percent Tetralin	448	0.986

A comparison among the outlet bulk temperatures and unreacted fuel fractions for the above fuels indicates that none of the fuels shows a significant amount of degradation at an outlet bulk temperature below 460 °C. These effects are observed because in a flow reactor with a maximum outlet bulk temperature of 460 °C, only a very small portion of the fuel is exposed to temperatures (≥ 400 °C) where pyrolytic reactions are dominant. However, in a batch reactor the fuel experiences greater degradation because all of it is exposed to a constant temperature exceeding 400 °C during a longer residence time. The general trend shown in Table 5 appears to be the same as that shown in Table 4 with the fuel and additive mixtures undergoing less degradation when compared with the pure fuel.

The pyrolysis model is validated using experimental data taken from the flow reactor after stressing dodecane at five different flow rates. The experimental data serves a dual purpose. First, it enables comparison with the numerical results, thereby evaluating the validity of the numerical model. Second, it helps in estimating the effects of both experimental and physical parameters on the predicted bulk temperatures and unreacted-fuel fractions. The parameters chosen for the parametric sensitivity analysis are fuel flow rate and fuel density.

The flow-reactor tube used for stressing dodecane is made of stainless steel with a 0.00635- m (0.25-inch) outside diameter and 0.003175-m (0.125-inch) inside diameter and an effective heated section of 0.889 m (35 inches). The simulation runs were done for two different sets of densities. For the first set of simulation runs, the density of the dodecane was estimated at the outlet bulk temperatures measured during the experimental runs. For the second set of simulation runs, the density of dodecane was taken at a temperature of 500 °C instead of the outlet bulk temperatures predicted by the experimental runs. A temperature of 500 °C was chosen because the experimentally measured wall temperatures for different flow rates reach 600 °C. Since the majority of fuel degradation takes place between 400 and 600 °C, a mean temperature of 500 °C serves as a more relevant estimate for density estimation of the fuel than do the outlet bulk temperatures.

For each flow rate, the fuel spends a different residence time inside the flow reactor. Table 6 shows the mean residence times for five different flow rates at which the fuel was stressed. The mean residence time of the fuel in the flow reactor increases with decreasing flow rate.

The outlet bulk temperatures measured experimentally and calculated by the numerical model for two different sets of densities at five different flow rates are shown in Table 7. Table 8 shows the unreacted-dodecane fraction measured experimentally and calculated by the numerical model for the same sets of densities and flow rates.

Table 6. Mean Residence Time for Dodecane Stressing at Different Flow Rates

Flow Rate (m ³ /sec)	Mean Residence Time (sec)
3 x 10 ⁻⁷ (20 mL/min)	24.1
2.67 x 10 ⁻⁷ (16mL/min)	30.2
2 x 10 ⁻⁷ (12 mL/min)	40.2
1.67 x 10 ⁻⁷ (10 mL/min)	48.3
1.33 x 10 ⁻⁷ (8 mL/min)	60.3

Table 7. Comparison of Experimental and Calculated Outlet Bulk Temperatures

Flow Rate (mL/min)	Experimental (°C)	Calculated* (°C)	Calculated** (°C)	Deviation* (percent)	Deviation** (percent)
20	430	343	397	20.26	7.70
16	468	420	446	10.20	4.71
12	492	504	509	2.56	3.47
10	498	533	534	7.05	7.18
8	513	550	547	7.19	6.73

* Simulation results for densities estimated at experimentally measured outlet bulk temperatures.

** Simulation results for densities estimated at a temperature of 500 °C.

Table 8. Comparison of Experimental and Calculated Outlet Unreacted Fuel Fraction

Flow Rate (mL/min)	Experimental	Calculated*	Calculated**	Deviation * (percent)	Deviation** (percent)
20	0.995	0.999	0.999	0.442	0.412
16	0.987	0.994	0.993	0.689	0.557
12	0.931	0.925	0.921	0.687	1.031
10	0.833	0.808	0.806	3.061	3.277
8	0.752	0.612	0.627	18.617	16.635

* Simulation results for densities estimated at experimentally measured outlet bulk temperatures.

** Simulation results for densities estimated at a temperature of 500 °C.

The percentage deviation for both the bulk temperature and the unreacted fuel fraction is calculated as in equations (14) and (15)

$$\% \text{ Deviation}^* = \frac{|\text{calculated}^* - \text{experimental}|}{\text{experimental}} \times 100 \quad (14)$$

$$\% \text{ Deviation}^{**} = \frac{|\text{calculated}^{**} - \text{experimental}|}{\text{experimental}} \times 100 \quad (15)$$

Figure 13 shows the outlet bulk temperatures measured experimentally after stressing dodecane at five different flow rates. The experimentally measured outlet temperatures are accurate to within ± 2 °C. It also shows the calculated bulk temperatures from the simulation runs at two different sets of densities. The calculated bulk temperatures show a deviation in the range of 2-20 percent from the experimentally measured values when the dodecane density was estimated at the experimentally measured outlet bulk temperatures. However, the calculated bulk temperature values show a deviation in the range of 3-7 percent when the dodecane density was estimated at 500 °C. This shows that the calculated values are in reasonable agreement with the experimentally measured values, but show variation with changing density. The simulation results calculated with the dodecane density estimated at 500 °C are closer to the experimentally measured outlet bulk temperatures. This shows that the simulation results are sensitive to the density parameter. Figure 13 also shows that the calculated outlet bulk temperature increases with decreasing density and vice versa. For example, at a fuel flow rate of 20 mL/min, the calculated outlet bulk temperature was found to be 397 °C when the density was estimated at 500 °C, but was found to be 343 °C when the density was estimated at the experimentally measured outlet temperature of 430 °C.

Figure 14 shows plots of experimentally measured outlet unreacted fuel fractions and the calculated numerical results for two different sets of densities at varying flow rates. The experimentally measured unreacted dodecane was estimated by averaging the results from three samples of the unreacted dodecane at each flow rate to reduce experimental error. However, the calculated results for the unreacted dodecane fraction may be accurate only up to ± 10 percent [39] because of extreme sensitivity to the kinetic parameters of dodecane degradation. The

calculated results for two different sets of densities show a deviation in the range of 1-18 percent from the experimentally measured values. However, the variation in the calculated unreacted fuel fraction shows very little change with density as compared with that observed for the outlet bulk temperatures. It appears that the density parameter has a much greater impact on the temperature profiles compared with the unreacted fuel-fraction profiles.

Both the experimental and numerical results also show that as the fuel flow rate increases, the outlet bulk temperature decreases and the unreacted fuel fraction increases. These trends can be justified on the basis of the residence time of the fuel in the flow reactor and the temperature experienced by the fuel during that period. At a lower flow rate the fuel spends more time in the flow reactor, hence absorbing more heat and, in the process, suffering more degradation.

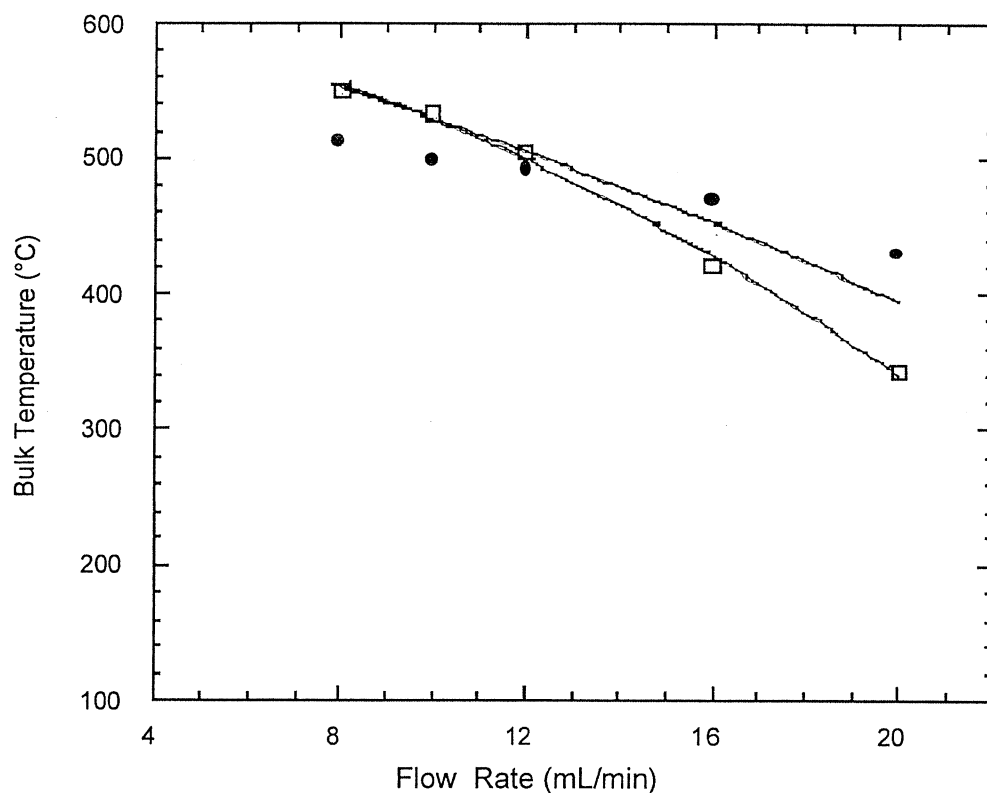


Figure 13. Experimental and Calculated Bulk Temperature Profiles.
(● experimental, □ calculated)

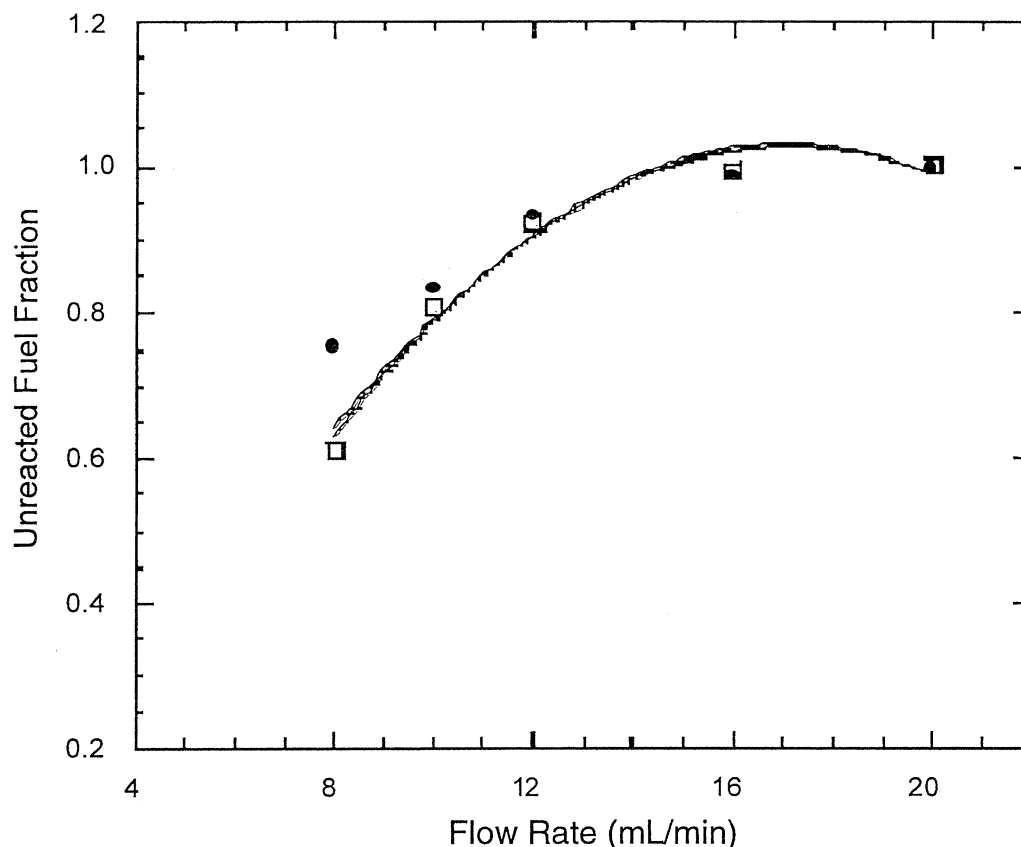


Figure 14. Experimental and Calculated Unreacted Fuel-Fraction Profiles (● experimental, □ calculated)

Since jet fuel will be used as the primary coolant for removing excess heat generated onboard military and commercial aircraft, the numerical model was also used to study the endothermic performance of the fuel. NORPAR-13 was chosen to demonstrate the endothermic effect of aviation fuels and so the results from the present study could be compared with prior work by Sheu *et al.* [24], on the same fuel. Figure 15 shows the endothermic effects on the predicted bulk temperature profiles using the numerical model with and without considering pyrolytic reactions. The results are consistent with the trends observed by Sheu *et al.* [24]. In the upstream region, for approximately half the flow-reactor length (0.6 meters), the temperature profiles predicted by both the pyrolytic and nonpyrolytic models are equal. This occurs because in the upstream region the fuel temperatures are too low for NORPAR-13 pyrolysis to have an endothermic effect. However, in the downstream region (from an axial distance of 0.6 meter to reactor outlet) of the flow reactor, the pyrolytic endothermic effect is more pronounced because the higher temperatures enhance the endothermic effect that leads to higher predicted temperatures for the nonpyrolysis model compared with the pyrolysis model.

The variation of the local Nusselt number along the reactor length has also been evaluated using the numerical model and the results are plotted in Figure 16. For a constant wall temperature, the Nusselt number approaches a value of 3.658 for a fully developed flow, whereas for a uniform heat flux at the wall, the Nusselt number approaches a value of 4.364 [46]. However, in the present study, the wall temperature changes along the reactor length so the local

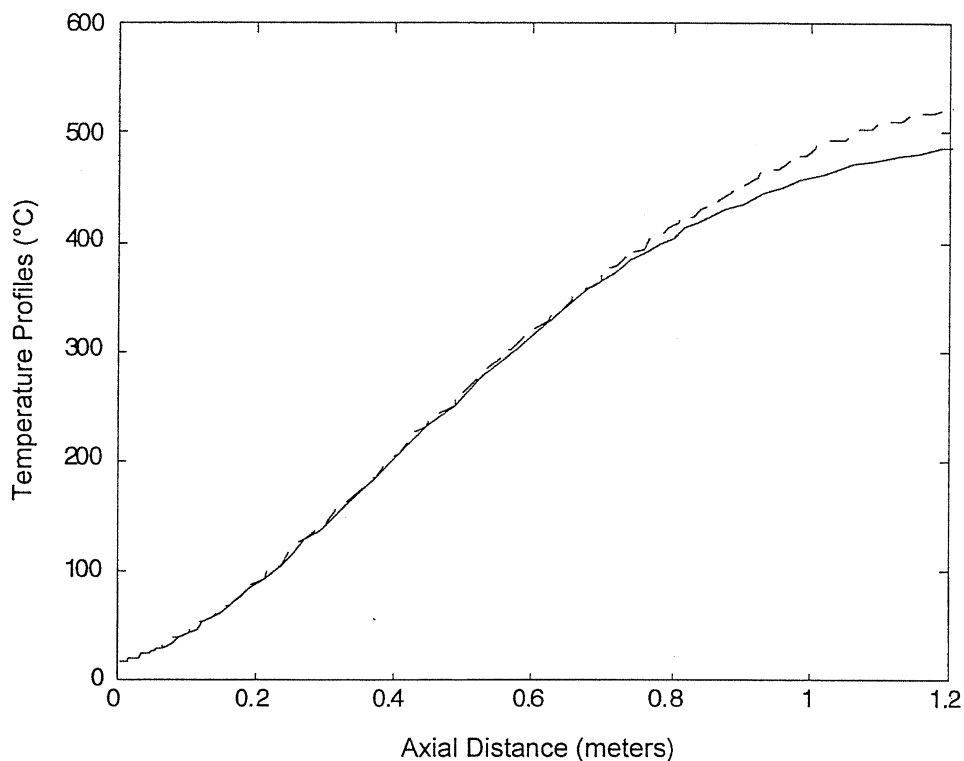


Figure 15. Temperature Profiles Predicted by Nonpyrolysis and Pyrolysis Model for NORPAR-13 Stressing
(----- nonpyrolysis model, ——— pyrolysis model)

Nusselt-number profile does not approach these values. The Nusselt number shows a decreasing trend in the upstream region reaching a value of 4.38, but increases initially in the downstream region before flattening out near the end. This shows that in the upstream region, the flow-reactor behavior resembles that of constant heat flux at the wall, but in the downstream region, the pyrolytic endothermic effect takes over resulting in a higher Nusselt number. The Nusselt-number profile flattens out toward the end of the flow reactor because the temperature at the wall decreases in that section of the flow reactor.

6.6 Conclusions

The present study demonstrates the use of numerical modeling in studying jet-fuel degradation in a heated-flow environment. A one-step global model is proposed to describe the pyrolysis of jet fuels under high-pressure conditions. The proposed model is validated using the experimental data obtained stressing the model jet fuel, dodecane, at different flow rates. For the conditions examined, the model's predictions agree well with the experimentally measured results. This numerical model can also be used as a tool to bridge the gap between batch- and flow-reactor studies of jet-fuel degradation. The model also serves as a comprehensive simulation tool to examine the effects of various physical and experimental parameters on jet-fuel degradation. The numerical simulations can be used in place of experiments and as a means of complementing and analyzing experimental results. The results predicted from the numerical simulation also provide an effective means of evaluating the performance of various additives, thereby determining the best fuel/additive mixture. Both the experiments and simulations yield

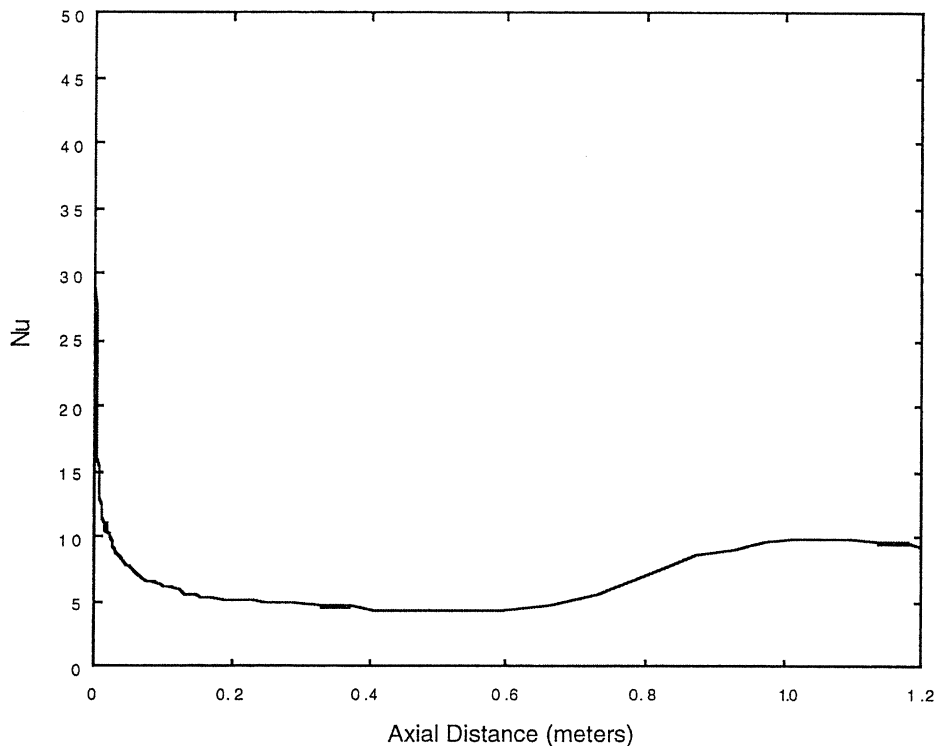


Figure 16. Variation of Local Nusselt Number along the Flow Reactor for Dodecane Stressing

similar results for the effect of increasing fuel flow rate on the outlet bulk temperature and unreacted fuel fraction. The outlet bulk temperatures and degree of fuel degradation are found to decrease with increasing fuel flow rates. The numerical model also predicted the endothermic nature of jet-fuel pyrolysis by means of a simulation on NORPAR-13.

The most important feature of the numerical model is that it is generic and can be used in a number of applications including the prediction of jet-fuel degradation in a flow reactor, irrespective of its size, fuel flow rate, and wall temperature. The present study demonstrates the use of this feature by simulations on two different sets of flow reactors. Finally, the model can also be used for predicting jet-fuel degradation onboard an actual aircraft if the conditions therein satisfy the design basis and assumptions used in the development of the numerical model.

7.0 DEGRADATION OF INDIVIDUAL COMPONENTS IN FUEL

7.1 Introduction

In an aircraft, fuel is used as a coolant for the engine lubricant, hydraulic controls, and environmental systems before being injected into the propulsion system. In the future, these systems will be required to operate at much higher temperatures. Jet fuels will have to be formulated to be operational at temperatures of 400 to 500 °C for periods of several hours. [47, 48] It has been shown that pyrolysis degradation is predominant in fuels at high temperature [49] and that reactive free-radical reaction mechanisms may eventually lead to the formation of gums or insoluble solids. [50, 51] These undissolved products may plug filters and generally reduce the performance of fuel heat exchangers. The accumulation of insoluble products on surfaces may result in the fouling of fuel lines, valves, and nozzles, which can lead to potential catastrophic failures [48].

To increase the thermal stability and to improve fuel characteristics, small quantities of additives may be required [52]. Several studies have shown the influence of different additives on jet fuels [53]. Mixtures of the following four classes of additives appeared to yield significant improvement in fuel thermal stability [54]: antioxidants, detergents, dispersants, and metal deactivators.

To develop a fundamental understanding of the processes involved, fuel degradations in tubing bombs were performed by studying model compounds. It is hypothesized that high-quality thermal stabilizers can be found among the more conventional hydrogen donors [55-57], and some authors have also tested the importance of some specific factors in the thermal stabilization of jet fuel [58].

Several reaction mechanisms have been proposed [59, 60], and it appears that hydrogen donors can act as radical scavengers by donating hydrogen to the radical from reactive compounds [61]. In addition, work on solid deposits formed during pyrolytic degradation has shown that these products can be attributed to the formation of polyaromatic hydrocarbons and condensation reactions [62].

From these results, new points of interest drew attention, and further studies were conducted to answer the question whether some specific hydrogen donors could be considered as high-temperature thermal stabilizers of jet fuels. However, the degradation rate of fuel components seemed to be strongly related to temperature when above 400 °C. Yoon *et al.* [63] concluded that temperature (when above 500 °C) is a limiting factor for the stabilization of jet fuels with hydrogen donors.

Other studies were not only focused on the effects of thermal stabilizers but on a model solvent (an n-alkane mixture). Some kinetic data were obtained for liquid and gas phases [64]. The amount of solid deposit has also been measured [65].

An important fact is that most of these quantitative data were obtained by either spectroscopic analyses (FTIR) [56] or gas chromatography [63-65]. The magnitude of error

inherent to these measurements may increase if the sample is a fuel mixture. In particular, jet fuel is a complex mix of hydrocarbons, and detailed molecular-level transformations are easily masked by product redistributions from almost an infinite number of compounds present.

To overcome this problem, the present study employed a different quantitative analytical method that we feel is better adapted to determine the conversion rate of fuel components when thermally stressed. Use of a labeled compound, specifically ^{13}C , has been shown to be an excellent technique for following target compounds in complex systems [66-72] as was demonstrated in the final report for Delivery Order No. 2 of this Jet Fuels Program [73]. Gas Chromatography / Selected Ion Monitoring / Mass Spectrometry (GC-SIM-MS) combined with the monitoring of a ^{13}C -labeled standard spiked at a known concentration into a jet fuel was developed as a method for determining the product loss of a compound of interest. In the current study, the reproducibility and accuracy of this method was tested by comparison with the gas chromatography / flame ionization detection technique (GC-FID) used in the large number of previous studies associated with this program. This quantitative method will provide the data accuracy required for the determination of kinetic parameters for a target compound, namely hexylbenzene, in the presence of the complex fuel mix. A second major objective of this study was to evaluate differences between static-reactor and flow-reactor conditions on the rate of model-compound degradation in the presence of the jet fuel.

The original scope of this work included a study of a second labeled compound, 1,5- ^{13}C -methylcyclohexane and examination of the degradation under oxygenated conditions. Unfortunately, problems arose, particularly with regard to the flowing-reactor section of the work and on synthesis of the methylcyclohexane. Under the original experimental plan, the flowing-reactor studies would be performed on an existing reactor already operational at Penn State. Delays in learning of its lack of availability caused by delays in construction and testing at Penn State and the need to construct a similar flowing-reactor system at Ohio State University severely limited the time available for experimentation on the reactor within the time frame of this project. The result of this delay was a reduction of the experimental work to a comparison of the degradation of neat ^{13}C -hexylbenzene and spiked JP-8 fuel under static conditions, as well as the spiked JP-8 in more realistic flowing conditions. The ^{13}C -labeled methylcyclohexane could not be synthesized in reasonable amounts needed without expenditures far beyond those anticipated, especially if we were to utilize it for the flowing-reactor pyrolysis.

7.2 Experimental Section

7.2.1 Sample Selection

The chemical reagents used in this study, including those required for the synthesis of ^{13}C -1-hexylbenzene, were purchased from Aldrich and ^{13}C -labeled material ($\text{Ba}^{13}\text{CO}_3$) was obtained from Isotech Inc. (99 atom percent, Cambridge Isotope Laboratories). To understand the thermal stability of fuel used in an aircraft at a fundamental level, we selected JP-8 jet fuel as the most appropriate sample to be studied. This fuel contains some conventional anti-oxidants and other

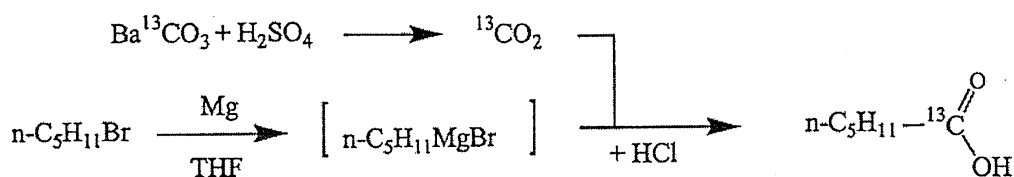
military-specified additives. [50, 74-76] 1-¹³C-hexylbenzene (abbreviated as Hb in this study) was then mixed with JP-8 at a known concentration, quantified by GC-FID.

7.2.2 Synthesis of the Labeled 1-¹³C-hexylbenzene

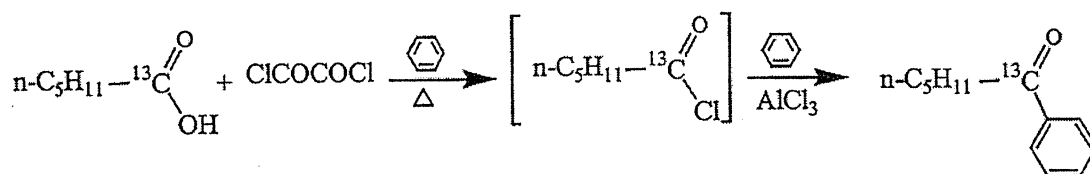
Because labeled compounds are either not commercially available or prohibitively expensive, they were synthesized in-house for the study. The synthesis of the 1-¹³C-hexylbenzene was developed in collaboration with Jack Richman at the University of Minnesota. This was accomplished using a three-step synthetic pathway (Figure 17). A description of the synthesis procedure, modified from Eberle and Kahle [77] and Szmant and Roman [78], is given below.

Based on the predicted experimental scheme for thermal-decomposition studies for both the static and flowing reactors, the quantity of this needed labeled compound was estimated to be 20 g.

STEP 1



STEP 2



STEP 3

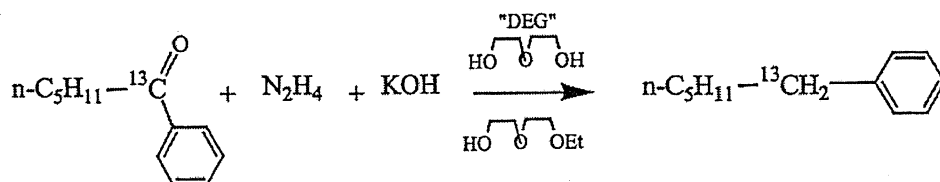


Figure 17. Schematic Presentation of the Procedure Used for the Synthesis of the Labeled Compound 1-¹³C-hexylbenzene

Step 1

A 1-liter, 3-neck flask with mechanical stirrer, condenser, and an addition funnel with nitrogen lines was oven-dried, assembled, and purged with nitrogen. Initial charges of the Grignard preparation were 10.15 g (0.422 mol) of Mg, 63.5 g (0.42 mol) of 1-bromopentane, and 500 mL of THF (divided into 50 mL portions). The reaction mixture was refluxed 2 hours with a slow N₂ flush and then cooled.

The mixture was then exposed to ¹³CO₂, produced from the reaction of 250 mL of hot H₂SO₄ (50 to 70 °C) with 41.83 g (0.21 mol) of Ba¹³CO₃. The mixture was then quenched with 225 mL of concentrated hydrochloric acid and allowed to stand overnight. After filtration through a glass plug to remove Mg particles, 100 mL of hexane were added. The resulting solution was washed six times with H₂O. After being dried with Na₂SO₄ in a cotton swab-plugged funnel, the mixture was vacuum stripped at 70 °C/0.1 mm, leaving behind 22.5 g of crude 1-¹³C-hexanoic acid.

Step 2

The crude hexanoic acid was washed with 50 mL of warm, dry benzene for dissolution in a stirred 500-mL flask. Approximately 25.5 g of oxalyl chloride and 70 mL of benzene were added to the solution. The reaction mixture was refluxed for 1 hour (bp 75 to 76 °C) and then slowly distilled at a bp of 80 °C to collect a total of 80-90 mL of distillate. The distillate was cooled to 0 °C and 34.7 g of AlCl₃ were added. The reaction mixture was stirred and warmed to room temperature under nitrogen. The crude reaction mixture was worked up by pouring onto 500 g of ice and stirring. Then, 100 mL of concentrated hydrochloric acid was added, and the solution was extracted with CH₂Cl₂ until colorless. The organic solution was then washed with H₂O. The water phase was drained, and the organic layer was dried through Na₂SO₄. Vacuum pumping to 60 °C/0.05 mm Hg left 28.82 g of crude product. The nuclear magnetic resonance shows an 85-wt percent yield of ¹³C-hexanophenone, the impurities being C₂₂H₄₆ and diketone.

Step 3

A charge of 28.8 g of the crude ketone mixture, 31.5 g of (KOH) (85 percent), 2.1 mL of H₂O, 230 mL of diethylene glycol (DEG), 23 mL of DEG monoethyl ether, and 21 mL of hydrazine (98 percent) was added to a 500-mL flask and heated at a fast rate (10 °C/min) to 100 °C. The heating was then slowed down and the temperature increased to 140 °C, and held constant for 1 hour. The mixture was then heated to 240 °C and held at this temperature for 39 hours by distillation of DEG. The reaction mixture was cooled down and washed four times with hexane. The resulting hexane phase was washed twice with H₂O+HCl (ca 0.1 M), once with H₂O, and once with H₂O+KOH (ca 0.1M). The hexane phase was stripped at 60 °C/0.05 mm Hg to provide 19.6 g of ¹³C-hexylbenzene; however, the purity was only 98 wt percent. Further purification was achieved on a silica-gel column eluted with hexane. The purity of the product,

determined by ^1H and ^{13}C -liquid nuclear magnetic resonance and gas chromatography analyses was estimated to be above 99 wt percent.

7.2.3 Instrumentation

7.2.3.1 Gas Chromatography

An important part of the work was to quantify individual compounds in the fuel. To this end, we utilized a GC-FID equipped with an on-column injector. A convenient software package with the quantification capabilities required for the study was also employed.

With deposition directly on the column, mass discrimination in the injector is not a problem, and satisfactory quantitative data can be obtained. We would be able to determine the GC-amenable compounds of the injected fraction in order to determine the percentage of the high-molecular-weight compounds included in the fraction. By use of an internal standard, we would also be able to quantify the chemical composition changes that occurred during the thermal stress of the fuel sample.

The GC-FID analyses were conducted on an HP6890 with an HP6890 series injector auto sampler. The diluted sample was introduced via an on-column injector in 1- μL injections. The column used for the GC was a 15-m, 0.2-mm ID, 0.2- μm film thickness (95 percent dimethyl - 5 percent diphenyl siloxane), fused-silica capillary column (J&W Scientific, Inc., DB-5). The temperature program used for the analyses ranged from 40 $^{\circ}\text{C}$ (held 2 minutes) to 330 $^{\circ}\text{C}$ (held 5 minutes), heated at 6 $^{\circ}\text{C}/\text{min}$. The data acquisition used for peak area measurements was carried out with EZChrom Elite software (version 2.31).

To obtain quantitative data, the error or instrumentation variations had to be minimized by using an internal standard, added to each sample before injection. Squalane was selected to quantify the degradation of either neat hexylbenzene or ^{13}C labeled hexylbenzene spiked into the JP-8 jet fuel sample.

Each quantification by GC-FID required a calibration curve determined as follows: labeled hexylbenzene and squalane were mixed in pentane at four different concentration levels of hexylbenzene (25, 50, 80, and 150 ng/L), whereas the squalane concentration remained constant in each of the four standards (80 ng/L). Injecting each standard solution three times tested the reproducibility of the method.

A calibration curve was drawn, and the following linear-fit parameters were determined:

$$\text{AREA}_{\text{Hexylbenzene}} / \text{AREA}_{\text{Squalane}} = 1.0090 \text{ wt-Hexylbenzene} / \text{wt-Squalane}$$

The correlation coefficient was $R^2 = 0.9999$.

7.2.3.2 Gas Chromatograph Coupled to a Mass Spectrometer

Because the GC-FID quantified the hydrocarbons without differentiation of the isotopically enriched and natural-abundance compounds, a complementary method had to be utilized. The

GC-SIM-MS was used to follow the chemical changes in the fuel involving the ^{13}C -enriched compounds. The GC-SIM-MS analyses were performed on a Kratos MS-25 RFA, a high-resolution gas chromatograph/double-focusing sector mass-spectrometer system. One liter of the diluted sample was injected on-column (30 m, 0.25-mm i.d., 0.25- μm film thickness; 95 percent dimethyl-5 percent diphenyl siloxane); fused-silica capillary column (J&W Scientific, Inc., DB-5). The temperature program of the oven was the same as that of the GC-FID described above.

The GC-SIM-MS quantification was based on monitoring a selective ion for each compound, which we quantified by measuring its corresponding intensity. However, some problems occurred using perfluorokerosene (PFK) lock masses and automatic magnet switching during the (SIM) run. The mass stability could not be maintained by the software, and the reproducibility of the runs was not acceptable. Therefore, we decided to disable all automatic mass positioning based on software and calibrate at the beginning of each run by using the PFK standard, relying on the mass stability established at that time. The reproducibility was increased and the standard deviation did not exceed 5 percent.

The same standard solution (mixture of squalane and hexylbenzene) used to calibrate the GC-FID was also utilized here. Each of these samples was analyzed by monitoring the m/z 163.144 ion ($\text{M}^+ + 1$ ion of the neat unlabeled hexylbenzene) and the m/z 183.211 fragment ion of the squalane. We made the assumption that the calibration curve for labeled hexylbenzene, using its $\text{M}^+ + 1$ ion, m/z 164.146, would be the same as the one calculated from unlabeled hexylbenzene using the m/z 163.148 ion. The linear-fit parameters of the calibration curve were the following:

$$\text{AREA}_{\text{Hexylbenzene}} / \text{AREA}_{\text{Squalane}} = 0.506 \text{ Wt.}_{\text{Hexylbenzene}} / \text{Wt.}_{\text{Squalane}}$$

The correlation coefficient was $R^2 = 0.9974$.

7.2.4 Static Reactor

7.2.4.1 Pyrolysis in Tubing Bomb Reactor

To continue the study previously begun at Penn State, a new set of static reactors was designed and constructed on site. These were more appropriate and convenient for the thermal-degradation study taking place at Ohio State University. Figure 18 shows this reactor design as being similar to those described by Coleman *et al.* [56]. The main modification made was to design the stem for sample insertion such that it occupied a low dead volume and remained unheated.

A spike of a model compound should be added to the JP-8 at a concentration in the same range as for the other compounds present in the oil mixture. Therefore, we quantified one of the highest n-alkanes present in the JP-8 and spiked the labeled compound at a similar concentration. This quantification was conducted using a GC-FID. The content of one of the highest n-alkanes (dodecane in this case) of the JP-8 was determined by injecting a solution of JP-8, including the squalane internal standard at a concentration of 1.5 mg/mL, into the GC-FID. The percentage of

dodecane present in the JP-8 mixture was found to be 4.12 wt percent. Based on this result, the fuel was spiked at approximately 5 wt percent with the labeled hexylbenzene.

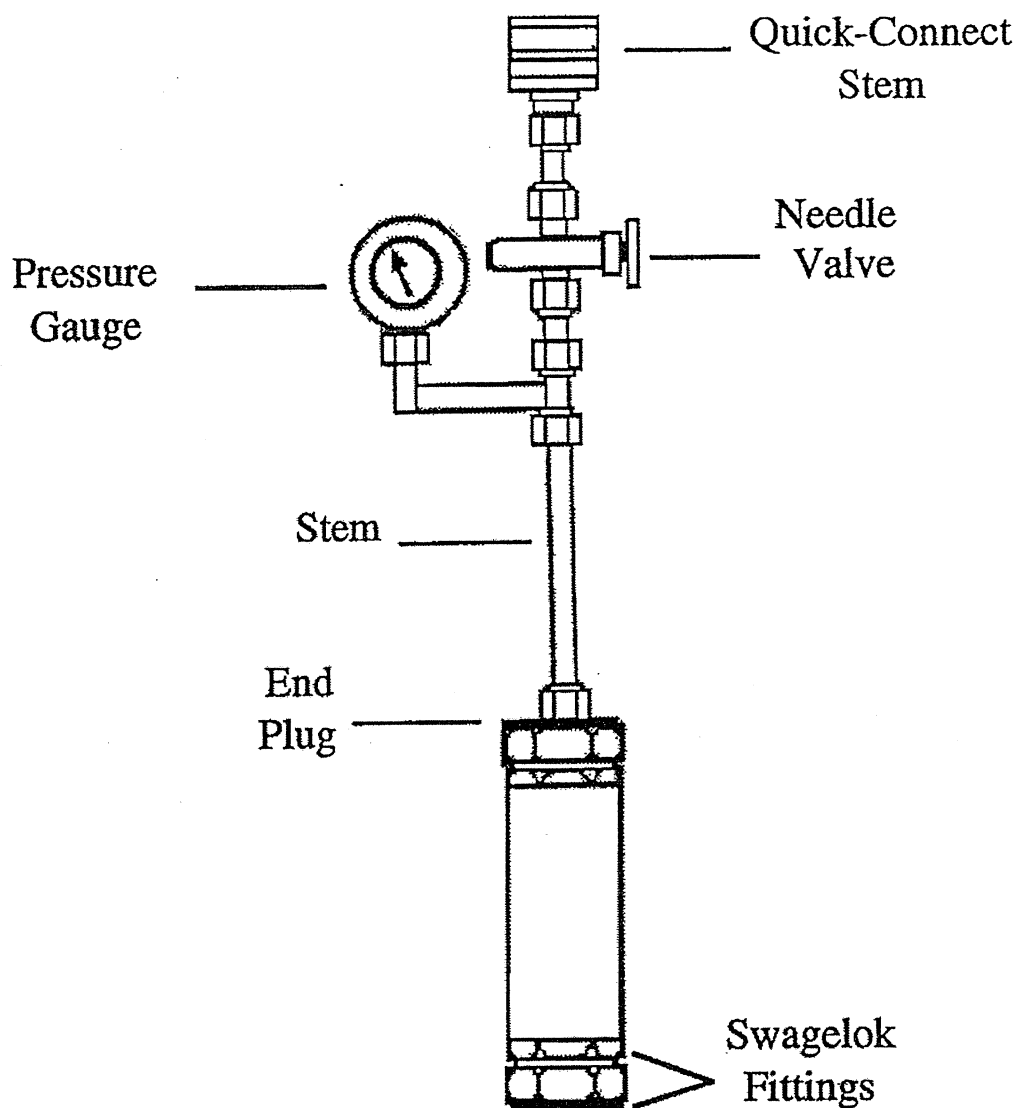


Figure 18. Schematic Presentation of the Stainless-Steel Autoclave Reactor for Jet-Fuel Stressing.

7.2.4.2 Spike of the JP-8 with I^{13} C-hexylbenzene

Because the GC-FID quantified the hydrocarbons without differentiation of the isotopically enriched compounds, the abundance of the hexylbenzene contained in the unstressed JP-8 had to be determined. It was found to be 1.53 wt percent. After the labeled hexylbenzene was added, the JP-8 was injected once again into a GC-FID instrument to determine precisely the new concentration of hexylbenzene. Taking into account the natural abundance of the hexylbenzene

in the oil mixture, the amount of the labeled compound added to the JP-8 was found to be 4.8 wt percent.

7.2.4.3 Pyrolysis Experiments

The pyrolysis experiments were performed in 25-mL stainless-steel autoclave reactors formerly described by Coleman *et al.* [56]. However, the sand bath described in this previous work was replaced by a muffle furnace, heating only the reactor itself and not the upper part of the apparatus (see Figure 18).

The experiment involved the pyrolysis of 10 g of sample at a temperature of 400 °C for 1, 2, 4, and 6 hours. The sample was previously purged with UHP-grade nitrogen 10 times at 1000 psi to minimize the presence of dissolved oxygen and finally pressurized with 100 psi of nitrogen. It was then placed in the preheated furnace at 400 °C for the required reaction time. After pyrolysis, the reactor was directly quenched into cold water and then depressurized. The gases were not recovered. Each experiment was repeated three times to check the reproducibility. The reactors were first tested with the hexylbenzene as a neat compound and then with the JP-8 spiked with labeled ¹³C-hexylbenzene in the known concentration mentioned above.

Before each injection, the internal standard was added to the pyrolyzed samples. The samples were first analyzed by GC-FID; then the same samples were injected and analyzed by GC-SIM-MS by monitoring the $m/z = 164.148$ ($M^+ + 1$ ion of the neat labeled hexylbenzene) and $m/z = 183.211$ (squalane fragment) ions. Each sample was injected three times to check the reproducibility of both methods. For our data, standard deviations of 0.2 percent and 0.8 percent were measured for the GC-FID and GC-SIM-MS methods, respectively.

By monitoring selected ions, the natural abundance of the hexylbenzene contained in the JP-8 does not interfere in the quantification of the labeled hexylbenzene. The monitored ion, $m/z = 164.148$, corresponds to the $M+2$ parent ion of unlabeled hexylbenzene. This ion can contribute significantly if the molecule has a large number of carbon atoms. However, the intensity of the $M+2$ ion in the mass spectrum of the natural hexylbenzene is negligible. The SIM method is preferred over the GC-FID method to determine the conversion of ¹³C-labeled hexylbenzene spiked into the JP-8. Due to the complexity of the oil mixture and the inherent coelutions observed on FID, having a method involving minimal interferences is of great benefit.

7.2.5 Flow Reactor

7.2.5.1 Flow Reactor Design

This reactor (Figure 19) was a single-pass design similar in concept to the near-isothermal flowing test rig (NIFTR) described by Jones and Balster [79], although with several changes outlined below. The fuel was supplied from two 316 stainless-steel reservoirs, a large (>15 L) tank containing neat JP-8 and a smaller (~2 L) tank containing the fuel spiked with the labeled hexylbenzene. A nitrogen-handling system was incorporated to allow independent sparging of the reservoir contents and to maintain a slight overpressure above the liquid to minimize diffusion of atmospheric oxygen into the tank after sparging was completed. Unlike the NIFTR,

the tanks were unheated, lacking the ability to precondition the fuels thermally, in addition to dissolved gas composition. All transfer lines and fittings were constructed of 1/16" 316 stainless- steel.

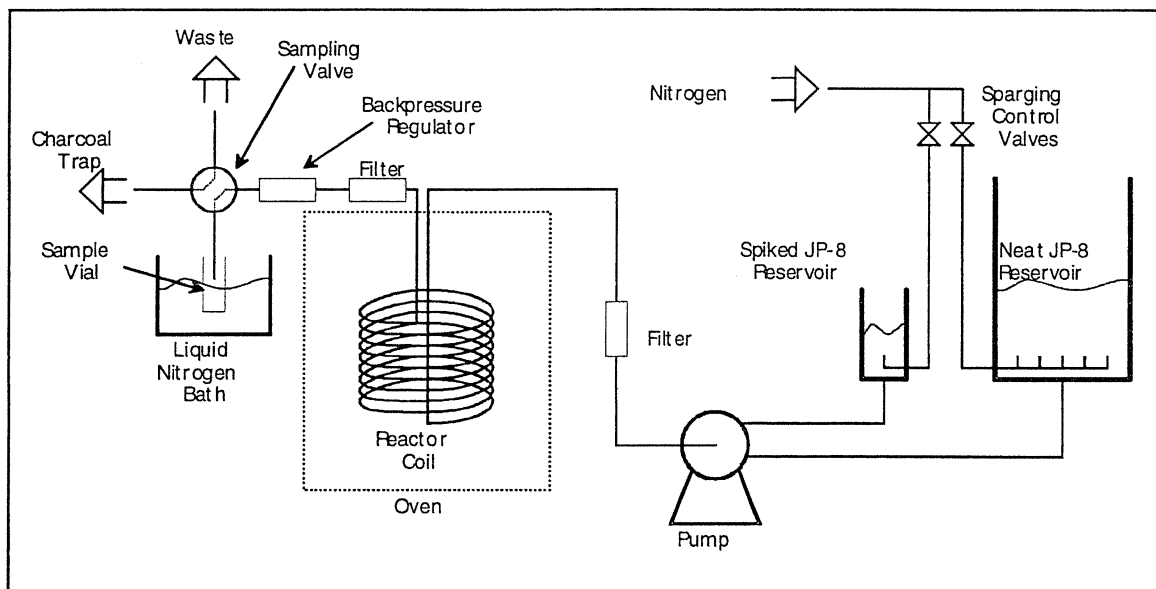


Figure 19. Schematic of the Flowing Reactor

Both reservoirs are sparged to remove oxygen from the fuel. The flow rate is selected at the pump to yield an appropriate residence time in the reactor. The sampling valve allows the eluent to either be shunted to waste or collected in a liquid nitrogen cooled sample vial. The charcoal trap is for fume reduction.

Both reservoirs fed into separate input lines on a Waters 6000A liquid pump (0.2 - 9.9 mL/min at 0-6000 psig). The input line is selectable, but internal mixing, as is available on a binary pump, is not possible. The pump was calibrated by timing the flow eluting from the vial connection at the sampling valve into a graduated cylinder. As the flow rates are quantized (no partial settings are possible on the pump controller), the residence time is also limited to certain values based on the reactor length.

The pump output stream passed through a 0.5- μ m sintered stainless-steel screen filter entering the heated zone. The reactor consisted of a 15-m length (as opposed to 0.56 m on the NIFTR) of stainless-steel tubing (1/8" OD) wound into a 20-cm diameter coil and placed inside an oven (Thermolyne Model 30400). The coil was modular, due to the arrangement of the fittings outside the heated zone, to allow for ease of replacement. The heated section of the reactor consisted of one continuous length of tubing, with no fittings exposed to the high temperature. The interface through the top (originally intended as a thermometer mount) was insulated with rock wool and the internal temperature monitored by a suspended thermocouple.

The reactor eluent then left the heated zone and passed through a 2- μ m screen filter (to remove the largest particles which might have formed in the reaction region, preventing damage to upstream flow-handling devices) and a back-pressure regulator set to 300 psig, used to

maintain the flow condition over a range of temperatures and flow settings. The stressed fuel was then directed by a two-position, four-port valve to either waste or a sample vial kept at liquid-nitrogen temperature. The sample vial was mounted to the system by a modified screw cap, allowing the venting of the gases only after their passing through the cooled surface of the vial, thereby effectively trapping all the condensable products from the fuel stream.

7.2.5.2 Flow Reactor Experiment

A fresh reactor coil was installed and both reservoirs were degassed for 1 hour prior to each experiment. Neat JP-8 was passed through the system at 5 mL/min to flush the system and ensure all surfaces were wetted in the reactor coil. The flow of neat fuel was slowed to 2 mL/min while the furnace was reaching operating temperature and stabilizing, requiring approximately 1 hour. This served a dual purpose. The relatively high flow (residence time of 30 minutes) minimized both the possible deposits formed from static fuel in the flow coil and waste of the spiked mixture.

Once the temperature was stable, the spiked-fuel stream was selected and allowed to purge the system for ~1.5 hours (3 reactor volumes), at which time the flow rate for the experiment was selected. The calculated residence time for the experiment was exceeded by >1 hour to minimize any effects from diffusion.

Samples were collected by mounting a 2-mL vial on the collection port of the sampling valve and cooling the vial with liquid nitrogen. Once the vial was at liquid-nitrogen temperature, the sampling valve was switched from waste to collect, diverting the fuel stream into the vial. Samples were collected for time periods corresponding to 1-2 mL of fuel (based on the flow rate).

Once the sample was collected, the valve was returned to the waste position and the vial removed from the mounting point. The vials were capped and placed aside until the solid melted, then the cap was loosened to allow the light gases to vent. This was necessary to prevent over-pressurization and subsequent destruction of the vial. Aliquots from the vials were taken and used for the GC-SIM-MS quantitation and analysis as described in the previous section.

7.3 Results and Discussion

7.3.1 Pyrolysis of the Neat Unlabeled Hexylbenzene

From the calibration curves on either of the GC-FID and GC-SIM-MS systems, the amount of residual hexylbenzene and thus the percentage of conversion could be determined in static-reactor pyrolysis experiments. Both techniques were used to calculate the conversions. Each pyrolysis experiment was reproduced three times, and the average of these runs was used to determine the conversion. The conversion percent is defined as follows:

$$\text{percent conv.} = 100 \times [1 - (C / C_0)]$$

where C is the residual hexylbenzene, and C_0 the initial hexylbenzene amount.

The results, summarized in Table 9, show that the percentages of conversion determined by the GC-FID and GC-SIM-MS techniques are very similar at each time interval. Assuming an apparent-first-order kinetic expression, the kinetic coefficient k (s^{-1}) was determined by plotting $\ln(C/C_0)$ versus the pyrolysis time (s).

Table 9. Conversion Percentage of Neat Unlabeled Hexylbenzene Pyrolyzed in a Tubing Bomb at 400 °C at Each Time Interval. Quantification by GC-FID (standard deviation = 0.2 percent), GC-SIM-MS (standard deviation = 0.8 percent). Determination of the kinetic coefficient k for each analytical method.

Time (h)	Conversion (percent)		
	GC-FID	GC-SIM-MS	GC-FID (McKinney) ⁵¹
0	0	0	0
1	6.3	5	16.7
2	24.3	25.3	33.3
4	41.3	44.5	49.4
6	57.7	56.7	64.9
k (s^{-1})	3.86×10^{-5}	3.90×10^{-5}	4.76×10^{-5}

The linear regression yielded correlation coefficients of 0.986 and 0.983 for the GC-FID and GC-SIM-MS methods (Figure 20), respectively. The pyrolysis of the neat hexylbenzene was confirmed to be a first-order reaction between 0 to 6 hours of thermal stressing. The rate of the degradation (kinetic coefficient k), ranged from 3.86×10^{-5} to $3.90 \times 10^{-5} s^{-1}$. Comparison of the results obtained by the two different methods showed that the GC-SIM-MS was as reproducible and reliable as the GC-FID method. However, GC-SIM-MS allows the differentiation between hydrocarbons enriched with ^{13}C and those at natural abundance. Furthermore, the accuracy of the technique has been determined by injecting each sample in triplicate. The results showed good reproducibility with standard deviations lower than 0.8 percent. Being precise and reproducible, this GC-SIM-MS method facilitates the improved quantitative determination of conversion percentages [72] compared with other techniques [80].

Previous studies by Peng [81] showed that the thermal degradation of neat hexylbenzene gives rate constants of $4.76 \times 10^{-5} s^{-1}$ and $1.04 \times 10^{-4} s^{-1}$, respectively. Compared with values obtained here, the previous studies are more consistent with our measured values. Perhaps the differences among all studies relate to the nature of the reactor and the method used for determining loss of product. That previous work used ^{13}C NMR in which the reactor was quenched, subsampled, and reheated to obtain temperature dependences. Peng [71] utilized a reactor with a substantial dead volume in the stem and quenched by cooling in water to 150 °C and letting the reactor cool to room temperature in air.

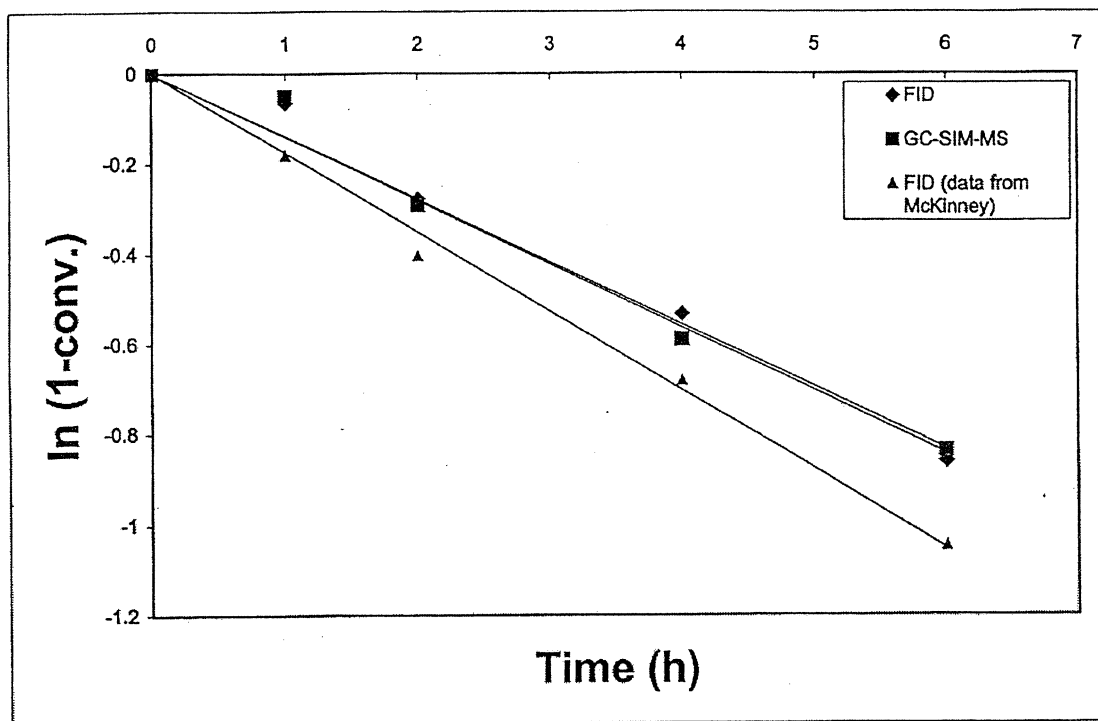


Figure 20. First-Order Plots of the Thermal Degradation of Neat Unlabeled Hexylbenzene Quantified by GC-FID and GC-SIM-MS, Compared with the GC-FID Data Obtained by McKinney [51]

7.3.2 Pyrolysis of the ^{13}C -Labeled Hexylbenzene Spiked into the JP-8 in the Static Reactor

As described previously, an internal standard (squalane) was added to each pyrolyzed sample before injection. To ensure reliability, the static reactor samples were also analyzed by GC-FID. The GC-SIM-MS results were obtained by monitoring the ions $m/z = 164.148$ and $m/z = 183.211$, assuming that the response factor of the $M+1$ parent ion of the unlabeled hexylbenzene ($m/z = 163.144$) equals that of the $M+1$ parent ion of the labeled hexylbenzene ($m/z = 164.148$). The results, obtained by the two methods are listed in Table 10. It is shown, as in the case of the neat experiments, that the conversion percentages determined by the GC-SIM and GC-FID methods were very similar to each other at each time interval. Some differences can be expected, particularly at high conversion levels where radical-recombination processes can lead to the production of 1-hexylbenzene as a product. It has been shown [82] that thermal cracking occurs predominantly by a step-wise free-radical mechanism in which the chain reaction can be terminated by recombination of two radicals to form a new C-C bond [59, 83, 84]. If this reaction occurs by reforming the hexylbenzene, a reduced conversion percentage would be detected by FID compared with that determined by GC-SIM-MS. Since the probability of recovering a 1- ^{13}C -hexylbenzene (^{13}C -Hb) is much lower than for ^{12}C -hexylbenzene (^{12}C -Hb), the amount of residual labeled ^{13}C -hexylbenzene measured by GC-SIM-MS would not increase significantly due to a potential contribution from molecular recombination. The unlabeled hexylbenzene could form from unlabeled alkylbenzenes pyrolyzed in the jet-fuel medium.

Table 10. Percentage of Conversion of ^{13}C -Labeled Hexylbenzene Spiked into JP-8 and Pyrolyzed in a Tubing Bomb at 400 °C at Each Time Interval. Quantification by GC-FID (standard deviation = 0.2 percent) and GC-SIM-MS (standard deviation = 0.8 percent). Determination of the kinetic coefficient k for each analytical method.

Time (h)	Conversion (percent)	
	GC-FID	GC-SIM-MS
0	0	0
1	3.9	4.3
2	10.1	11.2
4	21.5	20.7
6	32.9	32.3
$k \text{ (s}^{-1}\text{)}$	1.76×10^{-5}	1.73×10^{-5}

However, because GC-FID does not differentiate isotopically enriched hydrocarbons from those of natural abundance, the level of residual hexylbenzene determined by FID would be higher. The measured chromatographic peak detected by FID is a combination of the natural abundance-derived hexylbenzene (unlabeled), the ^{13}C -labeled hexylbenzene spiked in the oil mixture, and hexylbenzene originating from potential recombinations. This study did not reveal any significant differences between conversion rates measured by the two methods. Therefore, the probability of recombination reactions appears to be small for the 1-hexylbenzene under the pyrolysis conditions employed.

The GC chromatogram displayed in Figure 21 shows a typical profile of the prestressed jet fuel, JP-8, mixed with ^{13}C -1-hexylbenzene. Only four major groups of compounds are exhibited. The n-alkane series is dominant and ranges from C_8 to C_{16} with a maximum abundance for n- C_{11} . The other major compounds include the cyclohexane family alkylated from C_2 to C_{10} and the C_8 to C_{16} iso-alkanes. Finally, the C_8 to C_{14} mono-aromatic series, much less abundant than the others, is mostly alkylated from C_3 to C_{11} .

The static-reactor thermal stressing of the fuel sample during 1, 2, 4, and 6 hours (Figure 21b, c, d, and e, respectively) shows some changes in the absolute intensities of peaks but not in the general chemical composition. To visualize this trend, some major peaks were labeled in Figure 21a (peaks 1 to 20), and the percent changes were calculated between the prestressed and the 6-hour stressed JP-8. The results are listed Table 11. Basically, the data show a general decrease for all the families with a carbon number above C_9 (peaks 6 to 20) and a significant increase of the low-molecular-weight compounds (peaks 1 to 5). The same overall trend is shown for the ^{13}C -labeled hexylbenzene mixed in the JP-8: a slow loss of the compound is recorded as the pyrolysis time increases. This is due to the thermal cracking of longer alkyl chains. [61, 85, 86]

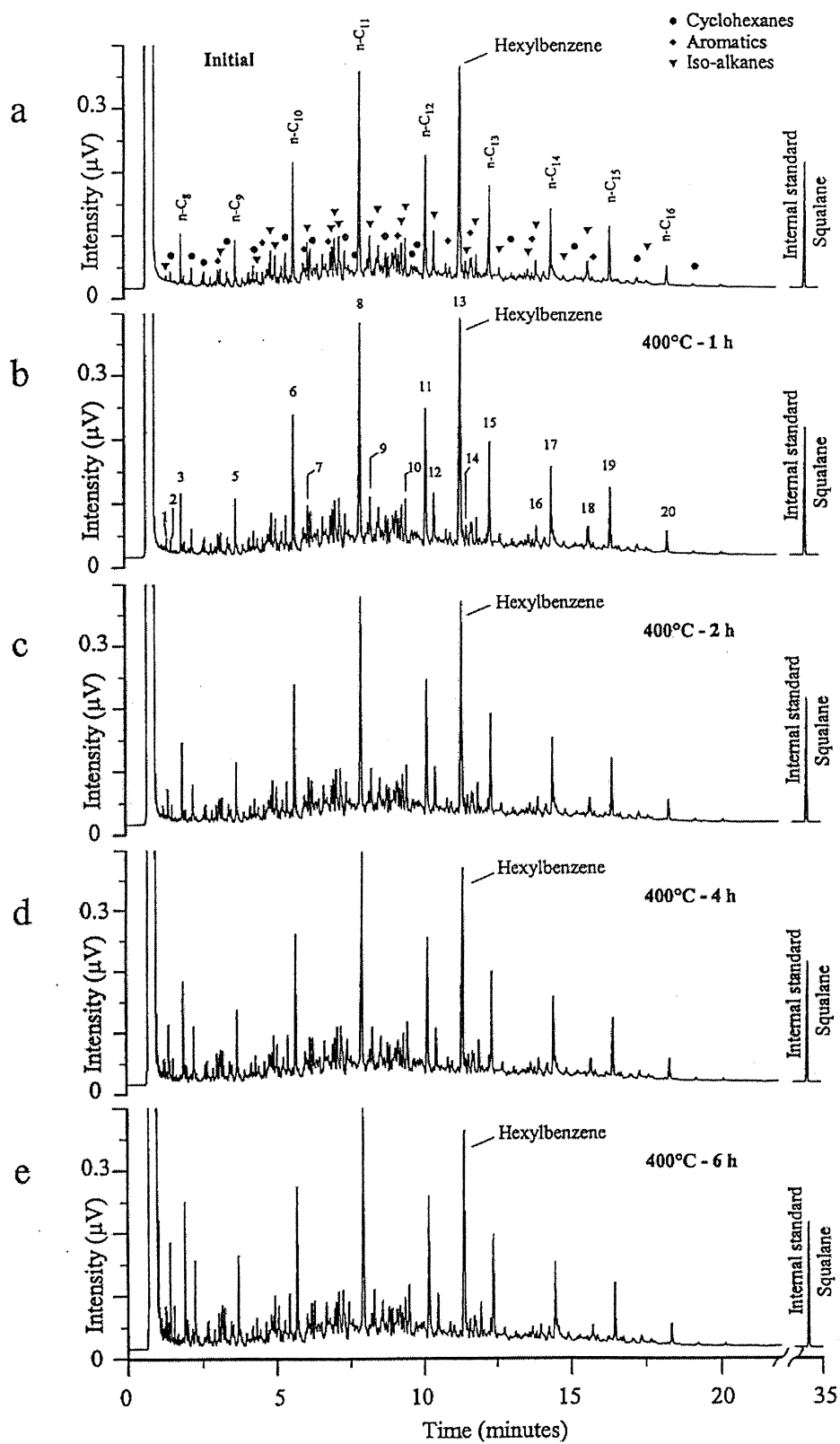


Figure 21. Gas Chromatograms of ^{13}C -Hexylbenzene Mixed with JP-8 (a) and Pyrolyzed in Static Reactor at 400 °C for 1 (b); 2 (c); 4 (d); and 6 hours (e)

Table 11. Percent Change of Abundance Relative to Initial Concentration of Peaks 1 to 20 (Figure 20a) during 6-Hour Pyrolysis

Peak Number	Nature	Change (percent)
1	C ₈ Iso-alkane	600
2	Alkyl Cyclohexane	100
3	Octane	120
4	Alkyl Cyclohexane	167
5	Nonane	44
6	Decane	-12
7	C ₁₁ Iso-alkane	-22
8	Undecane	-13
9	C ₁₂ Iso-alkane	-20
10	C ₁₂ Iso-alkane	0
11	Dodecane	-18
12	C ₁₃ Iso-alkane	-32
13	Hexylbenzene	-33
14	C ₁₃ Iso-alkane	-22
15	Tridecane	-22
16	C ₁₄ Iso-alkane	-33
17	Tetradecane	-13
18	C ₁₅ Iso-alkane	-33
19	Pentadecane	-31
20	Hexadecane	-33

The results listed Table 10 show that only 32 percent of the starting material has been degraded after 6 hours of thermal stressing, whereas it reaches 57 percent for the pyrolysis of neat hexylbenzene. This represents a 44 percent decrease in the conversion percentage relative to the initial amount. A plot of the natural logarithm of (1-conversion) versus time shows that the pyrolysis data provide a linear regression between 0 and 6 hours of stressing (Figure 22). The kinetic coefficient k ($k = 1.73 \times 10^{-5} \text{ s}^{-1}$) is, however, much lower than that of the neat compound ($k = 3.90 \times 10^{-5} \text{ s}^{-1}$). This indicates that the rate of degradation of the hexylbenzene is inhibited when mixed in the jet fuel JP-8 compared with thermal stressing of neat hexylbenzene, consistent with the findings of McKinney [72] who used NMR for rate determinations. The

suppressed rate is probably due to enhanced intermolecular reactions in the jet-fuel mixture that form more reactive compounds. From these results, we conclude that the oil matrix has an influence on the thermal degradation of the hexylbenzene. McKinney *et al.*, [72] observed a similar rate suppression for the thermal degradation of n-C₂₅ alkane in petroleum, compared with the thermal degradation of the neat compound.

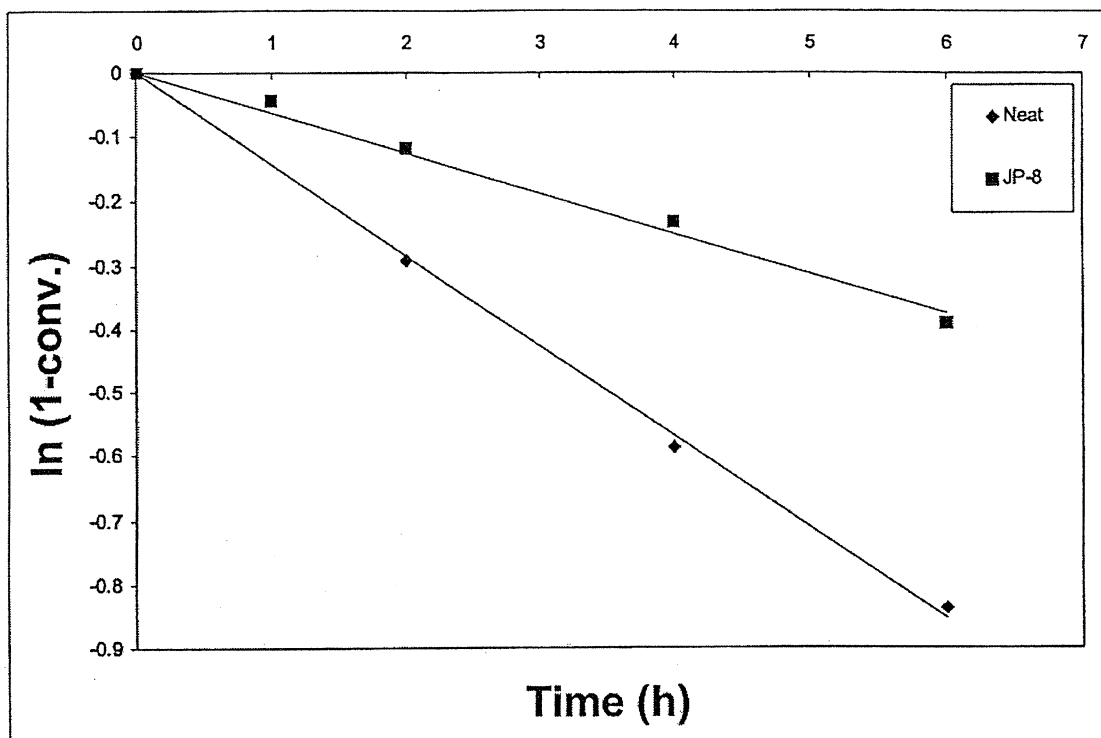


Figure 22. First-Order Plots for the Thermal Degradation of Neat Hexylbenzene and When Mixed in JP-8, Quantified by GC-SIM-MS

If we compare the data for thermal degradation of hexylbenzene in jet fuel with that obtained by McKinney [72], it appears obvious that the fuel can play an important role. He showed that hexylbenzene spiked into JP-8C derived from coal is 3.4 percent converted after 6 hours of thermal stressing, and the conversion rate is $1.61 \times 10^{-6} \text{ s}^{-1}$. If we consider the fact that the reaction rates for the neat hexylbenzene thermally stressed at 400 °C are in the same range in our studies and that of McKinney [72], it can be assumed that the rate of thermal degradation in the presence of jet fuel is dramatically lower, in the case of coal-derived jet fuel, by nearly an order of magnitude. Our JP-8 fuel is composed mostly of long-chain paraffins with low concentrations of alkylcyclohexanes, whereas the coal-derived JP-8C is enriched in cycloalkanes as well as hydroaromatics. [50, 74] This could result in differences in reactivity in static pyrolysis when we compare our results with that of McKinney [72]. The large pool of H-donors contained in JP-8C fuel could significantly suppress the thermal cracking of the hexylbenzene by capturing free reactive radicals, leading to an increased stability of the fuel.

7.3.3 Pyrolysis of the ^{13}C -Labeled Hexylbenzene Spiked into the JP-8 in the Flow Reactor

Samples collected from the flow reactor subjected to various times at 400 °C were analyzed only by GC-SIM-MS, because we established the validity of this method for obtaining accurate rate constants for thermal degradation. The samples were also analyzed by traditional GC-MS to obtain full-scan mass spectra so that redistribution of the label into compounds could be determined (see below). The conversion data for labeled hexylbenzene are shown in Table 12. The flow-reactor results show a conversion rate of $6.09 \times 10^{-5} \text{ s}^{-1}$ in the mixture, a significantly higher rate than either for the neat compound or for the static-reactor conversion. Figure 23

Table 12. Percentage of Conversion of ^{13}C -Labeled Hexylbenzene Spiked into JP-8 and Pyrolyzed in a Flowing Reactor at 400 °C at each Time Interval, as Defined by the Flow Rate of the Pump and the Reactor Length. Quantification by GC-SIM-MS (standard deviation = 1.0 percent).

Time (h)	Conversion (percent)
0	0
1.03	9.7
1.92	25.3
3.46	53.1
5.77	73.6
k (s ⁻¹)	6.09×10^{-5}

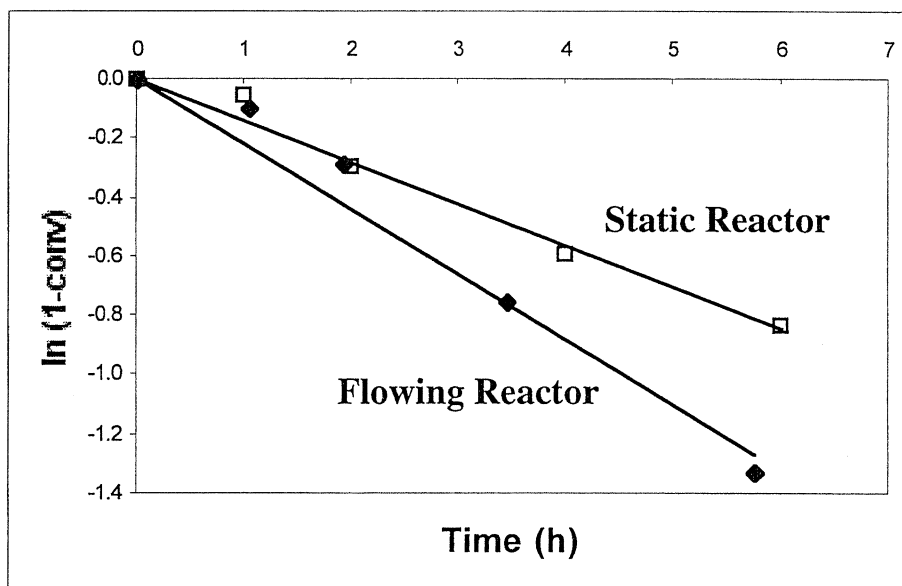


Figure 23. First-Order Plots for the Thermal Degradation of Hexylbenzene Mixed in JP-8, Compared with the Same Fuel in the Static Reactor as Quantified by GC-SIM-MS

shows a plot of $\ln(1 - \text{conversion})$ versus time for labeled hexylbenzene under both the static- and flow-reactor conditions. One can observe a significant difference between the two systems.

The difference between the flow- and static-reactor rates for the fuel is most likely the result of two factors. The design of the static reactor involves both a heated and unheated zone. The condensation that likely occurred would effect both the overall amount of sample available and discrimination toward the heavier compounds. The second factor is one of conditions. The flow reactor was operated at 300 psig, which almost surely placed the sample under supercritical conditions while conditions for the static reactor have not been established.

7.3.4 Measurements of Isotopic Enrichments for the Products

The use of a ^{13}C -labeled compound mixed into the fuel allowed us not only to quantify accurately the conversion percentage but also to develop an attractive way to characterize the reaction products and, eventually, the reaction mechanisms. Analyzed by the GC-SIM-MS method, the products from thermally stressed ^{13}C -labeled species can be identified within the distribution of products by tracing the isotopic enrichment of each compound. Products and initial compounds can then be related to each other. These results provide important information essential to a full understanding of the reaction mechanisms occurring in JP-8 pyrolysis. For the experiments discussed here, this ability is limited to tracing products that retain the labeled benzylic carbon. Thus, only products such as toluene, ethylbenzene, styrene, and other alkylbenzenes can be expected to show an enrichment in the label. We also expect the label to be incorporated into multi-ring compounds produced from condensations occurring during thermal degradation.

This concept has been applied to the JP-8 fuel spiked with labeled hexylbenzene and pyrolyzed for 4 h in both the static reactor and the flow reactor; however, in the interest of brevity, only the flow reactor details will be discussed here. The GC-SIM-MS analyses yield a chromatogram from which the ^{13}C -isotope enrichment of each compound can be calculated. This is accomplished by slowly scanning a narrow mass range during GC-MS to obtain a more accurate measure of the peak intensities and measuring enrichments by the isotopic distribution of molecular ions as well as fragment ions. A more precise measure of isotopic enrichment can be made by use of a GC-ir-MS system that is commonly used for studies of the isotopic patterns of natural-abundance compounds, but such an instrument was not available to us for such measurements. Only four ^{13}C -enriched compounds were characterized in the chromatograms: toluene, ethylbenzene, styrene, and C_3 -benzene. However, the complexity of the fuel mixture (hundreds of compounds) can cause difficulty in the determination of other ^{13}C -enriched compounds due to the uncertainty of measurements on small peaks, only partially enriched. In addition to these four most important peaks, some other compounds may be enriched but cannot be determined.

To estimate the relative amount of unknown enriched compounds, a mass balance of the ^{13}C -content was made to follow the distribution of the ^{13}C -labeling of the hexylbenzene when pyrolyzed in JP-8 under existing experimental conditions. From the mass balance, the relative amount of the unknown labeled compounds was calculated which included ^{13}C -enriched compounds present in the chromatogram but not characterized and tar components present in the

fraction but not GC-amenable peaks. Because the gases released during pyrolysis were not quantified in the flow-reactor experiments, the recovered liquid fraction was overestimated. However, we assumed that the amount of ^{13}C -enriched gases was negligible. Consequently, the ^{13}C -mass balance is defined as follows:

$$^{13}\text{C}_{\text{Hb initial}} = ^{13}\text{C}_{\text{Hb residual}} + ^{13}\text{C}_{\text{tol.}} + ^{13}\text{C}_{\text{ethylb.}} + ^{13}\text{C}_{\text{styrene}} + ^{13}\text{C}_{\text{C3-benz.}} + ^{13}\text{C} [\text{unknown}]$$

The ^{13}C enrichment was calculated for each compound as:

$$^{13}\text{C} = R \cdot \text{Peak Area}$$

$$\text{with R the ratio: } \frac{(M+1) - [(M) \times \#C \times 0.011]}{(M) + (M+1) - [(M) \times \#C \times 0.011]} \quad (16)$$

(M) abundance of the molecular ion of unlabeled compound

(M+1) abundance of the molecular ion of labeled compound that is +1 mass unit higher than M.

#C carbon atom number of the molecule

The term [(M) - #C - 0.011] represents the isotopic contribution of M to M+1.

For toluene, the tropillium-ion fragment ($m/z=92$) of the labeled toluene fragment also corresponds to the molecular ion of the unlabeled toluene. The abundance of M, used in the ^{13}C -calculation, is thus not measurable. However, the ratio (M-1)/(M) of unlabeled toluene (1.7) can be determined from a standard mass spectrum. The ratio R used in that particular case becomes:

$$R = \frac{(M+1) - \left[\frac{(M-1)}{1.7} \times 7 \times 0.011 \right]}{\frac{(M-1)}{1.7} + (M+1) - \left[\frac{(M-1)}{1.7} \times 7 \times 0.011 \right]} \quad (17)$$

Note that each measured peak area should be corrected by a response factor peculiar to the compounds themselves. However, the chemical composition of each component being nearly similar, the error is not expected to be higher than the mass spectrometer error measurement.

The mass balance of the ^{13}C -isotopic partition between initial hexylbenzene and pyrolysis products is described in Table 13. Fifty-six percent of the initial hexylbenzene remained in the pyrolyzed mixture (in the flow system) which correlates with the results obtained from GC-FID (48 percent conversion).

Besides the residual hexylbenzene, toluene and ethylbenzene are the two most important ^{13}C -enriched peaks identified in the chromatogram with a ^{13}C -content of 6 percent of the total for each, whereas the ^{13}C -contents of styrene and C_3 -benzene are only minor (0.3 and 0.5 percent of the total, respectively). The relative distribution of labeled products analyzed among the products identified to be enriched is listed Table 14. Eighty-one percent of the identified ^{13}C -enrichment was assigned to residual hexylbenzene, followed by 9 percent for toluene and ethylbenzene. The

contribution of styrene and C₃-benzene only counted for 0.4 percent and 0.7 percent, respectively.

Table 13. Mass Balance of the ¹³C from the Thermal Degradation (flow reactor, 4 hours) of ¹³C-Hexylbenzene Spiked in JP-8 and Showing the Redistribution of the Label into Other Compounds. The percentage of ¹³C-enriched unknown compounds is determined by difference.

Compounds	¹³ C-enriched compounds (percent)
Hexylbenzene Initial	100
Hexylbenzene Residual	56
Toluene	6
Ethylbenzene	6
Styrene	0.3
C ₃ -benzene	0.5
Unknown	31

Table 14. Relative abundance of the ¹³C-enriched compounds characterized by GC-SIM-MS. Pyrolysis of JP-8 spiked with ¹³C-hexylbenzene monitored in a flow reactor for 4 hours.

Products	Relative abundance (percent)
Hexylbenzene Residual	81
Toluene	9
Ethylbenzene	9
Styrene	0.4
C ₃ -benzene	0.7

Under the static-reactor reaction conditions (T = 400 °C, P > 100 psi), it is difficult to determine if a supercritical condition was achieved. The cracking reactions mainly involved radical mechanisms [87], and it seemed that hydrogen abstraction and β-scission determined the overall product distribution [81]. At a moderate conversion, two major pathways consumed the hexylbenzene, leading to the formation of styrene and toluene, respectively. However, styrene can be rapidly consumed to form ethylbenzene as a secondary but major product. [88] These reactions explain the presence of toluene, ethylbenzene, and styrene as reaction products. The formation of C₃-benzene may come from other minor reactions.

7.4 Conclusions

This research shows, in accordance with published information [50, 73, 89, 90], that the conversion rate of hydrocarbon compounds (alkanes, alkyl-aromatics) mixed within a fuel matrix and pyrolyzed in a tubing bomb depends mainly on the fuel chemical composition.

The pyrolysis experiments of ^{13}C -labeled hexylbenzene mixed in two different jet fuels (JP-8 in our study and JP-8C in the study by McKinney [72]) showed significant differences between the samples. In our study, a degradation rate of about 32 percent was recorded when the hexylbenzene was mixed with JP-8. The rate measured by McKinney [72] was only 3.4 percent with spiking into coal-derived JP-8C over a period of 6 hours (Table 15). Approximately 57 percent degradation was recorded for the neat system in our study. The major difference observed in the composition of the two jet fuels was the large concentration of cycloalkane and hydroaromatic compounds present in JP-8C. Such species can inhibit the thermal cracking of components by capturing free reactive radicals. It seems apparent that the H-donor propensity of a fuel is strongly related to its ability to suppress thermal degradation. The JP-8 fuel comprised of mostly alkanes exhibited a lesser ability to suppress hexylbenzene cracking but was significantly more prone to do so than the neat system. It is clear that fuel composition is an important criterion affecting the rate of thermal degradation at 400 °C.

Table 15. Percentage of Conversion of ^{13}C -Labeled Hexylbenzene Spiked into JP-8 and Pyrolyzed in a Flow Reactor at 400 °C at each Time Interval, as Defined by the Flow Rate of the Pump and the Reactor Length. Quantification by GC-SIM-MS (standard deviation = 1.0 percent).

Time (hours)	Conversion (percent)
0	0
1.03	9.7
1.92	25.3
3.46	53.1
5.77	73.6
k (s-1)	6.09×10^{-5}

Further studies need to be conducted with fuels of different characteristics. This will be necessary to understand fully the role of certain compounds that may be involved in various reactions when the fuel is exposed to extreme conditions such as those prevailing in an aircraft.

The ^{13}C -labeling method presented in this study suits this purpose well, especially in relation to the elaboration of the reaction mechanisms. The GC-SIM-MS technique is demonstrated to be a powerful method with good reproducibility and accuracy. By monitoring specific ions, the isotopic enrichment of each compound in the fuel distribution can be measured. The ^{13}C -labeled products resulting from the pyrolysis of the original labeled compound spiking the mixture can

thus be traced and identified. Results of such analyses will provide valuable information on the reaction mechanisms occurring during fuel degradation.

8.0 CLARIFICATION OF KEY INTERACTIONS AMONG FUEL COMPONENTS UNDER PYROLYTIC AND OXIDATIVE CONDITIONS

The present study has investigated three aspects of the clarification of key interactions among fuel components under pyrolytic and oxidative conditions. First, the key interactions between the hydrogen donors 1,2,3,4-tetrahydro-1-naphthol and 1,2,3,4-tetrahydroquinoline and the model compound n-tetradecane were investigated (section 8.1). Secondly, the chemical interactions between n-tetradecane and the hybrid hydrogen donors of benzyl alcohol and 1,2,3,4-tetrahydro-1-naphthol, and benzyl alcohol and tetrahydronaphthalene have been studied (section 8.2). Compared with the use of a single hydrogen donor, the hybrids resulted in synergistic effects toward reducing the pyrolytic degradation of alkanes in jet fuels, resulting in an enhanced suppression of the formation of free radicals. Finally, the thermal stability of n-tetradecane, decahydronaphthalene, and the coal-derived jet-fuel, JP-8C, as they go through the autoxidative regime into the pyrolytic regime, has been studied (section 8.3), where the differences in chemical reactivity between the linear and cycloalkane have been related to the stability of the coal-derived jet fuel.

8.1 Suppression of Pyrolytic Degradation of n-Alkanes in Jet Fuels by Hydrogen Donors

8.1.1 Introduction

The use of hydrogen donors to suppress pyrolytic degradation of jet fuels [91-93] is a potential route to reach the JP-900 thermal-stability requirement set up by the US Air Force [94]. The pyrolytic conversion of alkanes, typically found in petroleum-derived jet fuels, is generally considered to involve the formation of free radicals [95-96]. The propagation of these reactive intermediates results in a broad distribution of smaller alkane and alkene units, and triggers the aromatization of the liquid, which leads to undesirable solid depositions. As a solution, the free radicals can be halted immediately after the initiation step by the use of hydrogen donors. [91-93] However, the chemistry involved in inhibiting free-radical reactants during thermal degradation of fuels is not fully understood. This is addressed in this section, where the suppression of thermal degradation of n-tetradecane by the use of the hydrogen donors 1,2,3,4-tetrahydro-1-naphthol and 1,2,3,4-tetrahydroquinoline has been characterized at temperatures ranging from 425 to 475 °C under nitrogen.

Experimental

The compounds used were n-tetradecane (TD, Aldrich 99 percent+), 1,2,3,4-tetrahydro-1-naphthol (THNol, Acros 97 percent), and 1,2,3,4-tetrahydroquinoline (THQ, Aldrich 99 percent). A detailed description of the experimental setup and analytical determination of the product distribution using GC and GC/MS has been reported elsewhere. [91, 95]

Results and Discussion

The thermal stability of tetradecane (TD) during the pyrolytic stressing can be expressed on the basis of the amount of TD remaining in the liquid divided by the amount in the original

mixture weighted against the liquid yield of the experiment. This ratio ($TD_r:TD_o$) is, therefore, normalized, and its enhancement when a hydrogen donor is added, compared with that of the TD alone, indicates that the hydrogen donor does indeed improve the thermal stability of the paraffinic compound. Figure 24 shows $TD_r:TD_o$ for various mixtures with THNol, stressed at 425, 450, and 475 °C for 30 minutes. With increasing temperature there is a dramatic decrease in the amount of TD remaining with no THNol added, from around 85 mole percent at 425 °C to 27 mole percent at 475 °C. When the hydrogen donor is added, there is a significant increase in $TD_r:TD_o$ at all the temperatures for the first half-mole percent THNol added. A slower but steady rise is observed thereafter up to 5-mole percent THNol at all three temperatures; this tendency is marked more at higher temperatures. The comparison of for TD alone and with 0.5-mole percent THNol added is plotted in Figure 25. The effect of adding a small amount of THNol is clearly dependent on the temperature (for 30 minutes stressing), where the enhancement of 0.5-mole percent THNol is only 4 percent at 425 °C, rising significantly to nearly 35 percent at 475 °C.

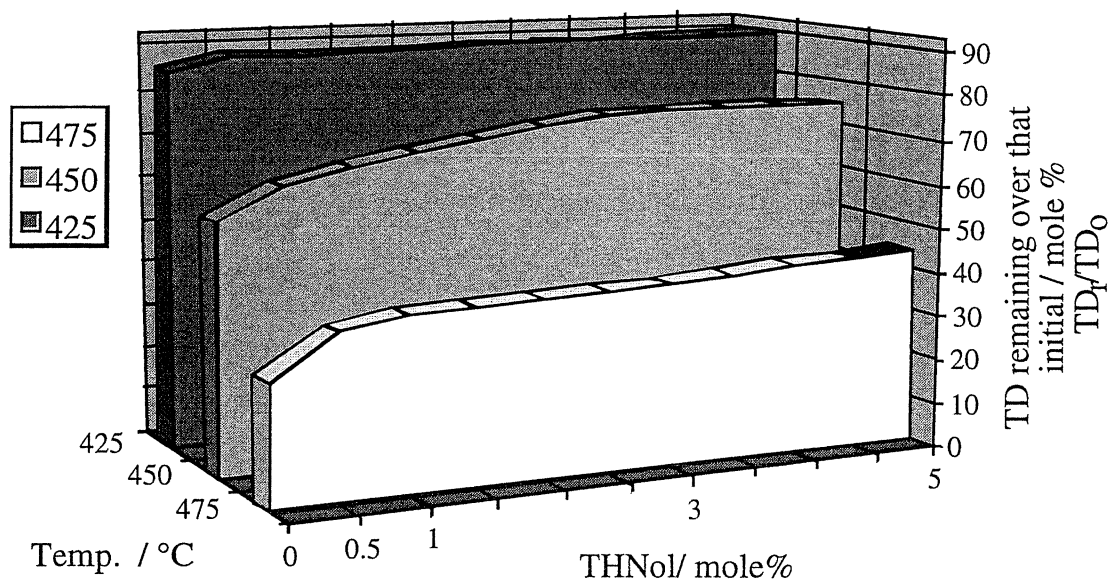


Figure 24. Comparison of Remaining TD Content Divided by its Initial Concentration for Different Mixtures with THNol, Stressed at 425, 450, and 475 °C for 30 Minutes

Figure 26 shows $TD_r:TD_o$ for various mixtures with THQ stressed at 425, 450, and 475 °C for 30 minutes. With increasing temperature, there is a dramatic decrease in the TD remaining with no THQ added, from around 85 mole percent at 425 °C to 27 mole percent at 475 °C. When the hydrogen donor is added, there is a significant increase in $TD_r:TD_o$ at all the temperatures for the first mole percent THQ added. A steady rise is observed thereafter up to 5-mole percent THQ for all three temperatures, especially at 450 and 475 °C. The comparison of $TD_r:TD_o$ for TD alone and with 5-mole percent THQ added is plotted in Figure 27. The effect of adding a small amount of THQ is clearly dependent on the temperature (for 30 minutes stressing), where the enhancement of 5-mole percent THQ is only 13 percent at 425 °C, rising significantly to nearly 120 percent at 475 °C.

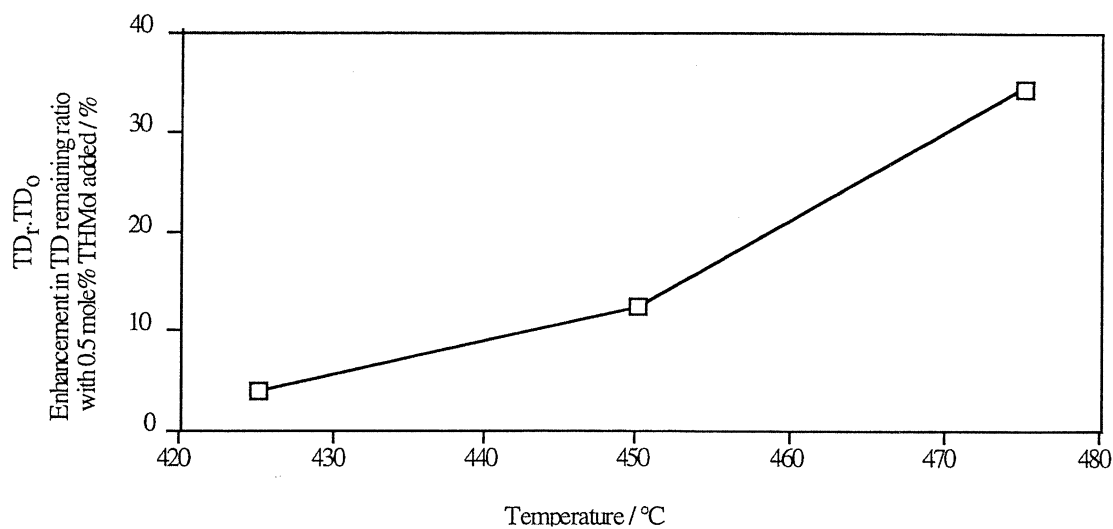


Figure 25. Comparison of the Ratio of the Remaining TD Content to its Initial Concentration for TD Alone and with 0.5-Mole Percent THNol Added, Stressed at 425, 450, and 475 °C for 30 Minutes

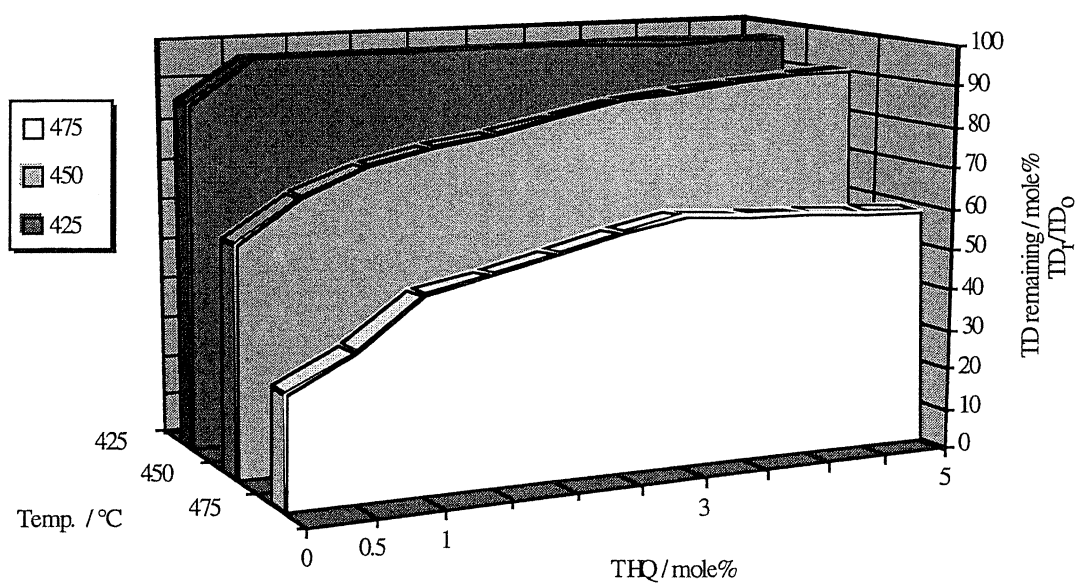


Figure 26. Comparison of Remaining TD Content Divided by its Initial Concentration for Different Mixtures with THQ, Stressed at 425, 450, and 475 °C for 30 Minutes

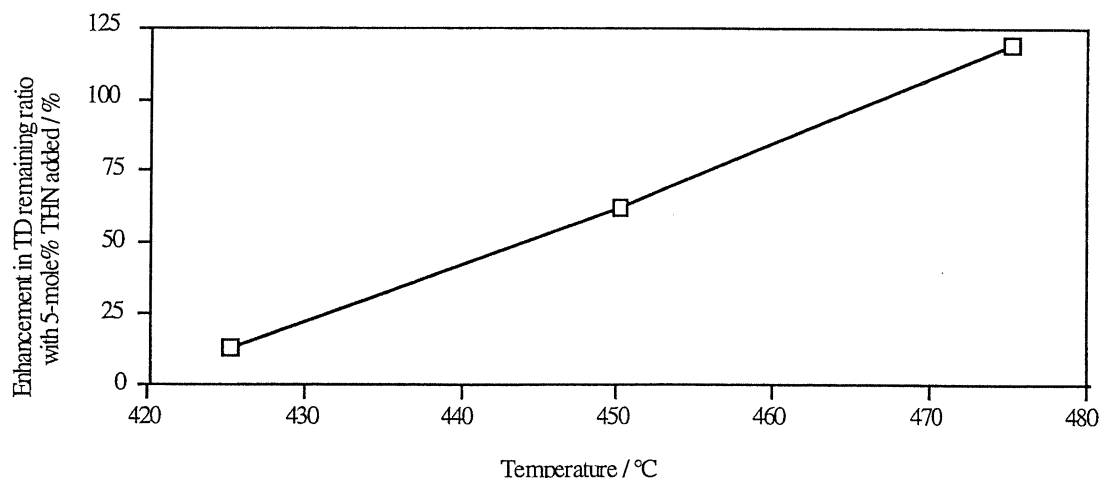


Figure 27. Changes in the Enhancement of the TD_r/TD_0 ratio with 0.5-Mole Percent THQ Added, Stressed at 425, 450, and 475 °C for 30 Minutes (TD_r/TD_0 for TD only is baseline)

Conclusions

The most significant effect of 1,2,3,4-tetrahydro-1-naphthol (THNol) and 1,2,3,4-THQ on the stabilization of n-tetradecane takes place with the addition of 1 mole percent. The increase in thermal stability of TD resulting from the presence of THNol and THQ appears to be comparable at low concentrations around 0.5 mole percent, but at higher concentrations, such as 5 mole percent, THQ performed better than did THNol.

8.2 Synergistic Effects of Hybrid Hydrogen Donors toward Stabilization of Paraffinic Jet Fuels in the Pyrolytic Regime

8.2.1 Introduction

The pyrolytic cracking of paraffins generates both primary and secondary free radicals, where a certain hydrogen donor may favor the interaction with only one type of free radical. This has been demonstrated previously, where the effects of hydrogen donors such as benzyl alcohol (BA) and 1,2,3,4-tetrahydro-1-naphthol (THNol) on the product distribution of pyrolytic-stressed tetradecane were studied. [97] Benzyl alcohol was found to reduce the amount of n-alkane-cracking products, whereas THNol greatly reduced 1-alkenes. This was associated with the ability of BA to target primary radicals and, correspondingly, the targeting of secondary radicals by THNol. Accordingly, section 8.2 focuses on the potential of hybrid hydrogen donors for enhanced pyrolytic stabilization of paraffinic compounds typical for jet fuels. Hybrids of benzyl alcohol with tetrahydronaphthalene and 1,2,3,4-tetrahydronaphth-1-ol have been studied, and their synergistic effect upon tetradecane has been characterized.

Experimental

The compounds used were n-tetradecane (TD, Aldrich 99 percent), benzyl alcohol (BA, Aldrich 99.8 percent), tetrahydronaphthalene (THN, Aldrich 99 percent), and 1,2,3,4-tetrahydro-1-naphthol (THNol, Acros 97 percent). Stressing of TD alone or in different mixtures with one or two hydrogen donors was performed for 30 minutes in a fluidized sand bath at 425, 450, and 475 °C. A detailed description of the experimental setup and analytical determination of the product distribution using GC and GC/MS has been reported elsewhere. [96]

Results and Discussion

It was shown in Delivery Order No. 2 [73], Subtask 2.1.2 that the addition of 1,2,3,4-tetrahydronaphthalene (THN) to n-tetradecane (TD) greatly reduced its thermal cracking, as evidenced by the reduction in the peak heights and areas of the alkane and alkene derivatives from TD by GC/MS. Furthermore, the introduction of THN reduced the 1-alkene peak in relation to the corresponding alkane peak when compared with the TD stressed alone. This indicates that THN, in particular, targets secondary radicals, a finding similar to that for THNol [97]. On the other hand, benzyl alcohol (BA) was shown to target n-alkane derivatives, indicating a tendency of BA to target primary radicals. [97] Figure 28 shows the ratio of the 1-alkene peak area to that of the corresponding n-alkane for TD alone and with 0.5-mole percent THN and BA. There is a clear increase in the alkene/alkane ratio for the BA mixture, indicating that BA is indeed targeting the primary radicals. However, for THN the ratios of the alkene to the alkane peaks are smaller than those observed for the TD alone, indicating that THN targets secondary radicals.

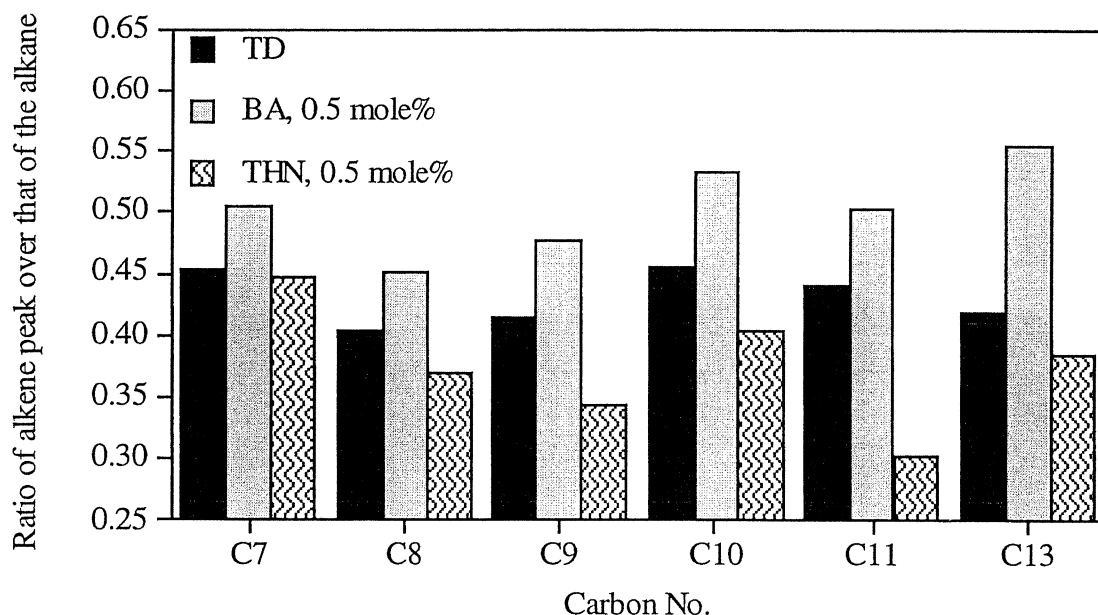


Figure 28. Ratio of the 1-Alkene Peak Area to That of the Corresponding Alkane for TD Alone and with 0.5-Mole Percent THN and 0.5-Mole Percent BA Addition Stressed at 475 °C for 30 Minutes

The observed effects on the thermal stabilization of TD by BA, THN, and THNol are summarized in Figure 29. The increased thermal stability of TD when hydrogen donors are added can be linked to the ability of the hydrogen donor to capture radicals formed during the stressing and therefore hinder cracking. This results in an increased liquid product and enhances $TD_i:TD_o$, when compared with TD stressed alone. Figure 29 presents in a simplified manner the role of the different hydrogen donors in the thermal stabilization of TD. A hydrogen is abstracted from the n-tetradecane due to the influence of heat resulting in a secondary radical. The additive can then cap the radical at this stage, preventing the propagation of the reaction and leaving the TD intact. Both THN and THNol have shown an ability to operate on secondary radicals in this fashion. However, if a secondary radical is not capped, it will undergo β -scission, yielding a 1-alkene and a primary radical. These primary radicals are targeted by BA. [97] Accordingly, hybrids of BA and THN or BA and THNol should, therefore, have a synergetic effect at low concentrations in enhancing the thermal stabilization of TD.

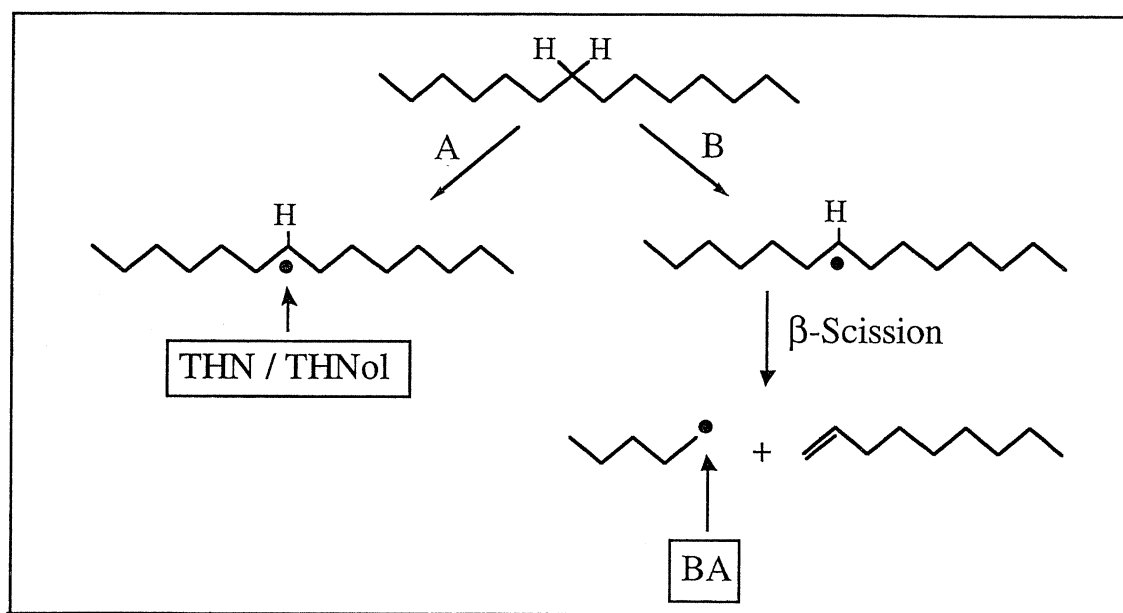


Figure 29. Simplified Role of the Hydrogen Donors, BA, THN, and THNol in the Thermal Stabilization of TD in the Pyrolytic Regime.

Figure 30 compares $TD_i:TD_o$ at 450 °C for the TD mixed with a single hydrogen donor, BA, THN, or THNol at 1-mole percent addition, with that for TD added to a hybrid of BA and THN or BA and THNol, at 0.5 mole percent each. Alone, both THN and THNol yielded a higher thermal stability than that using BA. However, the hybrid of 0.5-mole percent BA and 0.5-mole percent THN resulted in enhanced thermal stability when compared with the 1-mole percent single mixtures. This trend is further supported by the studies at 475 °C, as shown in Figure 31. For the single hydrogen-donor additions at 475 °C, $TD_i:TD_o$ increases from 27 percent for TD alone to around 35 percent with 1-mole percent BA addition; the use of THN has an even higher impact, where this ratio becomes 46 percent (Figure 31). The hybrid of BA and THN would be expected to be in the range of 35 to 46 percent, but gave a result of 52 percent showing a pronounced synergistic effect between these two hydrogen donors. Correspondingly, the effect from the hybrid of BA and THNol would be expected to be in the range 35 to 39 percent, but

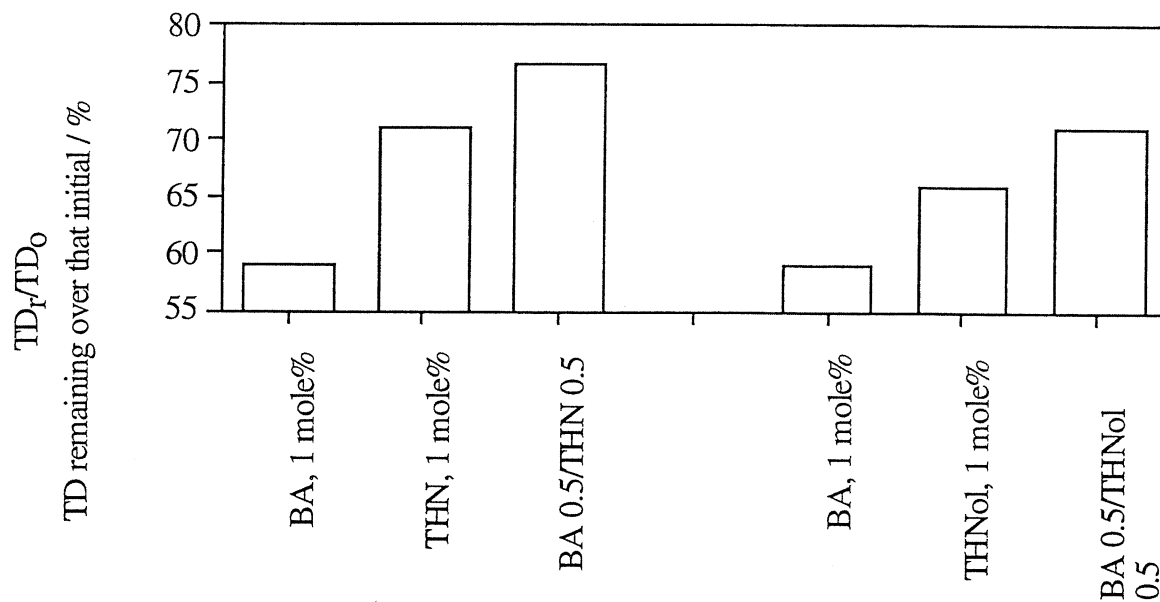


Figure 30. Comparison of the Ratio of TD Remaining to the Initial Amount for TD Mixed with 1 Mole Percent of the Single Hydrogen Donors BA, THN, and THNol, Individually, and with Hybrids at 450 °C

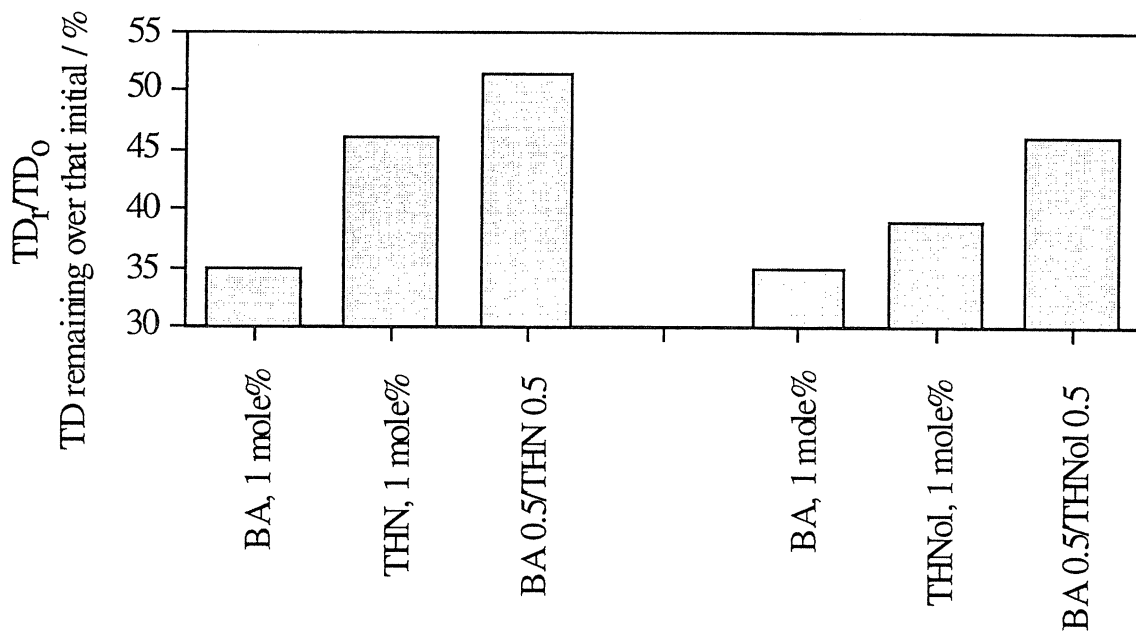


Figure 31 Comparison of the Ratio of TD Remaining to the Initial Amount for TD Mixed with 1 Mole Percent of the Single Hydrogen Donors BA, THN, and THNol, Individually, and with Hybrids at 475 °C

showed an enhancement of up to 46 percent. Although the BA/THN hybrid showed an overall higher thermal stability at both 450 and 475 °C, the synergistic effect from the BA/THNol hybrid was larger, taking into account the effect of the single hydrogen donors. These results are very

promising for the development of additives that can work in both the autoxidative regime (150 to 250 °C) and the pyrolytic regime; further research will study the effect in both these regimes using flow reactors.

8.2.4 Conclusions

Hybrid hydrogen donors of (i) benzyl alcohol (BA) and tetrahydronaphthalene (THN) and (ii) benzyl alcohol (BA) and 1,2,3,4-tetrahydro-1-naphthol (THNol) have shown a synergistic effect on the thermal stabilization of tetradecane (TD) in the pyrolytic regime. The BA/THN hybrid was most effective in stopping the thermal decomposition of the paraffinic TD, but the BA/THNol hybrid showed the highest synergistic effect compared with BA and THNol alone.

8.3 Thermal Stability of Coal-Derived Jet Fuels in the Autoxidative and Pyrolytic Regimes

8.3.1 Introduction

Coal-based liquids have a great potential as precursors for advanced jet fuels that meet the more stringent thermal stability requirements for the future high-Mach jet aircraft. [94] In current commercial planes, the fuel may be exposed to temperatures as high as 300 °C. [98] However, as the flight speed will be increased to high Mach numbers, the fuel is expected to experience temperatures as high as 480 °C (900 °F) in the future, since the jet fuel also functions as the main coolant for the different electronic and mechanical parts of the aircraft. Even though the residence time at such elevated temperatures is expected to be fairly short (matter of minutes), the jet fuels presently used have been shown to form a solid deposition that can lead to catastrophic malfunction of the jet aircraft. The current jet fuels are petroleum-derived and consequently rich in linear alkanes, which are highly susceptible to pyrolytic cracking resulting in coking. [96] The thermal stability of a jet fuel in the pyrolytic regime can be greatly enhanced by utilizing liquids rich in cycloalkanes. [99] This is the case for hydro-treated, coal-derived liquids, where the aromatic structures have been transformed into their corresponding cycloalkanes. [100] An additional problem with jet fuels is the presence of dissolved oxygen (from air), which reacts with the fuel during the autoxidative regime (150 to 250 °C) before the fuel and its oxygenated reaction products enter the pyrolytic regime (400 to 500 °C). [101] Accordingly, section 8.3 compares the thermal stability of a linear alkane (tetradecane), a cycloalkane (decahydronaphthalene), and a coal-derived jet fuel as they go through the autoxidative regime into the pyrolytic regime. Differences in chemical reactivity between the linear alkane and cycloalkane have been related to the stability of the coal-derived jet fuel.

8.3.2 Experimental

The compounds used were tetradecane (TD, Aldrich 99 percent), decahydronaphthalene (DHN, Aldrich 98 percent, a mixture of 46-mole percent cis- and 54-mole percent trans-decahydronaphthalene), and a coal-derived fuel named JP-8C. A volume of 5 mL was charged into a microautoclave with a total volume of 25 mL. [102] The system was pressurized with 100 psi of air and heated in a fluidized sand bath. The heating rate used was approximately 5 °C min⁻¹, and the microautoclaves were removed at 250, 350, 450, and 500 °C. After reaction, the microautoclaves were rinsed of sand and quenched. When the microautoclaves were cooled

to ambient temperature, the gas phase and liquid fraction were removed for analysis. The tube and the stem of the microautoclave were washed in pentane until a clear color was obtained and then dried. The amount of solid deposition was determined from the increase in weight of the tube and stem. The GC-MS was performed on a Shimadzu GC-174 coupled with a Shimadzu QP-5000 MS detector. The column used was a Restek XT15 column, and it was heated from 40 to 290 °C with a heating rate of 6°C min⁻¹.

8.3.3 Results and Discussion

8.3.3.1 *Comparison of Thermal Stability of the Liquids*

The content of liquid remaining for TD, DHN, and the coal-derived jet fuel JP-8C stressed under the influence of air in the temperature range 250 to 500 °C is compared in Figure 32. At low temperatures (250 and 350 °C), the formation of gas and solid products is very small. However, as the temperature is increased to 450 °C, and indeed for the one stressed at 500 °C, the amount of liquid remaining is reduced. The linear alkane TD experiences a drastic reduction in the liquid phase, reaching a level well below 80 percent. JP-8C shows an improved thermal stability relative to TD; more than 90 percent of the liquid remains. The cycloalkane DHN shows the highest ability to resist thermal cracking. The reduction in the liquid produces gas and solids; Figure 33 compares the solid deposition for tetradecane, decahydronaphthalene, and JP-8C stressed under the influence of air in the temperature range 250 to 500 °C. Already at 250 °C, the linear alkane shows a higher formation of solids than do JP-8C and DHN. The solid deposition is not significantly increased at 350 °C but rises sharply when stressed further to 500 °C, following a trend similar to the solid deposition found in flow-reactor studies [103-105]. The cycloalkane shows no solid deposition in the autoxidative zone and does not form solids at temperatures up to 500 °C, confirming the previous thermal-stressing behavior of DHN [99]. The coal-derived fuel also shows low solid deposition in the autoxidative zone, but at higher temperatures there is a significant increase in the formation of solids, which may be related to the chemical composition of JP-8C. Figure 34 shows the general composition of JP-8C, which consists of alkanes, cycloalkanes, hydroaromatics, alkyl-benzenes, and naphthalenes. Although the fuel is dominated by cycloalkanes (around 50 percent), there is a significant part consisting of 10 percent alkanes, which may be oxidized in the autoxidative zone, leading to increased thermal deposition in the pyrolytic regime.

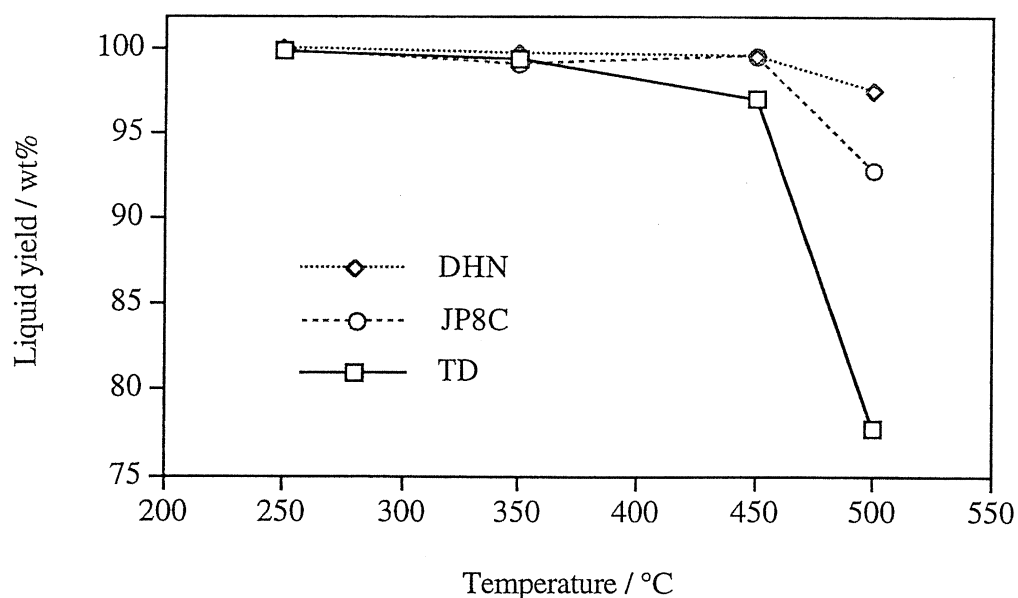


Figure 32. Comparison of Liquid Remaining for Tetradecane, Decahydronaphthalene, and the Coal-Derived Jet Fuel JP-8C Stressed Under the Influence of Air in the Temperature Range 250 to 500 °C

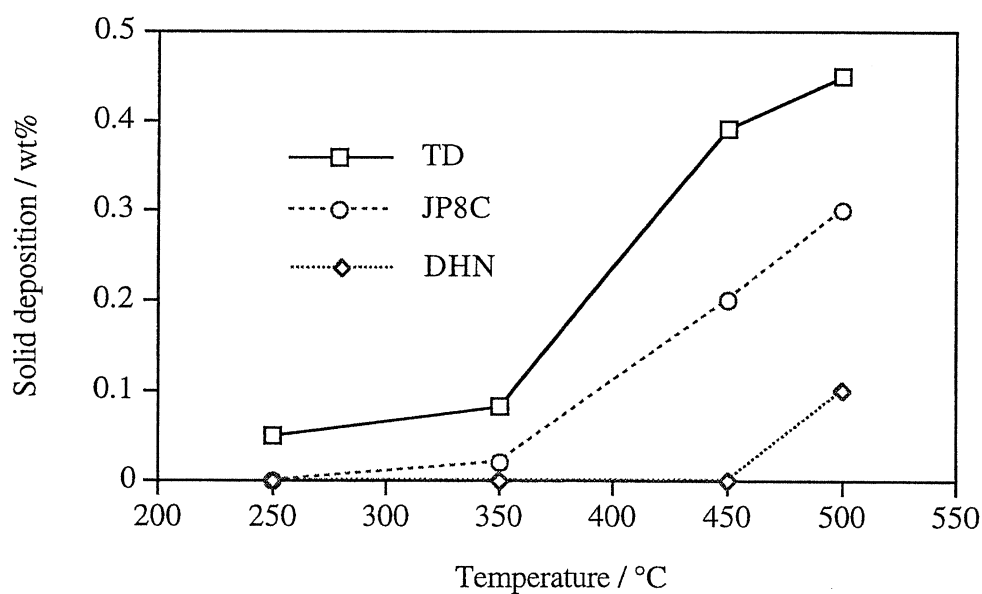


Figure 33. Comparison of Solid Deposition for Tetradecane, Decahydronaphthalene, and the Coal-Derived Jet Fuel JP-8C Stressed Under the Influence of Air in the Temperature Range 250 to 500 °C

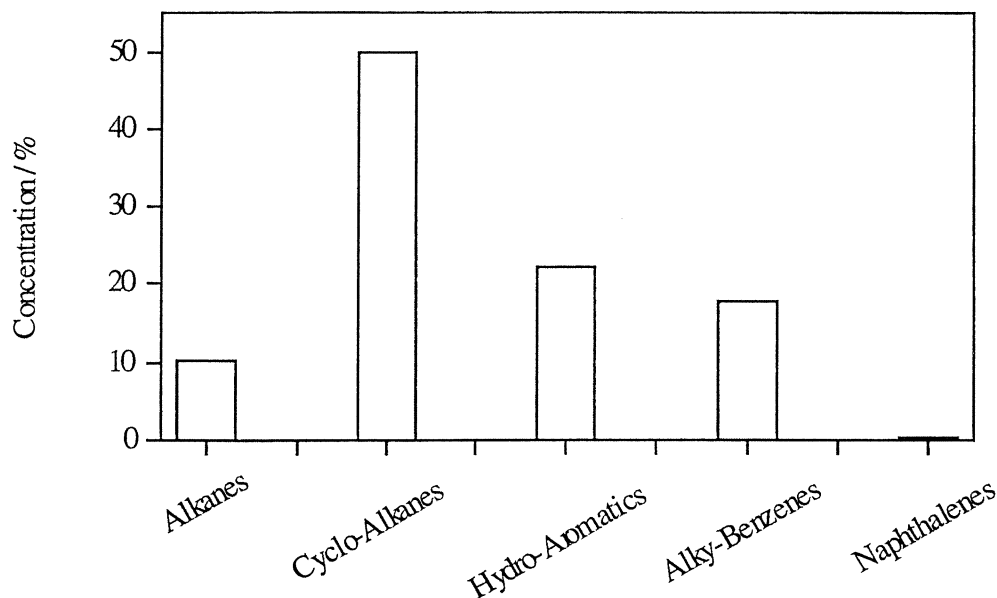


Figure 34. General Composition of the Coal-Derived Jet-Fuel JP-8C

The vast difference in liquid yield between liquids rich in linear alkanes and those containing mainly cycloalkanes (including the JP-8C), shown in Figure 32, can be explained further by studying the ability of the different hydrocarbons to resist thermal cracking. Figure 35 shows the variation in the remaining concentration of TD and DHN with temperature. In the autoxidative zone, the reduction in the concentration of the two compounds is small. However, as the temperature reaches the pyrolytic regime, a large difference in thermal stability between these two compounds appears. At 500 °C, only around 35 percent TD remains, whereas 85 percent of the DHN is unreacted.

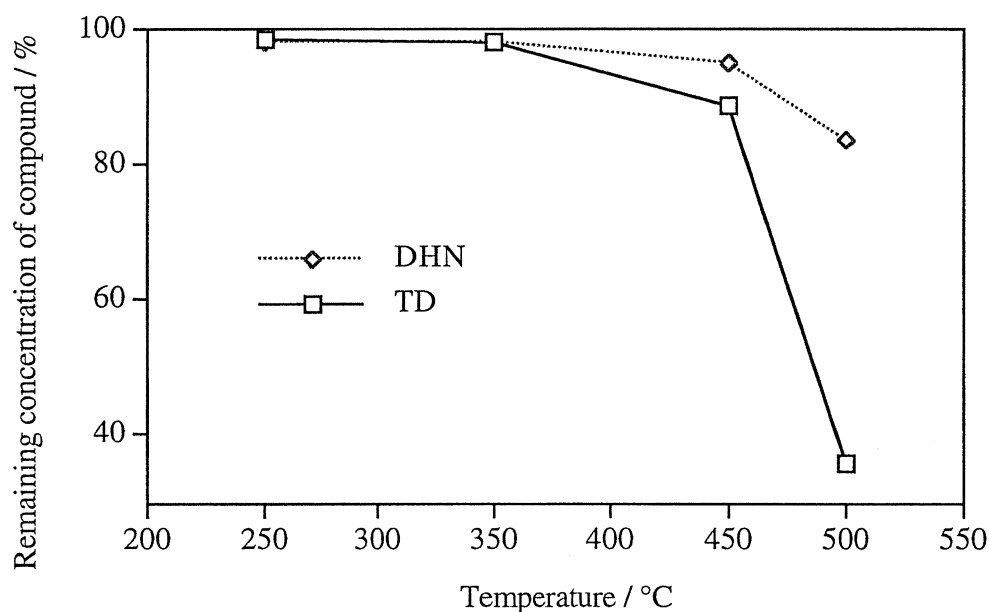
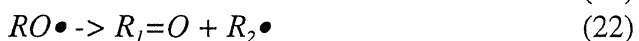
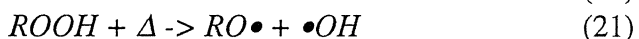
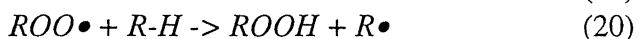
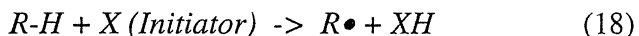


Figure 35. Variation in the remaining concentration of tetradecane (TD) and decahydronaphthalene (DHN) with temperature

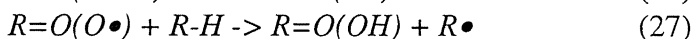
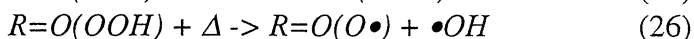
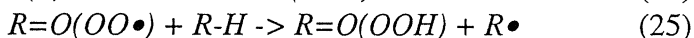
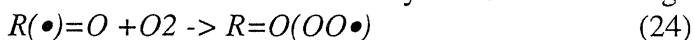
8.3.3.2 Thermal Cracking Products from Tetradecane under Autoxidative and Pyrolytic Conditions

The above differences in thermal stability can be related to the differences in the oxidation chemistry in the autoxidative zone and the thermal stability of the oxygenated compounds from linear alkanes and cycloalkanes remaining in the liquid. Figure 36 shows the GC/MS traces of the reaction products from stressing tetradecane under 100 psi air from room temperature up to 250, 350, 450, and 500 °C (listed from bottom to top, heating rate 5 °C/min). At 250 °C, a range of linear alkanes is present; at a 6-minute retention time, n-octane appears. A row of compounds with oxygen functional groups is associated with each linear alkane; for instance, butanoic acid, 2-hexanone, and hexanal appear next to n-octane. The production of acids, aldehydes, and ketones from oxidation in the autoxidative zone has been found previously; these species are derivatives of peroxides and alcohols formed at a lower temperature. The compounds present at 250 °C do not change when stressed up to 350 °C, but a drastic change in the product distribution appears as the temperature is increased to 450 °C. At this temperature, the concentration of n-alkanes is greatly increased; 1-alkenes are also produced as a result of thermal cracking [97]. Although some oxygenated compounds still remain in solution, the reactivity of these species clearly adds to the thermal degradation of the linear-alkane TD.

The differences in thermal stability found between tetradecane and decahydronaphthalene, as described here, can be related to the differences in the oxidation chemistry in the autoxidative zone and the thermal stability of the oxygenated compounds from linear alkanes and cycloalkanes remaining in the liquid. From Figure 36, a range of linear-alkane products is present; at a 6-minute retention time, n-octane appears. A row of compounds with oxygen functional groups that are derivatives formed from peroxides at lower temperatures is associated with each linear alkane. The main reaction mechanism is:



A hydrogen is abstracted from the hydrocarbon by an initiator such as a metal surface, creating a free radical (18). Further reaction with oxygen in the fuel forms a peroxy radical (19), which abstracts an H from another hydrocarbon and forms a hydroperoxide (20). Reactions 1 to 3 are well documented in the literature and cause great concern, even at room temperature; hence, most research has been focused at low temperatures [106, 107]. At elevated temperatures, which is the case for jet fuels, the hydroperoxide will auto-initiate as shown in reaction (21) to form an alkoxy radical. [108] The alkoxy radical then undergoes β -scission (22) to form ketones and aldehydes. [109] The array of alkanes is formed through hydrogen abstraction (23). Acids originate from the autooxidation of aldehydes as shown through reactions 24-27. [108]



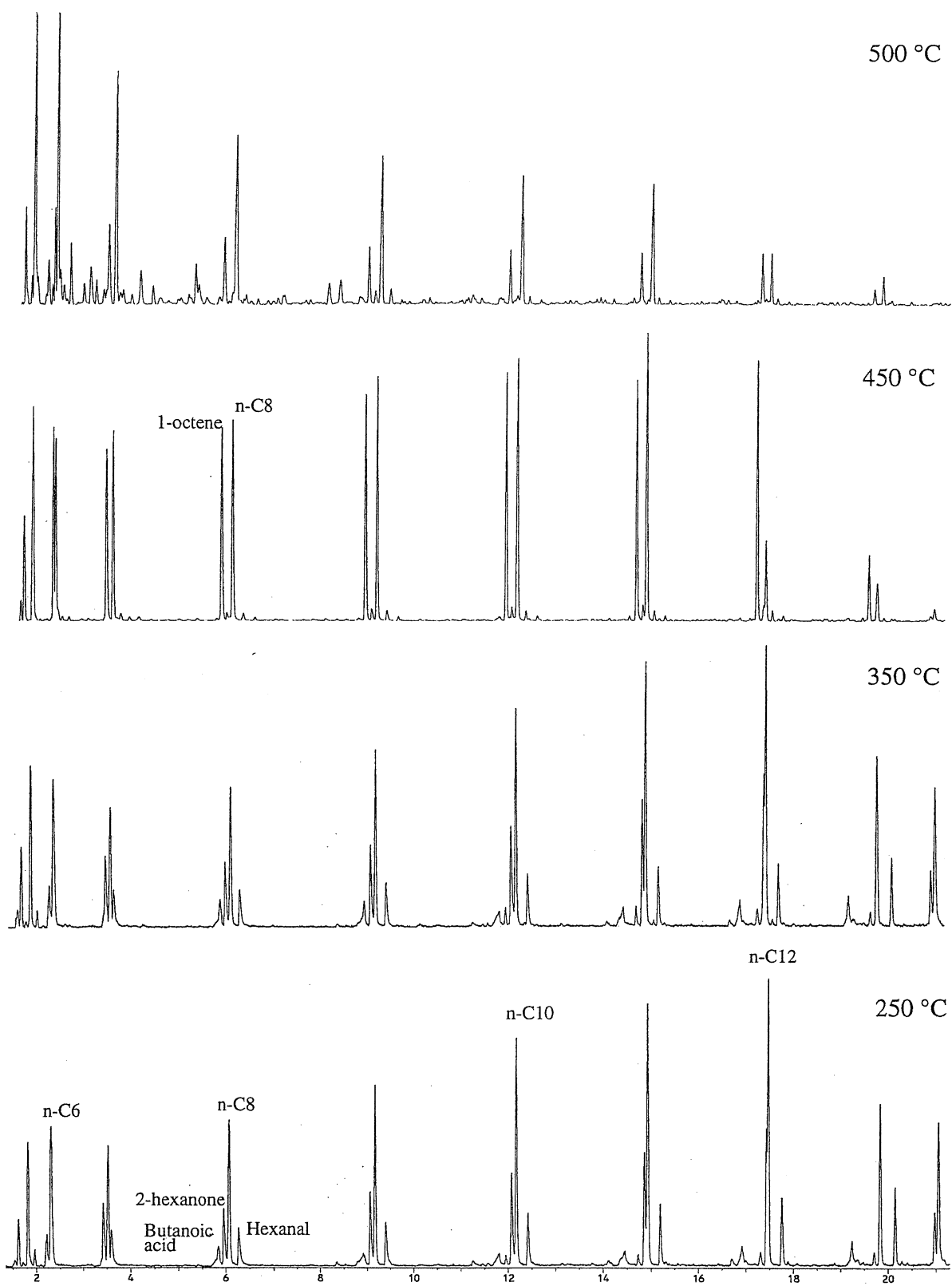


Figure 36. GC/MS Traces of the Reaction Products from Stressing Tetradecane in Air Up to 250, 350, 450, and 500 °C (listed from bottom to top and not to scale)

8.3.3.3 Thermal Cracking Products from Decahydronaphthalene under Autoxidative and Pyrolytic Conditions

The cycloalkane DHN also experiences oxidation in the autoxidative zone, as shown in Figure 37. The mixture of trans- and cis-decahydronaphthalene used here (retention times of 14 and 15 minutes, respectively) yielded only discrete groups of oxygenated products, which appear in a narrow retention-time range of 18 to 21 minutes. Figure 38 shows the GC/MS trace from the reaction products at these retention times from stressing DHN in air at temperatures reaching 250 °C. Ketones and alcohols, in particular, dominate; compounds such as 2-butyl cyclohexanone and decahydronaphthol are also abundant. The presence of alcohols in the products from DHN indicates that oxygenated cycloalkane compounds are more stable than their linear equivalents. Also, the very low concentration of acids indicates that a cycloalkane- rich liquid is less corrosive. As the temperature is increased to 450 °C, only small changes in the product distribution occur, again affirming the higher stability of cycloalkane-derived compounds resulting from the capture of oxygen. By increasing the stressing to 500 °C, non-oxygenated single-ring compounds such as 1-methyl cyclohexene appear at lower retention times, but the oxygenated compounds are still present. The development of the hydrogen-donor tetrahydronaphthalene may also further enhance the thermal stability of the liquid.

8.3.3.4 Structural Changes of JP8C under Autoxidative and Pyrolytic Conditions

The changes in the product distribution from the coal-derived jet fuel, JP8C, stressed under air at 250 and 500 °C are shown by the GC/MS traces in Figure 39. At 250 °C, JP8C is rich in one- and two-ring cycloalkanes, but at longer retention times, a series of long-chain linear alkanes in the range of C12 to C18 is present. When stressed to 500 °C, only small changes in the cycloalkane distribution occur, whereas the concentration of the linear alkanes has decreased drastically. Based on the study of TD stressing in both the autoxidative zone and the pyrolytic regime, the reduction in the linear-alkane concentration can be due to two reasons: First, the tendency of linear alkanes to react with oxygen and form less stable compounds, and second, the lower thermal stability of linear alkanes themselves in comparison with cycloalkanes.

8.3.4 Conclusions

The changes in product distribution for the linear-alkane tetradecane (TD) and the cycloalkane decahydronaphthalene (DHN) are related to the cycloalkane-rich, coal-derived liquid JP8C. Linear TD shows less thermal stability than do JP8C and, particularly, DHN. This is associated with the formation of a range of oxygenated compounds from TD such as acids, aldehydes, and ketones, which show a lower thermal stability than those oxygenated compounds derived from DHN. In the coal-derived liquid, the high content of cycloalkanes resulted in a significant amount of liquid remaining. However, a relatively high concentration of linear alkanes (10 percent) in the range C12-C18, with their tendency to oxidize and crack in the pyrolytic regime, resulted in higher solid deposition than observed for DHN.

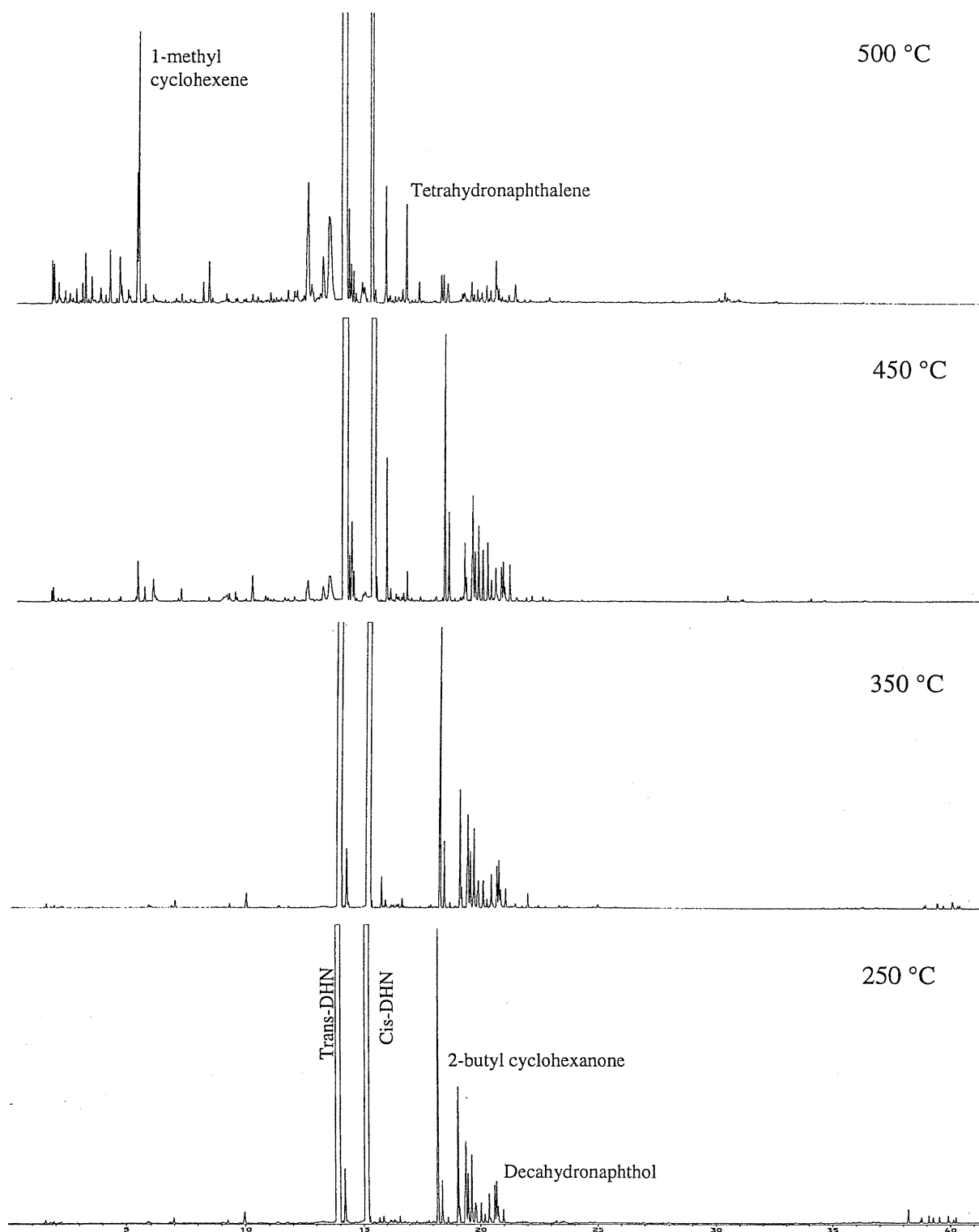


Figure 37. GC/MS Traces of the Reaction Products from Stressing Decahydronaphthalene in Air at 250, 350, 450, and 500 °C (listed from bottom to top and not to scale)

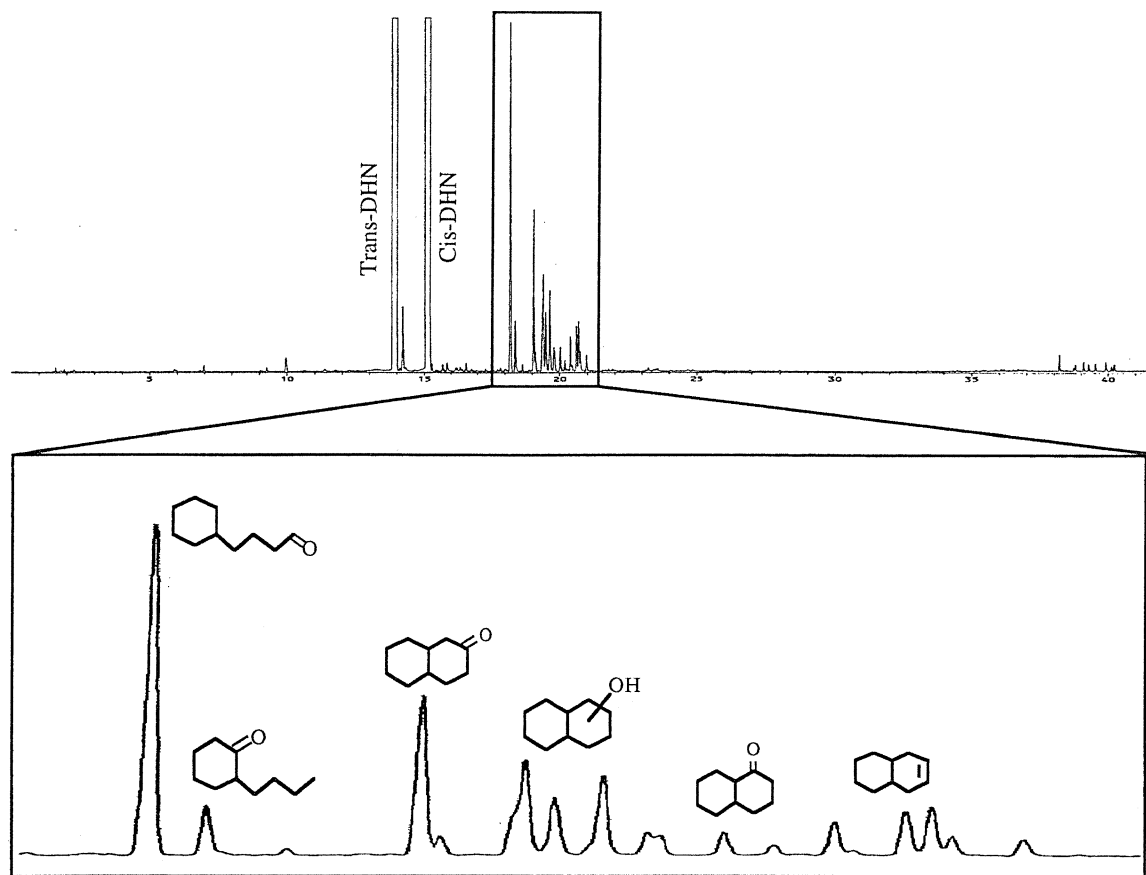


Figure 38. Major Oxygenated Compounds from Decahydronaphthalene Stressed Under Air and Heated to 250 °C

9.0 DECOMPOSITION AND SOLID DEPOSITION FOR COAL-BASED FUELS: FUEL COMPOSITION/PHASE AND SURFACE EFFECTS

9.1 Introduction

The principal objective of this subtask in conjunction with thermal stability of advanced jet fuel [110-112] was to study the effects of jet-fuel composition on deposit formation using model-compound mixtures. The experimental approach consisted of carrying out thermal-stressing experiments in a flow reactor with selected model compounds consisting of alkanes, cycloalkanes, and aromatics and their binary and ternary mixtures in the presence of Inconel 600 coupons. Thermal-stressing products were analyzed by GC-MS, and the carbonaceous deposits were characterized by both multiphase carbon analysis and scanning electron microscopy. The role of sulfur compounds in solid deposition on metal surfaces was also investigated with the addition of sulfur compounds like thiophene or dimethylsulfide (at ppm levels) to model compounds before thermal stressing.

9.2 Experimental

Thermal stressing of dodecane, methylcyclohexane, and toluene and their binary and ternary mixtures was carried out in the presence of Inconel 600 foil. The detailed nominal composition of Inconel 600 is Ni:74.4, Fe:8, Cr:15.5, Cu:0.5, Mn:1.0, Si:0.5, C:0.15, and S:0.0015 percentw. For stressing experiments, a 15 by 0.3-cm coupon of the superalloy foil was placed at the bottom of a 20-cm, 6.3-mm OD, and 4-mm ID glass-lined tube reactor. The thickness of the foils was 0.075 mm. Before introducing the model hydrocarbons, the reactor was heated to a 500 or 600 °C wall temperature, depending on the reaction temperature, for 2 hours under flowing nitrogen at 250/500/1000 psig. The hydrocarbon was preheated to 250 °C before entering the reactor. The reactor wall temperature and the fuel pressure were kept constant throughout the experiments at 500/600 °C and stressing pressure. Under these experimental conditions, hydrocarbons are in a supercritical state. The flow rate of model compound was maintained at 1 cc/min for 5 hours. The stressed foils were analyzed using a LECO-RC 412 Multiphase Carbon Determinator to obtain the total carbon deposition on the foils as well as the temperature-programmed oxidation (TPO) profiles of the deposits. The morphology of the deposits was examined with an ISI-DS 130 Dual Stage (SEM).

9.3 Results and Discussion

9.3.1 Single Compounds

Table 16 shows the carbon deposits collected on Inconel 600 surface from the thermal stressing of dodecane, toluene, and methylcyclohexane at 500 °C and 500 psig for 5 hours with 1 mL/min flow rate. The deposit amounts were determined by using an LECO carbon analyzer.

Table 16. Carbon deposits from stressing dodecane, toluene, and methylcyclohexane on an Inconel 600 alloy.

Compound	Carbon deposition ($\mu\text{g}/\text{cm}^2$)
Dodecane	19.0
Toluene	17.3
Methylcyclohexane	0.9

Thermal stressing of dodecane and toluene produced a much higher amount of deposit compared with that obtained from methylcyclohexane. The reaction products from n-dodecane are a series of n-alkanes and 1-alkenes lighter than n-dodecane. The decomposition of methylcyclohexane gave very low yields of liquid products that were not identified by GC analysis. The GC chromatogram of the liquid sample obtained after the reaction of toluene showed no significant difference from that of original toluene.

Dodecane and toluene gave almost the same amount of carbon deposits. Methylcyclohexane, however, produced 20 times less deposition than did the others. TPO profiles in Figure 40 show that the peak positions of the oxidation of the deposits to CO_2 are almost identical for the toluene and dodecane deposits. There are four basic peaks evolving at 350, 500, 650, and 750 °C indicating amorphous and catalytic deposit formation. For methylcyclohexane, there is a low-intensity peak that evolved between 250 and 450 °C. Figure 41 shows the SEM micrographs of the deposits obtained from the three single compounds. The deposits from dodecane (Figure 41a) and toluene (Figure 41b) contain both amorphous and filamentous structures, indicating both catalytic and thermal-deposition processes. In the case of methylcyclohexane (Figure 41c), the surface is almost clean except for the presence of some small filaments and particulate deposit formation along a scratch on the Inconel 600 surface. The deposit formation from methylcyclohexane appears to have begun after 5 hours of stressing in contrast to the complete coverage of the coupon surface by heavy deposition from dodecane and toluene stressing.

The thermal-stressing experiments on toluene, dodecane, and methylcyclohexane were also carried out in a glass-lined flow reactor at a 600 °C isothermal wall temperature, 500 psig, and a flow rate of 1cc/min. Thermal stressing was carried out in the presence of Inconel 600 coupons. Table 17 shows the amount of deposit collected on the Inconel 600 surface at a 600 °C stressing temperature for dodecane, toluene, and methylcyclohexane. In this case, toluene produced more deposit than did dodecane, but again, methylcyclohexane gave much less deposition than did dodecane. Figure 42 shows the TPO profiles of the deposits formed from the three different hydrocarbons. Unlike the TPO profiles of the deposits obtained at 500 °C, which contained three or four peaks at different temperatures, deposits produced at 600 °C gave a single peak at an intermediate temperature. The absence of low- and high-temperature peaks in the TPO profiles can be attributed to the dominance of thermal reactions at 600 °C with a less-pronounced effect from metal surface catalysis. Higher deposition from toluene compared with that from dodecane also points to the controlling role of thermal reactions leading to carbon deposition at this temperature.

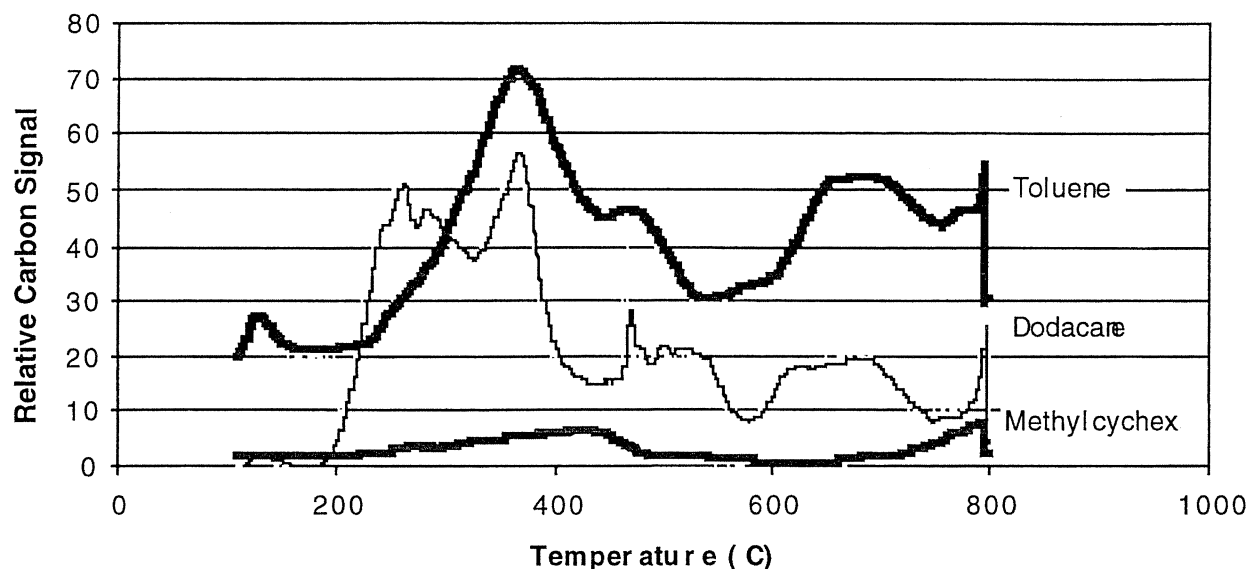


Figure 40. TPO Profiles of Carbon Deposits from Thermal Stressing of Dodecane, Toluene, and Methylcyclohexane at 500 °C and 500 psig for 5 h with a 1 mL/min Flow Rate

The SEM micrographs in Figure 43 show the morphology of the carbon deposits obtained from the three hydrocarbons on Inconel 600 at 600 °C. Figure 43a shows dodecane deposits where the coated tips of very short filaments can be observed. This indicates that the initiation of filamentous carbon formation was arrested by thermal deposition of amorphous carbon on active metal tips. Many areas on the coupon were covered with amorphous deposits. More extensive thermal deposition of carbon was observed with toluene stressing, as seen in the micrograph in Figure 43b. Many regions of the coupon surface show the formation of spherules on top of amorphous layers, indicating extensive deposition by thermal polymerization processes. Figure 43c shows coated fibers on the coupon surface stressed with methylcyclohexane, similar to those observed in the deposit from dodecane; however, only appearing on the surface defects, with the remaining surface still clean.

Table 17. The amount of deposit formed from toluene, dodecane, and methylcyclohexane at 600 °C and 500 psig with 1 cc/min flow rate for 5 h

Compound	Deposit ($\mu\text{g}/\text{cm}^2$)
Toluene	425.3
Dodecane	215.1
Methylcyclohexane	36.6

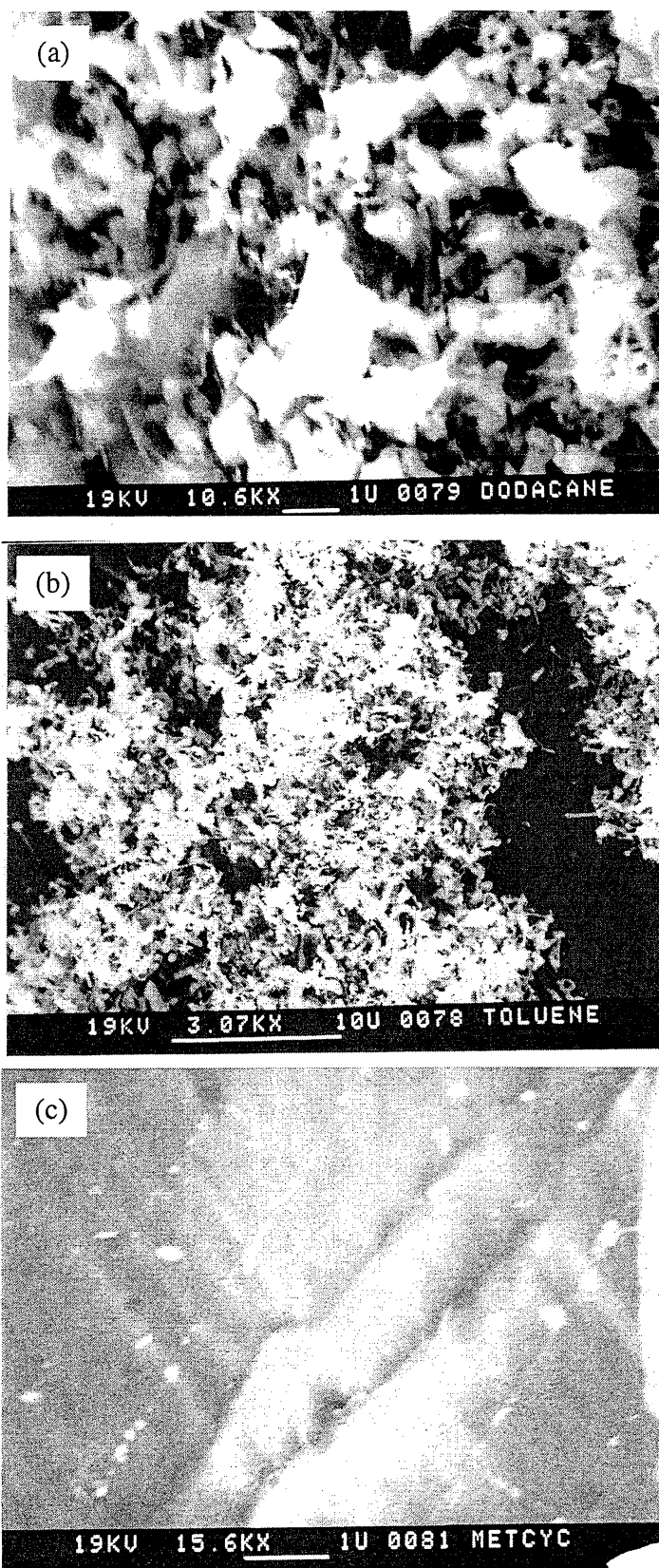


Figure 41. SEM Micrographs of Carbon Deposits from Dodecane (a), Toluene (b), and Methylcyclohexane (c) at 500 °C and 500 psig for 5 h with a 1 cc/min Flow Rate

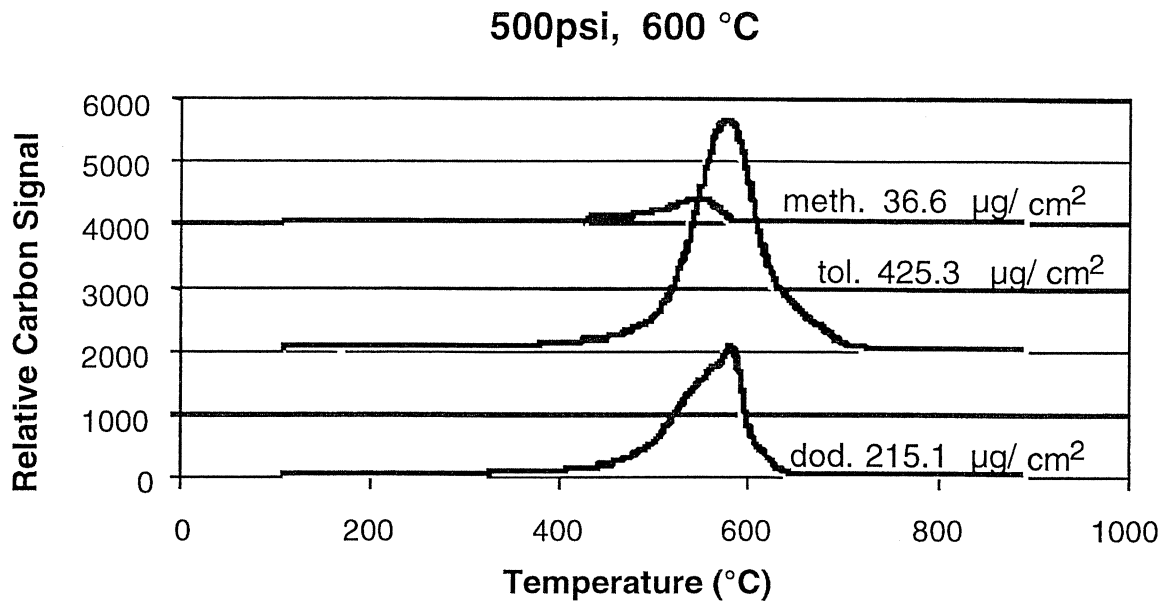


Figure 42. TPO Profiles of Carbon Deposits from Stressing Toluene, Dodecane, and Methylcyclohexane on Inconel 600 in a Glass-Lined Flow Reactor at 600 °C

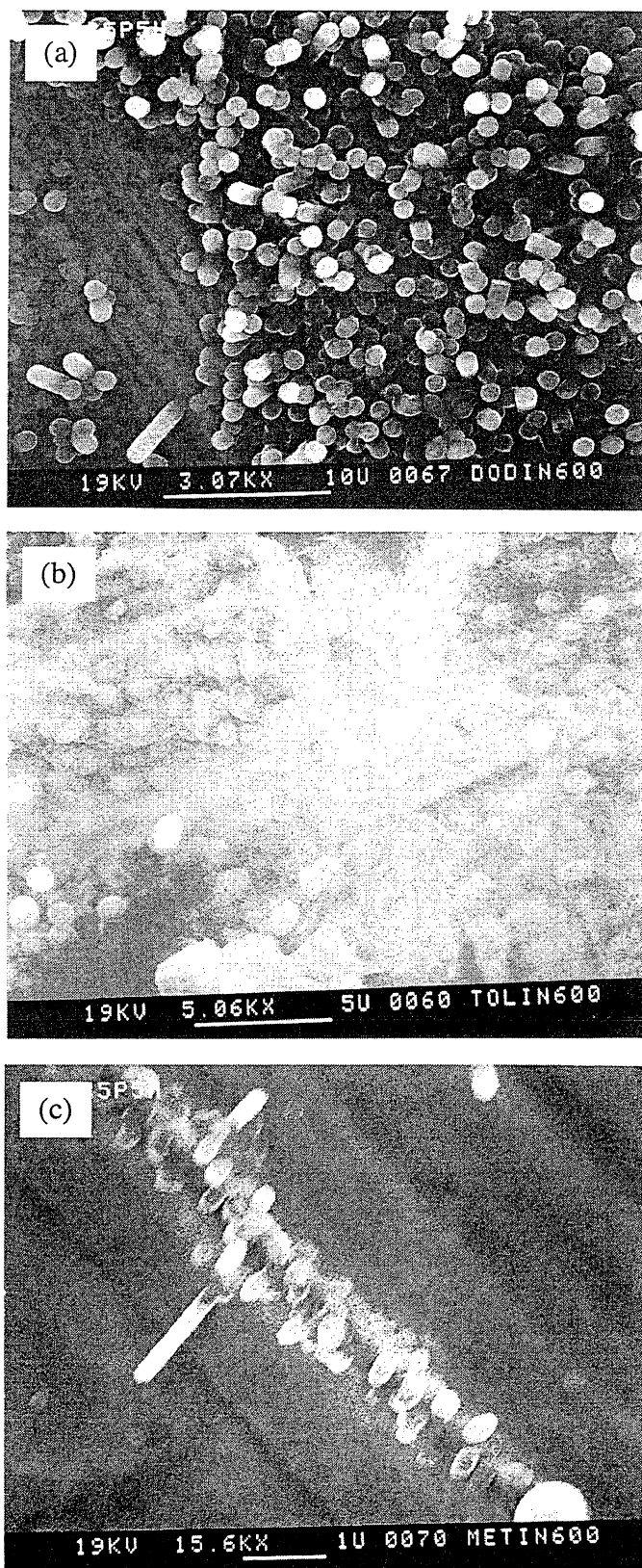


Figure 43. SEM Micrographs of Deposits from Dodecane (a), Toluene (b), and Methylcyclohexane (c) Decomposition at 600 °C and 500 psig for 5h with a 1 cc/min FlowRate

9.3.2 Binary Mixtures

Thermal stressing of 50 percent (vol.) of n-dodecane and methylcyclohexane and 50 percent (vol.) of n-dodecane and toluene mixtures was carried out in the presence of an Inconel 600 coupon at 500 °C and 500 psig with a flow rate of 1 cc/min. The amounts of carbon deposits obtained from stressing the binary mixtures are shown in Table 18. Both mixtures produced lower overall deposition compared with those obtained from single-compound stressing. Lower deposition from the n-dodecane and methylcyclohexane mixtures is understandable considering the hydrogen-transfer reactions between alkyl radicals and methylcyclohexane. It is, however, difficult to explain why the toluene and n-dodecane mixture gave a lower deposition compared with the amount calculated from the individual contributions of single components. What is clear is that the stressing of these mixtures shows nonadditive effects in terms of solid deposition, as would be expected in a chemically controlled process with interactions of reactive species produced from each component.

Table 18. Carbon deposits from dodecane+methylcyclohexane and dodecane+toluene mixtures on Inconel 600

Compound	Carbon deposition ($\mu\text{g}/\text{cm}^2$)
Dodecane+methylcyclohexane	6
Dodecane+toluene	11

As shown in Figure 44a, both mixtures produced similar types of deposits displaying similar reactivities toward oxygen during TPO analysis. Both mixtures produced two main peaks at burn-off temperatures of 400 and 750 °C. Figure 44b shows the SEM image of deposits produced from a dodecane+methylcyclohexane mixture at 500 °C. There are both filamentous and plate-like structures present in the deposits. These structures were also observed in deposits obtained from single dodecane decomposition at 500 °C. Although the presence of methylcyclohexane decreased the amount of deposit formation, there is no visible difference in the morphology of the deposits obtained from the mixtures.

Carbon deposition from binary mixture

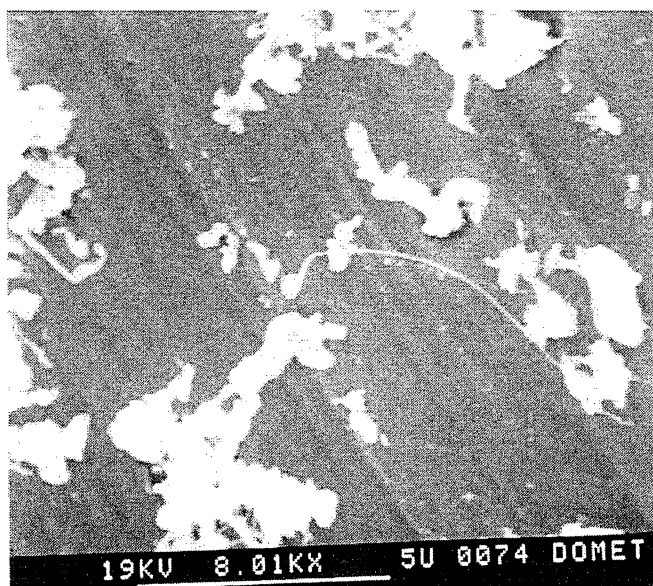
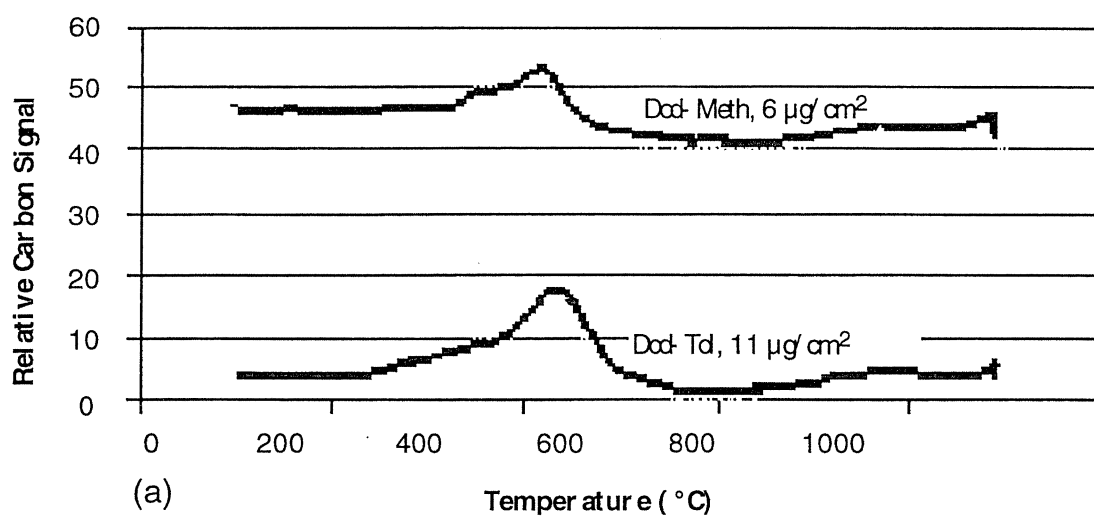


Figure 44. TPO Profiles of Carbon Deposits and SEM Micrographs of Carbon Deposits Formed from Dodecane and Methylcyclohexane.

9.3.3 Ternary Mixtures

Thermal stressing of a ternary mixture of n-dodecane, methylcyclohexane, and toluene was conducted in an isothermal flow reactor in the presence of Inconel 600 coupons at 500 °C and three different pressures, 250, 500, and 1000 psig. A constant-mass flow rate (1 cc/min of liquid sample) was used. The ternary mixture consisted roughly of one third of each component in volume. The critical temperature and pressure of the mixture are 336 °C and 560 psia, respectively, calculated using the methods recommended in the American Petroleum Institute Technical Data Book. The gaseous and liquid products were analyzed by a Perkin Elmer Auto System GC and a Perkin Elmer 8500 GC, respectively. The coupons with solid deposits were examined by SEM, and the amounts of the deposits were determined by an LECO Multiphase Carbon Analyzer.

The conversions of n-dodecane were lower than 1 percent because of the short reactant residence times (seconds) in the reactor. High-pressure conditions gave higher n-dodecane conversion than low-pressure conditions because of the longer residence times at high pressures. The reaction products were predominantly from the decomposition of n-dodecane, indicating that toluene and methylcyclohexane have a much higher thermal stability than does n-dodecane. At 500 °C, the individual n-alkane/1-alkene ratio from C₈ to C₁₁ decreased as the pressure and the conversion increased. These results are different from those obtained from the decomposition of n-dodecane in a glass-tube reactor at 425 °C and different pressures. In glass reactors, high pressures or high conversions favor the formation of the n-alkane over the 1-alkene with the same number of carbon atoms, for the C₆ to C₁₁ components. This difference may result from different reaction temperatures, different residence times, the presence of toluene and methylcyclohexane, or some other factors. One interesting observation is that among the C₇ to C₁₁ products, n-C₁₁ is the most abundant. This is unexpected because according to free-radical mechanisms, the n-C₁₁ yield should be lower than that of any n-alkane from C₆ to C₁₁.

The amounts of carbon deposits are given in Table 19. The deposits collected from each experiment have two different carbon burn-off phases, amorphous and catalytic. At 500 °C and 200 psig, both phases are low compared with those obtained at 500 and 1000 psig. The amount of deposits at 500 psig is higher than that for 1000 psig. The same result was obtained previously for JP-8 decomposition on an Inconel 600 surface.

Table 19. The amount of carbon deposit obtained from thermal stressing n-dodecane, methylcyclohexane, and toluene at 500 °C

P(psig)	Carbon deposit (μg/cm ²)
200	9.8
500	2.0
1000	0.8

In Figure 45, TPO analysis shows that the peak positions for the carbon burn-off reactivity of deposits in oxygen for different pressures are similar. Two peaks are observed for the deposits from stressed ternary mixtures at different pressures. The burn-off temperature of the deposits lies between 375 and 750 °C.

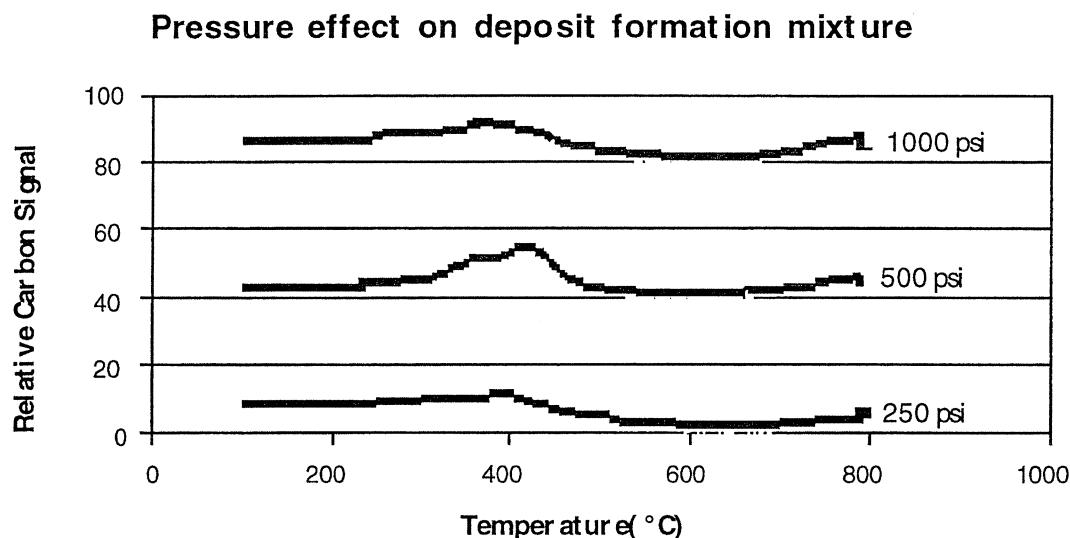


Figure 45. TPO Profiles of Deposits from Thermal Stressing of a Ternary Mixture of Dodecane, Toluene, and Methylcyclohexane for Different Pressures at 500 °C

The SEM micrographs in Figure 46 show the initiation of filamentous carbon deposition at 200 psig with the appearance of small filaments of 0.1- μm diameter. At 500 psig, more filaments formed with the appearance of some long filaments on the alloy surface. The length of longest filament is approximately 4 μm . At 1000 psig, thicker filaments with diameters between 0.2 and 0.3 μm were observed on the Inconel 600 surface. On the basis of the carbon burn-off results, the thickening of the carbon filaments can be attributed to secondary solid deposition on filament surfaces. It appears that decomposition of n-dodecane at very low conversion levels (~1 percent) provides the precursors for filamentous carbon formation

The observed effect of pressure can be explained by the following propositions.

- (1) Increasing the pressure (density increases) increases the residence time of fuel in the reaction zone.
- (2) At high pressure, radicals produced due to cracking may be terminated in high quantity.
- (3) Adsorption and diffusion of hydrocarbons through the metal surface is very low.

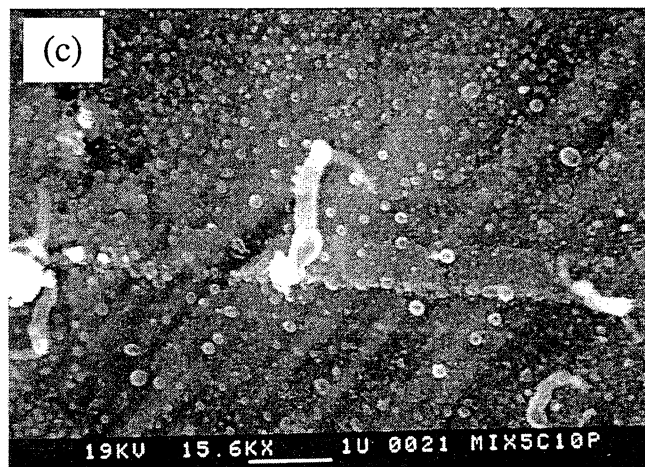
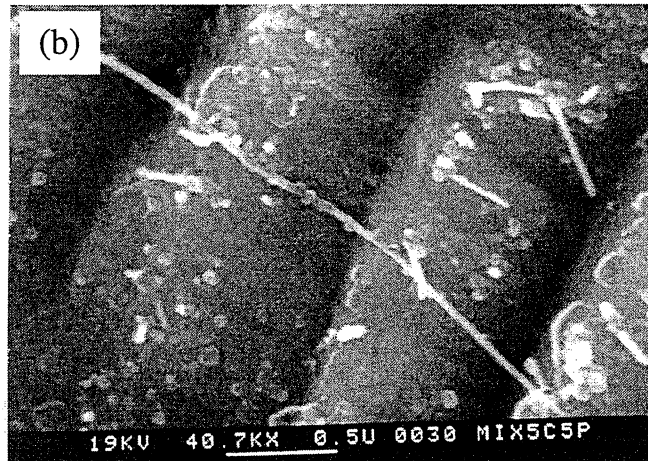
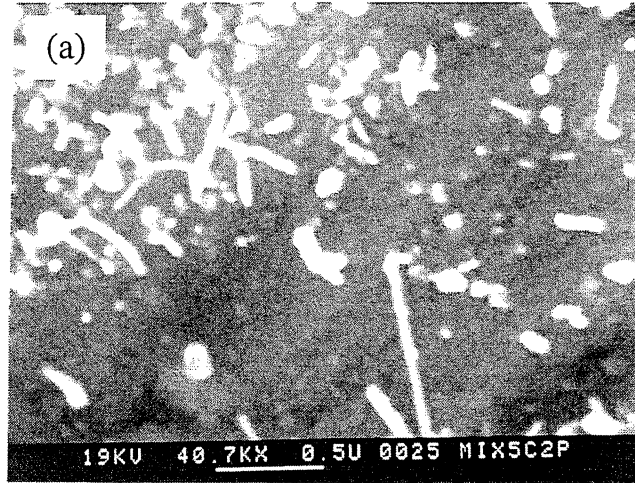


Figure 46. SEM Images of Deposits from Thermal Stressing of an n-Dodecane, Toluene, and Methylcyclohexane Mixture at Various Pressures

9.3.4 Effect of Sulfur Addition

In this part of the study, we carried out thermal-stressing experiments on dodecane and methylcyclohexane containing thiophene, C_4H_4S (as the sulfur source), in a glass-lined flow reactor at a 500 °C isothermal wall temperature, 500 psig, and a flow rate of 1 cc/min. Thermal stressing was carried out in the presence of Inconel 600 coupons. The sulfur content in both dodecane and methylcyclohexane was adjusted to 100 ppm.

Table 20 shows the amounts of carbon deposit formed from dodecane and methylcyclohexane on Inconel 600 foil with and without thiophene. Addition of thiophene increased deposit formation slightly with both dodecane and methylcyclohexane.

Figures 47a and 47b indicate that both reactive (possibly amorphous) and less-reactive (more ordered) deposits were increased by sulfur addition. A more pronounced effect was seen, however, with the catalytic deposition (ordered carbon). It should be noted that the addition of 100-ppm thiophene increased the area of the high-temperature peak appearing at 750 °C, shown in Figure 47a. Therefore, it is probable that an increase in sulfur content promotes the catalytic activity of the Inconel 600 surface by producing a highly stable (ordered) carbon deposit. Possible reasons for increased deposition of catalytically formed carbon with sulfur addition could be:

- (1) Enhanced solubility and diffusion of carbon through the metal surface [113]
- (2) Formation of hydrogen sulfide that attacks the alloy leading to grain boundary embrittlement [114]

Table 20. The Amount of Deposit Formed from Dodecane and Methylcyclohexane on Inconel 600 with and without Added Thiophene at 500 °C, 500 psig, with 1-cc/min Flow Rate for 5 h

Hydrocarbon	Deposit ($\mu\text{g}/\text{cm}^2$)	
	no S	100-ppm S
Dodecane	19	23
Methylcyclohexane	1	3

Addition of thiophene affected the morphology of the deposit, producing much higher concentrations of filamentous carbon on the surface compared with that obtained without thiophene. Figure 48 shows a SEM micrograph of the carbon deposit on Inconel 600 with 100-ppm thiophene at a magnification of 10K. Both coiled and straight filaments are visible in the micrograph. No coiled filaments were observed in the deposit obtained from n-dodecane without the added sulfur. The EDS elemental analysis was also conducted on the filamentous carbon shown in Figure 48. The EDS results gave a strong S peak, indicating that the carbon deposit had a high concentration of S, as expected.

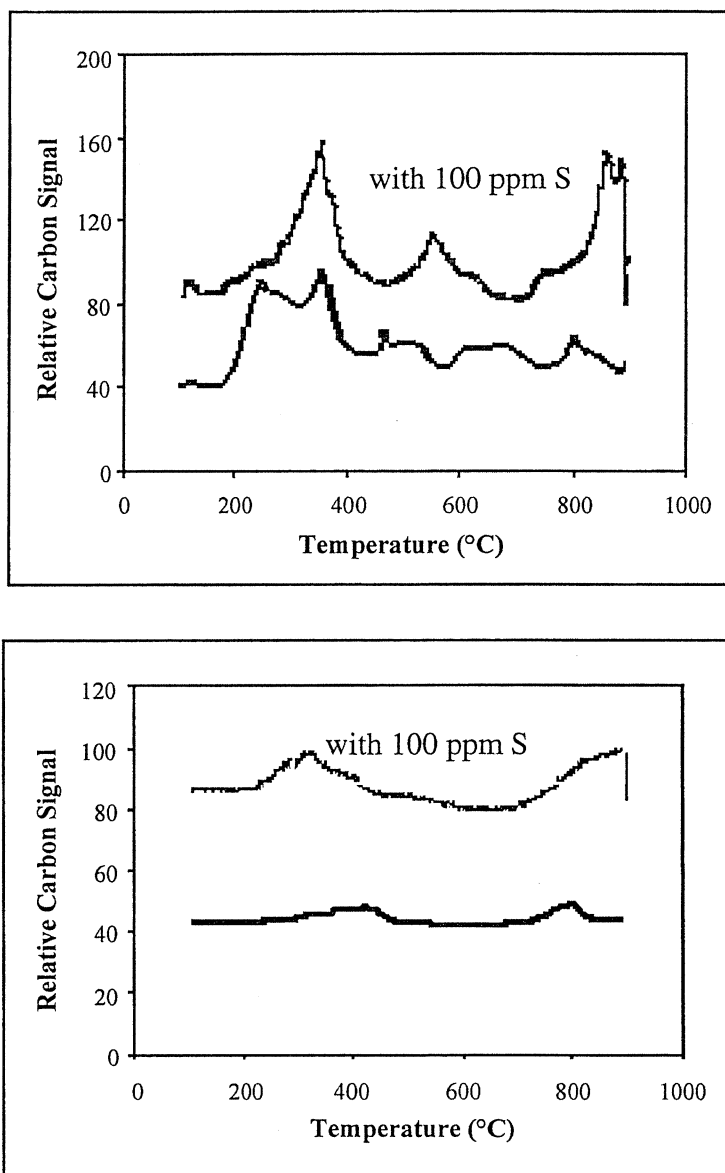


Figure 47. Carbon Burn-Off Profiles Showing the Effect of 100-ppm Thiophene Addition to Dodecane and Methylcyclohexane

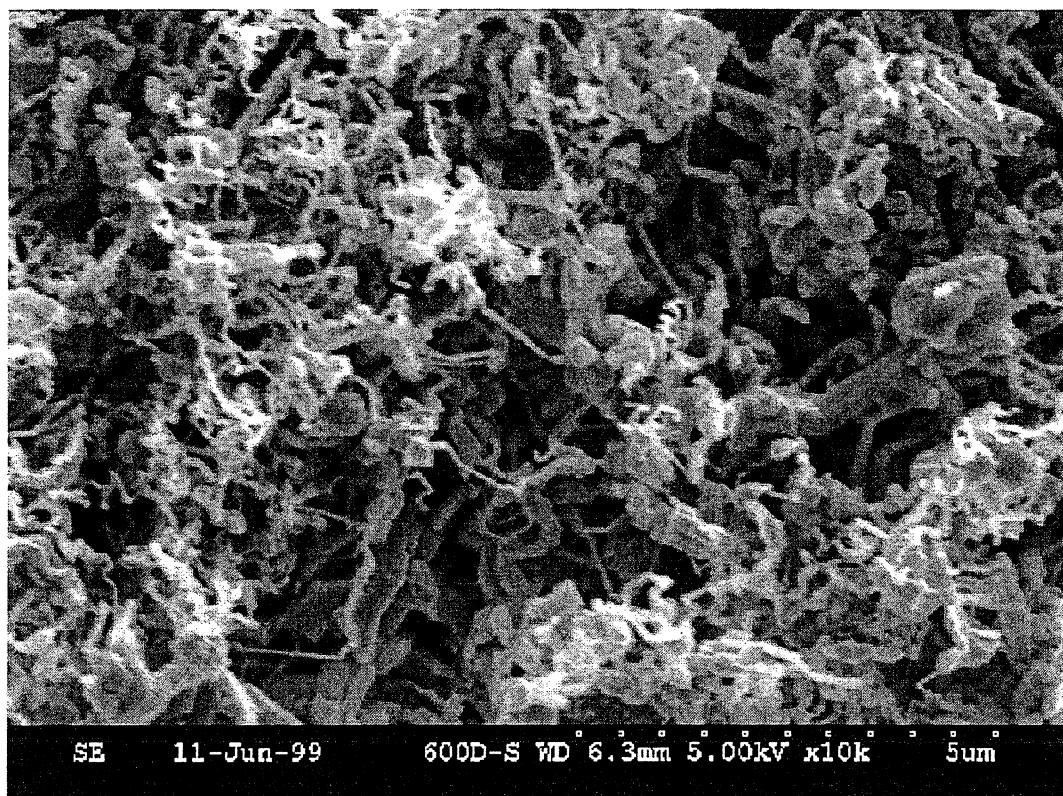


Figure 48. SEM Micrograph of a Carbon Deposit on Inconel 600 (100-ppm thiophene)

9.4 Conclusions

Stressing experiments with model compounds and their binary and ternary mixtures on Inconel 600 showed a strong dependence of the amount and type of carbon deposition on the chemical nature of the hydrocarbons, the reaction temperature, and the pressure. Nonadditive behavior was observed in the mixture studies. Addition of a sulfur compound (thiophene) in small concentrations to the hydrocarbons increased the amount of deposition.

10.0 REFERENCES

1. Katta, V. R., Roquemore, W. M., *Journal of Thermophysics & Heat Transfer*, **7**, 651 (1993).
2. Oliver, D. R., *Chem. Eng. Sci.*, **17**, 335 (1940).
3. Sieder, E. N., Tate, G. E., *Ind. Eng. Chem.*, **28**, 1429 (1936).
4. Gnielinski, V., *Int. Chem. Eng.*, **16**, 359 (1976).
5. Sobel, D. R., Spadaccini, L.J., *J. Eng. Gas Turbines Power*, **119**(2), 344-351 (1997).
6. Coleman, M. M., Schobert, H. H. Song, C., *Chemistry in Britain*, **29**(9), 760-762 (1993).
7. Edwards, T., *31st Aerospace Sciences Meeting & Exhibit*, Reno, NV, AIAA 93-0807 (1993).
8. Kazakova, E., *M. S. Thesis 1998*, The Pennsylvania State University.
9. Yoon, E. M., *Ph.D. Thesis 1996*, The Pennsylvania State University.
10. Song, C., Lai, W. C., Schobert, H. H., *Ind. Eng. Chem. Res.*, **33**(3), 534-547 (1994).
11. Selvaraj, L., *Ph.D. Thesis 1995*, The Pennsylvania State University.
12. Song, C., Lai, W. C., Schobert, H. H., *Ind. Eng. Chem. Res.*, **33**(3), 548-557 (1994).
13. Selvaraj, L., Sobkowiak, M., Song, C., Stallman, J. B., Coleman, M. M. *Energy Fuels*, **8**(4), 839-845 (1994).
14. Heneghan, S. P., Martel, C. R., Williams, T. F., Ballal, D. R., *J. Eng. Gas Turbines Power*, **115**(3), 480-485 (1993).
15. Mushrush, G. W., Hazlett, R. N., *Ind. Eng. Chem. Res.*, **23**(3), 288-294 (1984).
16. Heneghan, S. P., Chin, L. P., *Paper Presented at 5th International Conference on Stability and Handling of Liquid Fuels*, Oct. 3-7 (1994).
17. Chin, L. P., Katta, V. R., *33rd Aerospace Sciences Meeting and Exhibit*, Reno, NV, AIAA 95-0497 (1995).
18. Katta, V. R., Jones, E. G., Roquemore, W. M., *AGARD-CP-536*, Paper No. 19, Sep. 1992, 1-11.

19. Katta, V. R., Roquemore, W. M., AIAA, Reston, VA, AIAA 97-3040 (1977).
20. Mandal, T. K., Kunzru, D., *I&EC Process Design and Development*, **25**, 794-799 (1986).
21. Kopinke, F. D., Zimmermann, G., Reyniers, G. C., Forment, G. F., *Ind. Eng. Chem. Res.*, **32**, 2620-2625 (1993).
22. Kopinke, F. D., Zimmermann, G., Reyniers, G. C., Forment, G. F., *Ind. Eng. Chem. Res.*, **32**, 56-51 (1993).
23. Edwards, T., Zabarnick, S., *Ind. Eng. Chem. Res.*, **32**(2), 3117-3122 (1993).
24. Sheu, J., Zhou, N., Krishnan, A., Jones, A. G., Katta, V. R., *Prepr. Am. Chem. Soc., Div. Pet. Chem.*, **43**(3), 390-393 (1998).
25. Krazinski, J. L., Vanka, S. P., WRDC-TR-89-2139, Aero Propulsion and Power Laboratory, Wright Research Development Center, Dec. (1989).
26. Edwards, T., Anderson, S. D., Pearce, J. A., Harrison, W. E., USAF Wright Laboratory, WL/PSOF, Wright-Patterson AFB, OH 45433.
27. Fogler, H. S., *Elements of Chemical Reaction Engineering*; 2nd Edition, Prentice Hall of India Private Limited, New Delhi, 1995.
28. Bird, R. B., Stewart, W. E., Lightfoot, E. N., *Transport Phenomena*; John Wiley and Sons, Inc., Singapore, 1994.
29. Rice, R. G., Do, D. D., *Applied Mathematics and Modeling for Chemical Engineers*; John Wiley and Sons, Inc., New York, 1995.
30. Forment, G. F., *Ind. Eng. Chem. Res.*, **59**(2), 18-26 (1967).
31. Carberry, J. J., Varma, A., *Chemical Reaction and Reactor Engineering*; Marcel Dekker, Inc., New York, 1987.
32. Ahmed, M., Fahien, R. W., *Chemical Engineering Science*, **35**, 889-895 (1980).
33. Ahmed, M., Fahien, R. W., *Chemical Engineering Science*, **35**, 897-904 (1980).
34. Finlayson, B. A., *Chemical Engineering Science*, **26**, 1081-1091 (1971).
35. Edwards, J. T., Anderson, S. D., *31st Aerospace Sciences Meeting and Exhibit*, Reno, NV, AIAA 93-0806 (1993).
36. Krazinski, J. L., Vanka, S. P., WRDC-TR-89-2139, Aero Propulsion and Power Laboratory, Wright Research Development Center, Dec. (1989).
37. Yu, J. *Ph.D. Thesis 1996*, The Pennsylvania State University.

38. Schiesser, W. E., *The Numerical Method of Lines: Integration of Partial Differential Equations*, Academic Press, Inc., New York, 1991.
39. Oran, E. S., Boris, J. P., *Numerical Simulation of Reactive Flow*, Elsevier Science Publishing Co., Inc., New York, 1987.
40. Shampine, L. W., Reichelt, M. W., *SIAM J. Sci. Comput.*, **18**(10), 1-22 (1997).
41. Karlekar, B. V., Desmond R. M., *Engineering Heat Transfer*; West Publishing Co., New York, 1977.
42. Atria, J. V., Edwards, T., *Prepr. Am. Chem. Soc., Div. Pet. Chem.*, **41**(2), 498-501 (1996).
43. Atria, J. V., Schobert, H. H., Cermignani, W., *Prepr. Am. Chem. Soc., Div. Pet. Chem.*, **41**(2), 493-497 (1996).
44. Goel, P., Boehman, A. L., *Prepr. Am. Chem. Soc., Div. Pet. Chem.*, **43**(2), 382-386 (1998).
45. Minus, D. K., Corporan E., *Prepr. Am. Chem. Soc., Div. Pet. Chem.*, **43**(2), 360-363 (1998).
46. Kays, W. M., *Convective Heat and Mass Transfer*; McGraw-Hill Book Company, New York, 1966.
47. Lee, C. M., Niedzwiecki, R. W., *Am. Chem. Soc. Div. Petrol. Chem.*, **34**(4), 911 (1989).
48. Roquemore, W.M., Pearce, J. A., Harrison III, W. E., Krazinski, J. L., Vanka, S.P., *Am. Chem. Soc., Div. Petrol. Chem.*, **34**(4), 841 (1989).
49. Frankenfeld, J. W., Taylor, W. F., *Ind. Eng. Chem. Prod. Res. Dev.*, **19**, 65 (1980).
50. Song, C., Eser, S., Schobert, H. H., Hatcher, P. G., *Energy Fuels*, **7**, 234 (1993).
51. Taylor, P. H., Rubey, W. A., *Energy Fuels*, **2**, 723 (1988).
52. Song, C., Eser, S., Schobert, H. H., Hatcher, P. G., 1991 Interim report for period July 1990 to July 1991, WRDC-TR-91, vol II.
53. Zabarnick, S., *Ind. Eng. Chem. Res.*, **32**, 1012 (1993).
54. Zabarnick, S., Grinstead, R., *Ind. Eng. Chem. Res.*, **55** (1994).
55. Burgess, C. E., Schobert, H. H., *Fuel*, **70**, 372 (1991).

56. Coleman, M. M., Selvaraj, L., Sobkowiak, M., Yoon, E., *Energy Fuels*, **6**, 535 (1992).
57. Selvaraj, L., Sobkowiak, M., Song, C., Stallman, J. B., Coleman, M. M., *Energy Fuels*, **8**, 839 (1994).
58. Yoon, E. M., Selvaraj, L., Song, C., Stallman, J. B., Coleman, M. M., *Energy Fuels*, **10**, 806 (1996).
59. Song, C., Peng, Y., Jiang, H., Schobert, H. H., *Am. Chem. Soc., Div. Petrol. Chem. Prepr.*, **37**(2), 484. *Energy and Fuels*, **8**, 839 (1992).
60. Ofosu-Asante, K., Stock, L. M., Zabransky, R.F., *Fuel*, **68**, 567(1989).
61. Song, C., Lai, W.-C., Schobert, H. H., *Ind. Eng. Chem. Res.*, **33**(3), 548 (1994).
62. Ballal, D. R., Byrd, R. J., Heneghan, S. P., Martel, C. R., Williams, T. F., Zabarnick, S., 1992 Interim report for period February 1991 to September 1992, WL-TR-92-2112.
63. Yoon, E. M., Selvaraj, L., Eser, S., Coleman, M. M., *Energy Fuels*, **10**, 812 (1996).
64. Yu, J., Eser, S., *Am. Chem. Soc., Div. Petrol. Chem.* (1996).
65. Atria, J. V., Edwards, T., *Am. Chem. Soc., Div. Petrol. Chem.* (1996).
66. McKinney, D. E., Bortiatynski, J. M., Hatcher, P. G., *Energy Fuels*, **7**, 578 (1993).
67. Burnham, A. K., Gregg, H. R., Braun, R. L., *Energy Fuels*, **9**, 190 (1995).
68. McKinney, D. E., Bortiatynski, J. M., Hatcher, P. G., *Prepr. Am. Chem. Soc., Div. Pet. Chem. Prepr.*, 534 (1996).
69. Schobert *et al.*, 1994 Advanced Thermally Stable Jet Fuels, Technical Progress Report, October 1994 to December 1994, 92PC92104-TPR-10.
70. Schobert, *et al.*, 1996 Advanced Thermally Stable Jet Fuels, Technical Progress Report, January 1996 to March 1996, 92PC92104-TPR-15.
71. Filley, R., Eser, S., *Energy Fuels*, **11**, 631 (1997). McKinney, D. E., Behar, F., Hatcher, P. G., *Organic Geochemistry*, **29**(1-3), 119 (1998). Schobert, H., Advanced Thermally Stable Jet Fuels, Contract # F33615-98-2802 0002
74. Lai, W.C., Song, C., Schobert, H. H., Arumugan, R., *Am. Chem. Soc., Div. Fuel Chem. Prepr.*, **37**(4), 1671 (1992).

75. Lai, W.C., Song, C., *Fuel*, **74**(10), 1436 (1995).
76. Song, C., Hatcher, P. G., *Am. Chem. Soc. Div. Petrol. Chem. Prepr.*, **37**(2), 529 (1992).
77. Eberle, N. K., Kahle, G. G., *Tet. Lett.*, **21**, 2303 (1980).
78. Szmant, H. H., Roman, M. N., *JACS*, **88**, 4034 (1966).
79. Jones, E. G., Balster, W. J., *Energy Fuels*, **7**, 968 (1993).
80. Burnham, A. K., Gregg, H. R., Ward, R. L., Knauss, K. G., Copenhaver, S. A., Reynolds, J. G., Sanborn, R., *Geochim. Cosmochim. Acta*, **61**, 3725 (1997).
81. Poutsma, M. L., *Energy Fuels*, **4**, 113 (1990).
82. Song, C., Lai, W.C., Schobert, H. H., *Ind. Eng. Chem. Res.*, **33**(3), 534 (1994).
83. Lai, W.C., Song, C., *Fuel Process. Techn.*, **48** (1), 1 (1996).
84. Behar, F., Vandenbroucke, M., *Energy Fuels*, **10**, 932 (1996).
85. Billaud, F., Chaverot, P., Berthelin, M., Freund, E., *Ind. Eng. Chem. Proc. Des. Dev.*, **20**, 307 (1988).
86. Edwards, T., Zabarnick, S., *Ind. Eng. Chem. Res.*, **32**, 3117 (1993).
87. Peng, Y., *Ph.D. Thesis*, 1995 The Pennsylvania State University.
88. Watkins, J. M., Mushrusch, G.W., Hazlett, R. N., Beal, E. J., *Energy Fuels*, **3**, 231 (1989).
89. Andresen, J. M., Strohm, J. J., Song, C., *Am. Chem. Soc., Div. Petrol. Chem.*, **43**(3), 412 (1998).
90. Strohm, J. J., Andresen, J. M., Song, C., *Am. Chem. Soc., Div. Petrol. Chem.*, **44**(3), 386 (1999).
91. Song, C., Lai, W.C., Schobert, H. H., *Ind. Eng. Chem. Res.*, **33**, 548-557 (1994).
92. Coleman, M. M., Sobkowiak, M., Fearnley, S. P., Song, C., *Prep. Am. Chem. Soc., Div. Petro. Chem.*, **43**(3), 353-356 (1998).
93. Venkataraman, A., Song, C., Coleman, M. M., *Prep. Am. Chem. Soc. Div. Petro. Chem.*, **43**(3), 364-367 (1998).
94. Edwards, T., *Prep. Am. Chem. Soc. Div. Petro. Chem.*, **41**(2), 481-487 (1996).
95. Song, C., Lai, W.C., Schobert, H. H., *Ind. Eng. Chem. Res.*, **33**, 534-547 (1994).
96. Andrésen, J. M., Strohm, J. J., Song, C., *ACS Petroleum Chemistry Division Preprints*, **43**(3), 412-414 (1998).

97. Andrésen, J. M., Strohm, J. J., Coleman, M. M., Song, C., *Prep. Am. Chem. Soc. Div. Fuel Chem.*, **44**(1), 194 (1999).
98. Yoon, E. M., Selvaraj, L., Song, C., Stallman, J. B., Coleman, M. M., *Energy & Fuels*, **10**, 806-811 (1996).
99. Andrésen, J. M., Strohm, J. J., Song, C., *Prep. Am. Chem. Soc. Div. Fuel Chem.*, **44**(1), 199-203 (1999).
100. Andrésen, J. M., Strohm, J. J., Song, C., *Prep. Am. Chem. Soc. Div. Petro. Chem.*, **44**(34), In Press (1999).
101. Hazlett, R. N., *Thermal Oxidative Stability of Aviation Turbine Fuels*, ASTM, Philadelphia, PA (1991).
102. Song, C., Eser, S., Schobert, H. H., Hatcher, P. G., *Energy & Fuels*, **7**, 234-243 (1993).
103. Edwards, T., Atria, J. V., *Prep. Am. Chem. Soc. Div. Petro. Chem.*, **40**(4), 649-654 (1995).
104. Edwards, T., Liberio, P. D., *Prep. Am. Chem. Soc. Div. Petro. Chem.*, **39**(1), 86-91 (1994).
105. Andrésen, J. M., Strohm, J. J., Song, C., *Prep. Am. Chem. Soc. Div. Fuel Chem.*, **44**(1), 194-198 (1999).
106. Reich, L., *Autoxidation of Hydrocarbons and Polyolefins*, Marcel Dekker, New York (1969).
107. Scott, G., *Atmospheric Oxidation and Antioxidants*, Elsevier Pub. Comp., Amsterdam (1965).
108. Scott, G., *Chapter 1* in "Atmospheric Oxidation and Antioxidants", Ed. Scott, G., Elsevier Pub. Comp., Amsterdam (1993).
109. Reddy, K. T., Cernansky, N. P., Cohen, R. S., *Energy & Fuels*, 205-213 (1988).
110. Edwards, T., Zabarnick, S., *Ind. Eng. Chem. Res.*, **32**, 3117 (1993).
111. Li, J., *Ph. D. Thesis*, 1998, The Pennsylvania State University.
112. Altin, O., Eser S., *Ind. Eng. Chem. Res.*, **39**(3), 642 (2000).
113. Bramley, A., *Trans. Faraday Soc.*, **31**, 715 (1935).
114. Reyniers, M. F. S. G., Froment, G. F., *Ind. Eng. Chem. Res.*, **34**, 773 (1995).

Nomenclature

A_o	preexponential factor, sec^{-1}
C_A	concentration of unreacted fuel, mol/m^3
C_{Ao}	initial concentration of entering fuel, mol/m^3
C_p	specific heat, $\text{J/kg}\cdot^\circ\text{K}$
D	diffusivity, m^2/sec
E_a	activation energy, J/mol
ΔH	enthalpy difference, J/kmol
L	length of flow reactor, m
k	rate constant, sec^{-1}
K	thermal conductivity, $\text{W/m}\cdot^\circ\text{K}$
r	radial coordinate
$-r_a$	rate of reaction, $\text{mol/m}^3\cdot\text{sec}$
r_w	radius of flow reactor, m
R	gas constant, $\text{J/mol}\cdot^\circ\text{K}$
T	temperature variable, $^\circ\text{C}$
T_b	bulk temperature, $^\circ\text{C}$
T_o	inlet temperature of the fuel, $^\circ\text{C}$
u	velocity in the flow reactor, m/sec
u_{\max}	centerline velocity in the flow reactor, m/sec
z	axial coordinate

Greek Symbols

ρ	density, kg/m^3
--------	--------------------------

List of Symbols, Abbreviations, and Acronyms

<u>Abbreviation</u>	<u>Definition</u>
API	American Petroleum Institute
BA	Benzyl Alcohol
BP	BP-Amoco Inc.
DEG	Diethylene Glycol
DHN	Dihydronaphthalene
EDTST	Extended duration thermal stability test
FID	Flame ionization detector
FTIR	Fourier-transform infra red
GC-FID	Gas chromatography-flame ionization detector
GC-MS	Gas chromatography-mass spectrometry
GC-SIM-MS	GasChromatography-SelectIon Monitoring-Mass Spectrometry
EDS	Energy-Dispersive Spectrometry
HPLC	High-Pressure Liquid-Chromatography
ID	Inside Diameter
JPTS	Jet Propellant Thermally Stable
LECO	(name of the company)
MOL	Method of Lines

NIFTR	Near-Isothermal Flowing Test Rig
NIST	National Institute of Standards and Technology
NMR	Nuclear Magnetic Resonance
OD	Outside Diameter
ODE	Ordinary Differential Equations
PDE	Partial Differential Equations
PFK	Perfluorokerosene
QCM	Quartz Crystal Microbalance
SEM	Scanning Electron Microscope
SIM	Secondary Ion Mass Spectrometry
SPR	Structure-Property Relationship
TD	Tetradecane
THN	Tetrahydronaphthalene
THQ	Tetrahydroquinoline
TPO	Temperature-Programmed Oxidation
UHP	Ultra High Priority